MATHEMATICAL MODELLING OF INVASIVE SPREAD IN THE HETEROGENEOUS LANDSCAPE

by

BRADLY F. DEELEY

A thesis submitted to
The University of Birmingham
for the degree of
DOCTOR OF PHILOSOPHY

School of Mathematics
College of Engineering and Physical Sciences
The University of Birmingham
September 27, 2023

Abstract

Invasive plant species pose a significant threat to biodiversity and the economy, and their management is often resource-intensive and expensive. Evidence suggests that roads can have an important effect on the spread of invasive plant species, although little is known about the underlying mechanisms at play. Further research and the application of mathematical models is required to make control measures more efficient.

In this thesis, we develop a novel mathematical model to analyse the impact of roads on the propagation of invasive plants in both the one-dimensional and two-dimensional spatial domains. An integro-difference equation model is formulated for stage-structured population and incorporates a road sub-domain in the spatial domain. We show that, depending on the definition of the growth function in the model, there are three distinct types of behaviour in front of the road. Roads can act as: (1) a barrier to invasion; (2) a temporary obstacle, leading to the formation of a beachhead; (3) as a corridor for invasion. Small changes in conditions favouring the invasive species can change the case for the road, allowing the invasive species to invade the domain in front of the road where it previously could not. We investigate the propagation regime of the invasive plant species studied at the short-time scale before a travelling wave is established and advances into space at a constant speed. Using this approach, we demonstrate how nonlinear spatio-temporal dynamics arise in a transient regime where the propagation speed depends on the detection threshold population density.

In the two-dimensional spatial domain, a long-distance dispersal kernel is incorporated along the road sub-domain. We show how long-distance dispersal along the road can lead to increased invasion in the domain.

Finally, additional landscape heterogeneities around the edge of the road, the edge effect, are investigated. Leading to an increase or decrease in the population density of the species in the spatial domain around the road.

Acknowledgements

First and foremost, I would like to thank Dr Natalia Petrovskaya for her excellent help, support, and guidance throughout my studies.

I thank Professor Rob MacKenzie, Dr Simon Dixon, and Deanne Brettle; through the Forest Edge Doctoral Scholarship Programme, we had many interesting conversations. I would also like to thank my friends and everyone I met in Birmingham who helped to make the time so enjoyable.

Finally, I would like to thank my family for all of their continual help and support throughout.

Contents

Chapter 1

Introduction

Biological invasion of animal and plant species pose a significant threat to the ecosystem and economy in the order of billions of pounds each year [54], with the rate of damage set to increase over the coming years [58]. Due to the importance of this issue, the United Nations has declared 2021-2030 the decade on ecosystem restoration. Part of the United Nations goals include the re-introduction of native species and increasing the biodiversity of the land. However, as the world becomes ever more connected [49], invasive plant species pose an increasing obstacle to this goal [18, 62, 10]. Invasive species cause both direct losses in biodiversity [55, 68, 7] and damage existing habitats in a multitude of ways [39]. For example, through alterations to: soil composition [30, 44]; hydrological properties [14]; and frequency of wild fires [19].

Due to the various ways invasive species can cause damage, it is highly desirable to manage invasive species. To do so, we need to understand the underlying behaviours of invasive plant species, the dynamics of the species and the ecosystems they are a part of. The better the understanding, the more effectively we can allocate the limited resources available for ecosystem management. Biological invasion can occur on scales as large as countries or continents and on time scales of decades. Effectively monitoring the spread of invasive species over these spatial-temporal scales is very costly, and anything that can be done to reduce this cost will be of benefit.

Mathematics can play an essential role in improving one's understanding of ecosystems by providing models that aim to quantify their complex behaviour. No mathematical model exists that can fully incorporate all of the interactions and complexities within an ecosystem. However, even a simple mathematical model can provide useful insight into its behaviour. Mathematics also offers a particular advantage, allowing one to create a 'virtual sandbox', wherein we can test hypotheses and make comparisons to real-world observations and field data [31].

Much of the work carried out in the area of mathematical ecology has taken place within around the last one hundred years, although some key initial results date back further. One of the key aims of mathematical modelling is to provide as realistic as possible representation of the problem; this means attempting to incorporate all components of the system into the model. Some of the components of the system include: how the species grows and spreads; how the species interacts with the environment; and how the species interacts with other species. One must start at a simple mathematical model and carefully incorporate new components into the model. Some of the earliest works considered a single species, discrete-time, non-spatial model that describes how the population density changes over this discrete time interval, with the most basic models only calculating the difference of the birth and death rates of the species. In 1748, Leonhard Euler created a discrete time single-species model [24] where the solution has geometric (exponentially behaving) growth. Fifty years later (1.1.6) in 1798, a continuous time single-species differential equation model was created by Thomas Malthus [5], known as the Malthusian model. The Malthusian model also results in exponential growth. Both models have unrealistic, unbounded growth. To address this issue, Pierre Verhulst [1838, [61]] added a density-dependent term to the model; this was intended to model intraspecific competition. Later, Raymond Pearl investigated a specific class of the model, which popularised the model now known as the Verhulst-Pearl logistic model [5]. This model added an important biologically realistic element to the problem, where the population no longer has unlimited resources.

In 1937, Fisher [26] extended these models to the spatial setting using reaction-diffusion equations. The Fisher–KPP equation yielded travelling wave solutions where, after establishment, the gene in Fisher's case or population spread at a constant rate at each generation. Early work by Skellam [64] and Kierstead and Slobodkin [33] investigated the minimum spatial area necessary for the population to survive, also known as the critical patch size problem, through the reaction-diffusion framework. Since then, reaction-diffusion continuous time and space equations have been used in answering many problems in ecology, from single-species to multi-species problems [38, 12, 40].

The dynamics of populations with discrete generations (e.g. insects) cannot be captured by a continuous time model. Instead, a discrete model is required in systems with discrete generations, for example. Difference equations that describe the population density of a species in discrete time have long been used in problems such as host-parasitoid systems [51]. However, in 1975, May created that simple difference equations could lead to chaotic behaviour [46], at which point the use of such discrete time models increased in popularity. Weinberger in 1982 [72], and Kot and Schaffer in 1986 [35] combined dispersal in continuous space with discrete time growth. These models are now known as integro-difference equations. Integro-difference equations have been applied to many problems in ecology, and their popularity has been increasing in recent years [43]. Integro-difference equations will be used as the basis of the mathematical model explored later in the text.

1.1 Background Mathematics

We will start with a single species model where the population density is given by $N \geq 0$. The change in the population density depends only on the discrete time increment Δt,

$$\Delta N_t(\Delta t) = N_{t+\Delta t} - N_t \tag{1.1.1}$$

$$= [B(N_t) - D(N_t)]\Delta t, \tag{1.1.2}$$

where $B(N_t)$ represents the birth rate for a given population density N_t, and D_t represents the death rate for a given population density. How the population density grows only depends on the density dependent birth and death rate. These terms can be combined in a single function describing the growth $G(N_t) = B(N_t) - D(N_t)$. The population density at the next time increment can then be found,

$$N_{t+\Delta t} = N_t + \Delta N_t \tag{1.1.3}$$

$$= N_t + G(N_t)\Delta t. \tag{1.1.4}$$

In the discrete case, one can take $\delta t = 1$ and simplify Eq. (1.1.3) as follows

$$N_{t+1} = N_t + G(N_t) \equiv F(N_t), \text{ for } t \geq 0,$$

where $F(N_t)$ is called the growth function. This defines a first order difference equation,

$$N_{t+1} = F(N_t), \text{ for } t \geq 0. \tag{1.1.5}$$

Now that we have constructed a model for the growth of the species, one might want to analyse its behaviour. For example, one may be interested in finding population density values that remain constant with time, known as the equilibrium solutions. These are precisely the solutions $\bar{N}$ to Eq. (1.1.5) when

$$\bar{N} = F(\bar{N}).$$

An equilibrium solution of a biological system is when a system is balanced. A population density is at equilibrium when the forces acting against the species growth, be that a lack of resources or predators, for example, is equal to the forces of growth of the species; therefore, the population density remains constant. In the real world, however, rarely something living remains constantly fixed. To address perturbations we introduce the

notion of the stability of the equilibrium state. If an equilibrium state is stable a small perturbation will converge back to the equilibrium solution, and unstable if it diverges from the equilibrium solution. For first-order difference equations, we have the following definitions [50].

Definition 1.1. Equilibrium Solutions and Stability in One-Dimension: Let F' be continuous on an open interval I containing the equilibrium point $\bar{N}$ of Eq. (1.1.5).

1. Then $\bar{N}$ is a locally asymptotically stable equilibrium if

$$| F'(\bar{N}) | < 1,$$

specifically we have,

   (a) monotonic convergence when $0 < F'(\bar{N}) < 1$, and

   (b) oscillatory convergence when $-1 < F'(\bar{N}) < 0$.

2. We also have that $\bar{N}$ is unstable if

$$| F'(\bar{N}) | > 1,$$

specifically,

   (a) monotonically unstable when $F'(\bar{N}) > 1$.

   (b) When $F'(\bar{N}) < -1$ several cases of behaviour can occur, the steady state can converge to a limit cycle or it can converge to a chaotic attractor [40, 45, 47].

One of the earliest population models is a discrete time single-species model created by Leonhard Euler [24],

$$N_{t+1} = (1 + \rho)N_t, \tag{1.1.6}$$

where $\rho \in \mathbb{R}^+$ is the growth rate, and $F(N_t) = (1 + \rho)N_t$. Solving (1.1.6),

$$N_t = (1 + \rho)^t N_0,$$

where N_0 is the initial population density. The solution grows geometrically (similar to exponentially) with time.

Finding the equilibrium solutions for the model (1.1.6) we have,

$$\bar{N} = (1 + \rho)\bar{N},$$

which simplifies to,

$$\rho\bar{N} = 0,$$

where $\rho > 0$, therefore, the only equilibrium solution is at $\bar{N} = 0$. For the stability of the equilibrium solution,

$$F'(\bar{N}) = (1 + \rho) > 1,$$

and is, therefore, a monotonically unstable equilibrium solution. This agrees with our understanding of the behaviour of the model. In particular, if $N_t = 0$ the population is extinct and remain extinct for all time. Otherwise, if $N_t > 0$, then due to geometric growth as $t \to \infty$, $N_t \to \infty$.

Later Thomas Malthus created a continuous time single-species differential equation model known as the Malthusian model [5],

$$\frac{dN_t}{dt} = \rho N_t, \tag{1.1.7}$$

where $\rho \in \mathbb{R}^+$ is the growth rate for the population. The growth rate $G(N_t) = \rho N_t$, where the growth function $F(N_t) = N_t + G(N_t) = (1 + \rho)N_t$ is the same as in the discrete time model (1.1.6). Solving the difference Eq. (1.1.7) gives

$$N_t = N_0 \exp(\rho t), \tag{1.1.8}$$

where N_0 is the initial population density, this also results in exponential growth. Both the discrete time and Malthusian models have unrealistic, unbounded growth. Let $f(N_t)$

denote the per capita growth rate then for both models (1.1.6), and (1.1.7) the per capita growth rate is density independent $f(N_t) = \rho$. This means that both models produce unbounded growth.

Then Pierre Verhulst [61] introduced a density-dependent mortality term into the model to address this issue,

$$\frac{dN_t}{dt} = \rho N_t - sN_t^2,$$

where s is the density dependent term. This density-dependent mortality term is typically interpreted as representing intra-specific competition. Later Raymond Pearl set $s = \frac{\rho}{K}$, which popularised the model now known as the Verhulst-Pearl logistic model [5],

$$\frac{dN_t}{dt} = \rho N_t \left(1 - \frac{N_t}{K}\right). \tag{1.1.9}$$

In this form, the growth rate of the population density is given by $G(N_t) = \rho N_t(1 - \frac{N_t}{K})$. This model is usually referred to as logistic growth or the logistic growth model. This model (1.1.9) can be solved to obtain [40],

$$N_t = \frac{KN_0}{N_0 + (K - N_0)e^{-\rho t}},$$

if $N_0 > 0$, then as $t \to \infty$, $N_t \to K$. This model has an important biologically realistic behaviour, the population no longer grows without an upper bound. Note that when the population density is small $N \ll 1$, one can write (1.1.9) as $\frac{dN_t}{dt} \approx \rho N$ [40]. Thus the Malthusian model (1.1.8) can approximate the logistic model (1.1.9) when the population density is small.

Despite these models, little attention was given to this area of research until 1917 when D'Arcy Thompson wrote the highly influential book 'On Growth and Form' [66] which has received much praise [40, 6]. Thompson outlined in numerous ways how mathematics can be applied to biology and ecology, writing

> "In general no organic forms exist save such as are in conformity with physical and mathematical laws".

This work demonstrated Thompson's belief that mathematics provided the tools necessary to solve these problem and inspired much future work in this area.

Up to this point, the models introduced have been non-spatial, describing only the growth of the population. However, populations do not just grow at one point in space; they also spread and move in space. When considering a spatial component of the model, it is essential to consider what type of movement the species uses. Do plant and animal species move and disperse deterministically or stochastically? When it comes to plant species, they do not typically move; however, the seeds disperse. Many factors affect how and where the seeds disperse, such as wind and animal movement. This means that one can consider seed dispersal stochastically. For animal movement, how animals move throughout the landscape is affected by many external factors, such as the weather, other animals, food, and many other stimuli. Thus, animal movement can also be appropriately modelled stochastically [40]. Because the dispersal component is stochastic one wants to find the probability that an individual at the point y moves to the point x after some time increment Δt. In the discrete time case we can consider $\Delta t = 1$. Due to the assumption of stochastic movement, the exact position x the individual will move to is uncertain. A probability density function

$$k(x, y), \tag{1.1.10}$$

known as the dispersal kernel, can be used to model the movement of the individual in space. Note the dispersal kernel is required to conserve the total population density in the domain,

$$\int k(x, y)\, dx = \int k(x, y)\, dy \equiv 1. \tag{1.1.11}$$

The diffusion equation [40],

$$\frac{\partial N_t(x)}{\partial t} = D\frac{\partial^2 N_t(x)}{\partial x^2}, \tag{1.1.12}$$

where D is the diffusion coefficient, is often used as a continuous approximation to the stochastic movement behaviours described above.

Now that we have defined models for the growth and dispersal for both discrete and continuous cases, these components can be combined to create a model that considers both growth and dispersal. We first will consider the continuous case where there exist overlapping generations. This model will combine the diffusive term (1.1.12) and the growth term,

$$\frac{\partial N_t(x)}{\partial t} = D\frac{\partial^2 N_t(x)}{\partial x^2} + G(N_t)$$

The resulting class of equations created by doing so are referred to as reaction-diffusion equations.

Reaction-diffusion equations have been widely used in the study of mathematical ecology [40]. However, this approach is not necessarily appropriate when modelling populations with distinct generations, where the demographic stage and dispersal happen on separate time scales. A discrete time framework is more appropriate in such cases as one requires a model which considers these processes separately, i.e. a stage-structured model. If one chooses a growth function (1.1.3) to represent the demographic stage,

$$N_t^{gr}(x) = F(N_t(x)),$$

and combines this with a dispersal kernel (1.1.10) to represent the dispersal stage in the following way,

$$N_{t+1}(x) = \int_\Omega N_t^{gr}(y)k(x,y)\,dy,$$

this forms what is known as an integro-difference equation model [43].

Now that spatio-temporal models have been introduced, one might be interested in how fast the population density propagates in the dispersal domain. When considering the propagation speed, one must first define what it means to reach/invade a given area. Many dispersal kernels result in a non-zero population density everywhere. Not only is this not very interesting, but it is also inaccurate to a real-world situation. Therefore, a detection threshold $\tilde{N}$ will be introduced, i.e. the population will be considered to have reached a point x in the domain if $N(x) \geq \tilde{N}$. As the population propagates the

position where this threshold density is observed changes. The speed of propagation can be calculated from the changes in the spatial extent of the detectable population as follows. The edges of this extent are given by,

$$x_t^+ = \max_{N_t(x) \geq \tilde{N}} x, \text{ and, } x_t^- = \min_{N_t(x) \geq \tilde{N}} x.$$

The propagation speed to the right and left can then be defined by,

$$c^+(t, \tilde{N}) = x_t^+(\tilde{N}) - x_{t-1}^+(\tilde{N}), \text{ and, } c^-(t, \tilde{N}) = x_{t-1}^-(\tilde{N}) - x_t^-(\tilde{N}),$$

respectively. Note that when using a symmetrical dispersal kernel, the left and right propagation speeds are identical; however, for general dispersal kernels, they can be different.

In Fisher's paper 'The wave of advance of advantageous genes' [26] the concept of a traveling wave solution was proposed. A traveling wave solution to a spatio-temporal model (*e.g.* a reaction-diffusion, or integro-difference equation) is one such that the propagation speed c is constant and the shape of the leading edge of the population density is preserved as it propagates.

Chapter 2

Propagation of Invasive Waves in the Homogeneous Landscape

We are interested in modelling the behaviour of invasive plant species. Many plant species reproduce at certain time intervals throughout the year, for example, on a yearly cycle through seed dispersal or pollination [40]. Therefore, the model will be a discrete-time model. There is a period where the demographic stage, which can include the growth of juveniles, their maturation, mating and reproduction, occurs, followed by a period where the demographic stage does not occur. Even though an individual's death can happen at any time through predators or a lack of resources, it is convenient to treat the whole system in discrete time. Therefore, we deal with all deaths between cycles at the beginning of the next cycle. The plants' position and the invaded area do not change between the demographic stage cycles. A first-order difference equation (1.1.5) will be used to model the demographic, growth only stage.

Throughout the model, we use set discrete time intervals, the time between generations, where an entire cycle of behaviour will occur over each time increment. Since the model assumes discrete time, we can set this time increment to one. We denote the current time by t, and note that the population density evolves from current generation t to generation $t + 1$. We will denote the population density of the species by N. Let

$N(t) \equiv N_t$ denote the population density at generation t.

Sections 2.1-2.10 are partially based on a published journal article [20].

2.1 The Growth Function

The choice of growth function that describes the demographic stage is an important one, and much consideration has previously been given to the problem [43]. When choosing a growth function for the model, we want it to be biologically realistic; this means we cannot have a growth function that leads to a negative population density. We also cannot have a growth function that leads to growth that tends to infinity within a region. This is because, for a given species, due to its size and the available resources, a species has a maximum population density within a region; the carrying capacity of the species. We firstly want to investigate a growth function that has positive growth for any population density N up to the carrying capacity. We therefore will consider the following growth function [2]

$$F(N) = AN\exp(-N),\ A > 0, \tag{2.1.1}$$

where A determines the carrying capacity. The exponential function acts as the limiting factor,

$$\lim_{N\to\infty} F(N) = 0.$$

From definition 1.1 the equilibrium solutions of the growth function (2.1.1) are the points where

$$\bar{N} = A\bar{N}\exp(-\bar{N}),$$

which has solutions $\bar{N}_1 = 0$ and $\bar{N}_2 = \ln(A)$. Investigating the stability of the equilibrium solutions one has

$$F'(N) = -A(N-1)\exp(-N),$$

where

$$F'(\bar{N}_1) = A.$$

Thus, the equilibrium solution $\bar{N}_1 = 0$ is locally stable with oscillatory convergence when $0 < A < 1$, and is locally monotonically unstable when $A > 1$. Further investigation is required [23] if $A = 1$. We have for the second equilibrium solution

$$F'(\bar{N}_2) = 1 - \ln A.$$

Then, if $1 < A < e^2$, the equilibrium solution $\bar{N}_2$ is stable, and if $A > e^2$ the equilibrium solution $\bar{N}_2$ is unstable. If $1 < A < e$ the equilibrium solution $\bar{N}_2$ converges monotonically, if $e < A < e^2$ then $\bar{N}_2$ converges with oscillatory behaviour. Throughout we will assume that $A < e^2$, and thus $\bar{N}_2$ can be treated as a stable equilibrium solution. Where $\bar{N}_1 = 0$ is the trivial equilibrium solution, if the population density is zero it remains at zero for all time increments. The equilibrium solution

$$\bar{N}_2 = \ln(A) \tag{2.1.2}$$

is the carrying capacity. Setting $F'(N) = 0$, we find (2.1.1) has a global maximum at

$$N^{max} = \frac{A}{e}. \tag{2.1.3}$$

In Fig. 2.1a, the population density after the growth function has been applied $F(N)$, is given for a range of $N \in [0, 8]$, for choices of $A = 0.75$, $A = 2.5$, and $A = 7$. In Fig. 2.1b, an example of how the population density evolves over time is given by the difference equation (2.1), for a starting density of $N_0 = 0.1$, and choice of $A = 0.75$, $A = 2.5$, and $A = 7$ is shown.

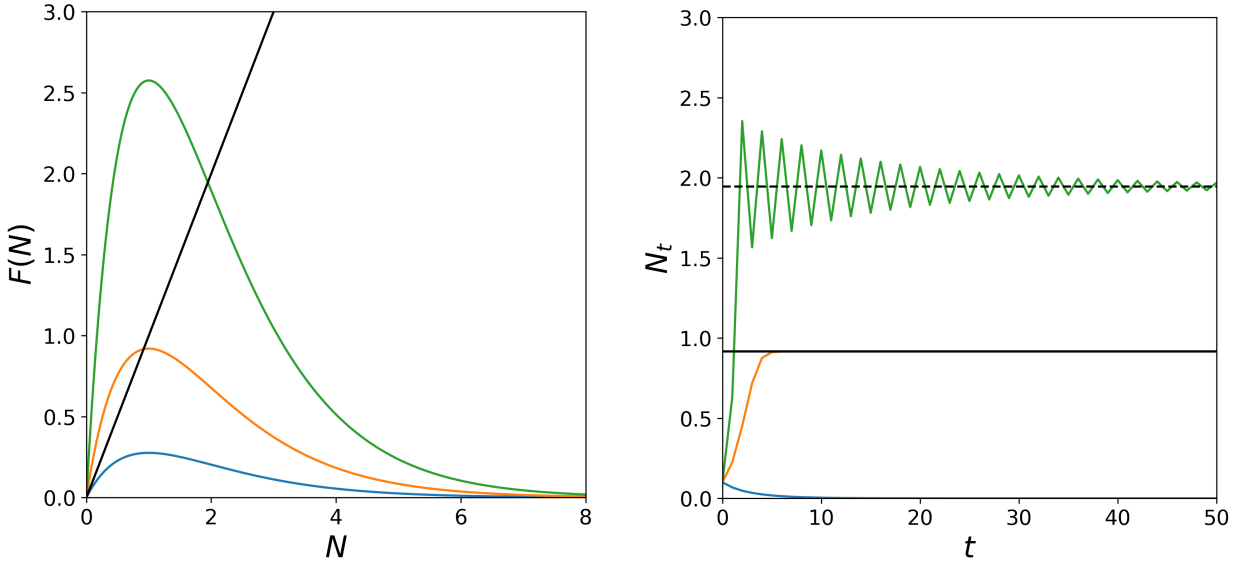

Figure 2.1: *(a) The growth function* (2.1.1) *for the range of population density* $N \in [0, 8]$*, and various values of* A*, where the equilibrium solutions are given by the intersection with the line* $N = F(N)$ *(solid black line). For* $A = 0.75 < 1$ *(blue solid line), one can see* $F(N) < N$ *for all* N*, and therefore the population density decreases after the growth function has been applied. For* $A = 2.5$ *(orange solid line), and* $A = 7$ *(green solid line), the growth function parameter* $A > 1$*. (b) The population density over time* N_t *given by the model* (2.1)*, for* $N_0 = 0.1$ *and various choices of* A*. For* $A = 0.75$ *(solid blue line), we are in an unconditional extinction case where* $N_t \to 0$ *as* $t \to \infty$*. For* $A = 2.5$ *(solid orange line), we are in an unconditional survival case. The carrying capacity* $\ln 2.5 \approx 0.916$ *(solid black line), is close to the maximum population density* $2.5 \exp(-1) \approx 0.920$*, and therefore we do not observe oscillatory behaviour as the population density tends towards the carrying capacity. For* $A = 7$ *(solid green line),* $A > e$ *and therefore oscillatory convergence behaviour occurs as the population density tends towards the carrying capacity (dashed black line).*

2.2 Spatio-Temporal Dynamics

So far, we have only considered a time-dependent difference equation model for the growth of the population. However, from a biological point of view, we are also interested in investigating how a species spreads throughout space, for example, a forest. To do so, we need to introduce a spatio-temporal model that considers both how the species grows and spreads in space throughout time. The population density N, now depends on time and space. Let $N(t, x) \equiv N_t(x)$ be the population density at generation t over continuous space x. We will use integro-difference equations as the basis of the model; this allows one to consider both the demographic stage and dispersal stage independently at every

time increment, i.e. a stage-structured model. The distribution of the population density is considered at generation t, after generation t has dispersed, but before the maturation stage is applied at generation $t+1$. In a biological context: the species has reached maturity; its seeds have dispersed; and then grow at the seeds' new location. The species first enters the demographic stage,

$$N_t^{gr}(x) = F(N_t(x)). \tag{2.2.1}$$

Once complete, the species now enters the dispersal stage which, when finished, produces the species' spatial distribution in the next generation,

$$N_{t+1}(x) = \int_\Omega N_t^{gr}(y)k(x,y)\,dy, \tag{2.2.2}$$

where Ω is a dispersal domain and $k(x,y)$ is the dispersal kernel. Now that we are working in space and time, we need to define a domain in which we will work. We will initially work in a one-dimensional dispersal domain

$$\Omega = [-L, L]. \tag{2.2.3}$$

A position in Ω is then denoted by x. The dispersal kernel is denoted by $k(x,y)$ where $y \in \Omega$, is the probability density function of the event that an individual moves from position y to position x after dispersal. For example, the probability of a seed at position y reaching position x. If we have a closed domain, none of the population density N can escape. Thus, the dispersal kernel conserves the total population density and satisfies

$$\int_\Omega k(x,y)\,dx = \int_\Omega k(x,y)\,dy \equiv 1.$$

If we substitute (2.2.1) into (2.2.2) we obtain the following integro-difference equation for the population density in generation $t+1$ in the spatial domain Ω:

$$N_{t+1}(x) = \int_{\Omega} F(N_t(y))k(x,y)\,dy. \tag{2.2.4}$$

This integro-difference equation model calculates the population density at the next time increment $t+1$, given the known population density at the current time t, therefore, one also needs to introduce an initial population density for $t = 0$.

2.3 Numerical Method

Although analytical solutions of the integro-difference equation can be found in some cases, and analytical solutions will be provided later in the text, numerical simulations are important to provide further understanding and confirmation of the analytical results, and to solve the integro-difference equation in cases that cannot currently be solved analytically. In numerical solutions, we approximate the continuous spatial domain, we do so by splitting the spatial domain into a discrete number of equally spaced sub-intervals.

For convenience, as will become apparent below, we split the domain into $K = (2^b+1)$ sub-intervals, where $b \in \mathbb{Z}^+$. This gives the distance between sub-intervals

$$\Delta x = \frac{2L}{2^b},$$

which defines how fine the grid is; the finer the grid, the better the approximation to the exact solution. In order to do so efficiently, a computer model needs to be developed.

Python will be used as the basis for the computational model. Python's standard numerical method package uses the composite trapezoidal rule. This method is very computationally expensive, $O(K^2)$ in one dimension, $O(K^4)$ in two dimensions. However, there are other algorithms for integration, including the fast Fourier transform (FFT). The FFT uses convolutions and the convolution theorem to rearrange the integral into a

product of Fourier and inverse Fourier transforms.

Definition 2.1. Fast Fourier Transform: Given a function $f(a)$ defined on $a \in (-\infty, \infty)$, the Fourier transform is defined by [11]

$$\mathcal{F}(\omega) = \int_{-\infty}^{\infty} f(a) \exp(-2\pi i a\omega) da,$$

and the inverse Fourier transform is defined by

$$f(a) = \int_{\infty}^{\infty} \mathcal{F}(\omega) \exp(2\pi i a\omega) d\omega.$$

Given two functions, $m(a)$ and $n(a)$ were $a \in (-\infty, \infty)$, their convolution is given by the following,

$$m(a) * n(a) = \int_{-\infty}^{\infty} m(b)n(a-b)db.$$

The convolution theorem states

$$m * n = \mathcal{F}^{-1}(\mathcal{F}(m) \cdot \mathcal{F}(n)), \tag{2.3.1}$$

where $\mathcal{F}(m)$ is the Fourier transform of m, and $\mathcal{F}^{-1}(m)$ is the inverse Fourier transform of m.

This can be generalised for the finite interval Ω, as long as Ω is large enough that the species N does not reach the boundary. Therefore, equation (2.2.4) can be written in the following way in terms of convolutions

$$N_t^{gr}(x) * k(x) = \int_{\Omega} N_t^{gr}(y)k(x-y)dy, \tag{2.3.2}$$

which allows us to rewrite (2.3.2) in terms of Fourier transforms given by equation (2.3.1),

$$\mathcal{F}^{-1}(\mathcal{F}(N_t^{gr}(x)) \cdot \mathcal{F}(k(x))) = \int_{\Omega} N_t^{gr}(y)k(x-y)dy.$$

For full details on the implementation of the FFT, see [57]. In the one-dimensional case, this allows us to calculate the integral in $O(K\log_2(K))$ operations. In the more realistic two-dimensional case, this allows us to calculate in $O(K^2\log_2(K))$ operations, compared to $O(K^4)$ operations for simple numerical methods as described above. It is not hard to see that, for large values of K, this will save a significant amount of computational time.

2.3.1 Validation of The Numerical Method

The error $e_i = \left|\bar{N}_t(x_i) - N_t(x_i)\right|$ of the numerical method will be computed for every point in the domain x_i, $i = 1, 2, ..., K$, where: K is the total number of sub-intervals in the domain; $N_t(x_i)$ is calculated through numerical integration; and $\bar{N}_t(x_i)$ is the exact solution. The overall numerical error is calculated using the error norm [57] is given by,

$$||e|| = \max_{i=1,2,...,K} |e_i|.$$

Throughout the calculations, we employ a computational error cutoff threshold of τ. This is due to the dispersal kernel producing non-zero values across the entire domain for every time-increment. There are no rules currently governing the interaction with the boundaries of the domain. The threshold τ prevents small computational errors, arising from interactions between this dispersal kernel and the boundary, from affecting the overall accuracy of the numerical method. If the population density is below the error cutoff at the end of a time-increment the population density is set to zero,

$$N_t(x) = \begin{cases} 0, & \text{if } \bar{N}_t(x) < \tau, \\ \bar{N}_t(x), & \text{otherwise.} \end{cases}$$

We now compute the error norm to compare the accuracy of the FFT method against

the actual result, using the normal distribution as the dispersal kernel

$$k(x-y) = \frac{1}{\sqrt{2\pi\sigma^2}} \exp\left(-\frac{(x-y)^2}{2\sigma^2}\right), \tag{2.3.3}$$

where $x, y \in \Omega$, with $\sigma = 0.1$, $\Omega = [-10, 10]$, and an error cutoff of $\tau = 10^{-7}$. The choice of computational error cutoff does not noticeably impact the speed of the computation in and of itself. However, if the error cutoff is too small, the population density will reach the edge of the domain in a shorter period of time. This would, therefore, require a larger grid size if this happens, which would then increase computational time. The dispersal kernel decays towards zero away from the center of dispersal, thus, the smaller the detection threshold, the further away the population density becomes non-zero from the centre of dispersal. This also means that the smaller the detection threshold, the sooner non-zero population density values spread to the boundaries of the dispersal domain. In order to continue the simulation for further time increments, the domain size and, therefore, the number of grid points has to be increased. However, for a higher detection threshold, the compilation can be computed for a greater number of time increments before non-zero population density values reach the edges of the domain. Here we have $k(x-y)$ instead of $k(x, y)$; this is because the dispersal kernel is symmetric[1]. We will also use the normal distribution for the initial population density

$$N_0(x) = \frac{1}{\sqrt{2\pi\sigma_0^2}} \exp\left(-\frac{(x-\mu)^2}{2\sigma_0^2}\right), \tag{2.3.4}$$

with $\sigma_0 = 1$ and mean $\mu = 0$. In order to have an exact result, we will consider a linear growth function

$$F(N) = BN_t(x). \tag{2.3.5}$$

[1]Note that, the general notation for the dispersal kernel k(x,y) has been used until now.

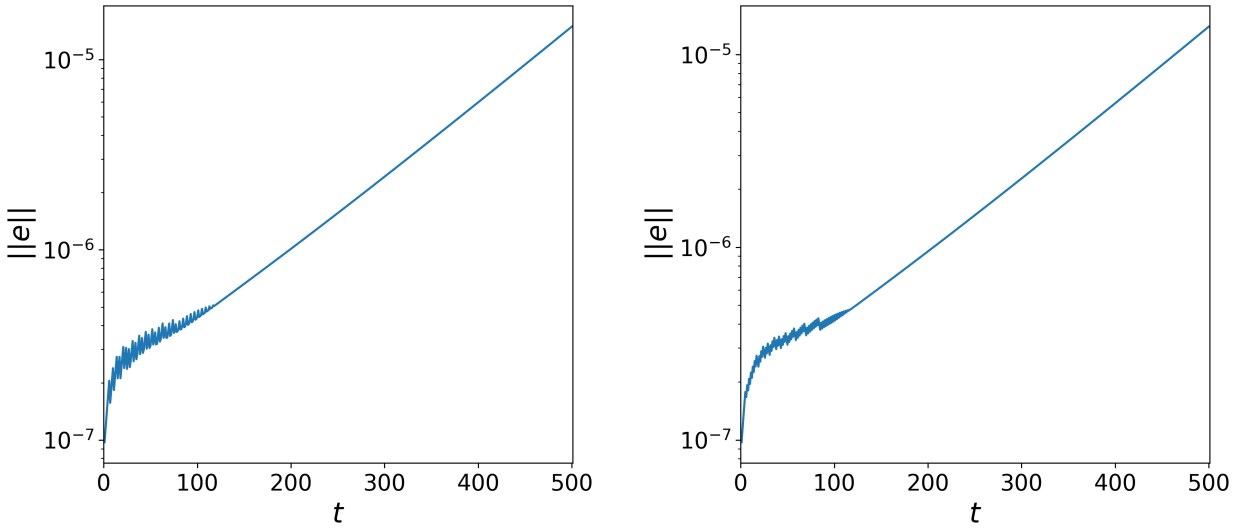

Figure 2.2: *Error norm computations against the exact solution of the integro-difference equation* (2.3.6)*,* ***(a)*** *over a grid step size of* $\Delta x = \frac{5}{128}$*, and* ***(b)*** *over a grid step size of* $\Delta x = \frac{5}{256}$*.*

We, therefore, have the following exact solution for the population density

$$N_t(x) = (BN_t(x))^t \cdot \frac{1}{\sqrt{2\pi\sigma_t^2}} \exp\left(-\frac{(x-\mu)^2}{2\sigma_t^2}\right), \tag{2.3.6}$$

where $B = 1.01$, $\mu = 0$ and $\sigma_0 = 1$.

We can see the plots of the error norm against time for $\Delta x = \frac{5}{128}$ in figure 2.2a and $\Delta x = \frac{5}{256}$ in figure 2.2b. From this we can see that both $\Delta x = \frac{5}{128}$, and $\Delta x = \frac{5}{256}$, provide sufficient accuracy for a long period of time. We conclude that the FFT method is a good numerical method, both in terms of computational time and accuracy, for evaluating integro-difference equation based models.

2.4 Results

We now want to solve the 1-D spatio-temporal problem. To do so the initial condition, dispersal kernel, and growth function needs to be chosen. The initial condition at $t = 0$ is chosen to be a Gaussian distribution with mean $\mu = 0$, standard deviation σ_0, and total

population density Φ,

$$N_0(x) = \frac{\Phi}{\sqrt{2\pi\sigma_0^2}} \exp\left(-\frac{x^2}{2\sigma_0^2}\right). \tag{2.4.1}$$

The height $h = N_0(0)$ of the initial condition is defined by the parameters Φ and σ_0 as follows,

$$h = \frac{\Phi}{\sigma_0\sqrt{2\pi}}. \tag{2.4.2}$$

The Gaussian dispersal kernel with standard deviation σ

$$k(x, y) = \frac{1}{\sqrt{2\pi\sigma^2}} \exp\left(-\frac{(x-y)^2}{2\sigma^2}\right), \tag{2.4.3}$$

will be used as the dispersal kernel throughout. Finally, for the demographic stage we need to select a growth function. In this section we will investigate the growth function (2.1.1). Now we have everything required to solve the model (2.2.4).

However, this initial value problem cannot be solved analytically, so we will use the numerical method described in Section 2.3. The error cutoff of $\tau = 10^{-7}$, and computational grid size of $\Delta x = \frac{5}{128}$ will be used throughout any numerical computations.

One can now investigate the behaviour of the model where several values of the growth function variable A are considered. The other variables in the problem are chosen to be $\sigma = 0.1$, $\Phi = 0.01$ and $h = 0.1$, where σ_0 is determined from (2.4.2). These values are fixed for this analysis. We first choose a spatio-temporal case with $A < 1$, specifically, $A = 0.75$, see Fig. 2.3. It can be seen that the population density diffuses and decays, going to extinction.

For the very high choice of $A = 7$ (see Fig. 2.5), strong oscillatory behaviour is observed around $x = 0$, however, a traveling wave solution is still observed in this case. This strong oscillatory response is unrealistic for invasive plant species, and therefore we will consider the case $A = 2.5$ (see Fig. 2.4).

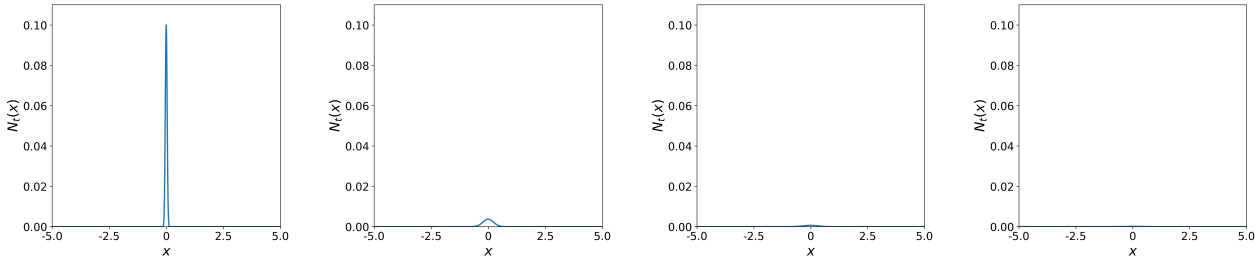

(a) $t = 0$ (b) $t = 5$ (c) $t = 10$ (d) $t = 15$

Figure 2.3: *The propagation of the invasive species for the growth function* (2.1.1) *where* $A = 0.75$. *The other parameters used in computation are* $\sigma = 0.1$, $\Phi = 0.01$, *and* $h = 0.1$. *(a) The initial population density at* $t = 0$ *is given by* (2.4.1). *(b) After some time* $t = 5$, *the population density has started to disperse into the domain. However, due to the choice of* $A = 0.75$, *the population density decays every time the growth function is applied. (c) By the time* $t = 10$, *the population density has been all but eliminated, and (d) for* $t = 15$ *the population density has visually disappeared and is tending to extinction.*

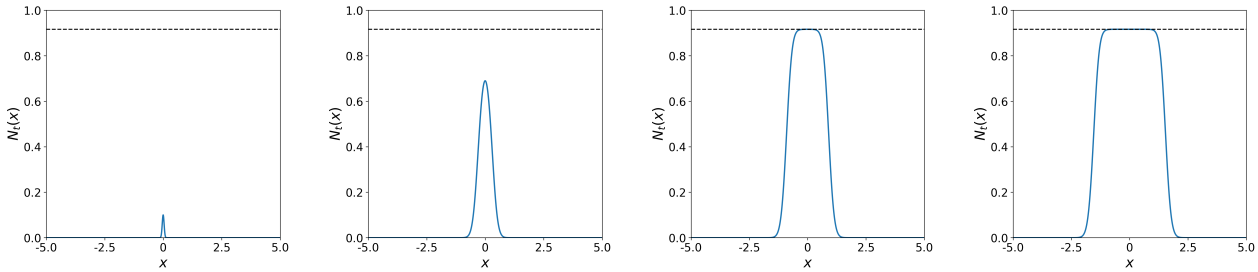

(a) $t = 0$ (b) $t = 5$ (c) $t = 10$ (d) $t = 15$

Figure 2.4: *The propagation of the invasive species for the growth function* (2.1.1) *where* $A = 2.5$, *with the carrying capacity given by* (2.1.2) *(black dashed line). The other parameters are the same as in Fig 2.3. (a) The initial population density at* $t = 0$ *is given by* (2.4.1). *(b) After some time* $t = 5$ *the population density grows and spreads further into the spatial domain. (c) As time continues* $t = 10$, *the population density continues to grow and spread into the domain, reaching the carrying capacity around* $x = 0$. *(d) This process continues* $t = 15$, *and will spread at a constant speed as the time continues (see section 2.11).*

2.5 Allee effect

So far, we have only considered the growth function (2.1.1). However, we may be interested in a case where the population density either increases or decreases depending on the population density. We, therefore, investigate the behaviour of a growth function with Allee effects.

The phenomenon of the Allee effect was first observed in the $1930's$ by Warder Clyde Allee [1]. A species with Allee effect has reduced fitness (reproductive success), and

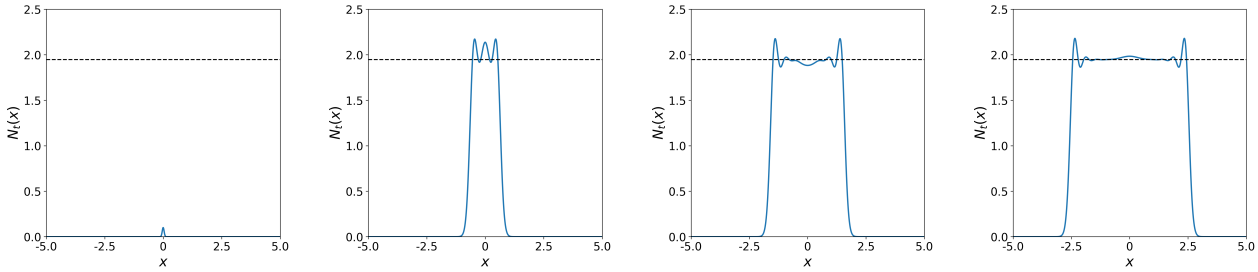

(a) $t = 0$ (b) $t = 5$ (c) $t = 10$ (d) $t = 15$

Figure 2.5: *The propagation of the invasive species for the growth function* (2.1.1) *where* $A = 7.5$*, with the carrying capacity given by* (2.1.2) *(black dashed line). The other parameters are the same as in Fig 2.3. (a) The initial population density at* $t = 0$ *is given by* (2.4.1)*. (b) After some time* $t = 5$ *the population density has reached and exceeded the carrying capacity, and has begun to display oscillatory behaviour. (c) As time continues* $t = 10$ *the population density continues to spread into the domain. The population density around* $x = 0$ *although still displaying oscillatory behaviour begins to dampen out to the carrying capacity (see the behaviour of* $A = 7$ *in Fig. 2.1b). (d) The propagation wave continues invading the domain at a constant rate of spread* $t = 15$*, (see section 2.11).*

therefore, a reduction in the growth rate at low population densities. In [65], Stephens et al. showed that the Allee effect could produce a threshold below which the population could not survive[70, 3]; this case is known as the strong Allee effect. Allee effects that do not give rise to a critical population size are referred to as the weak Allee effects [32, 59]. The Allee effect has not been widely documented in a real-world environment, however, they have been shown to occur in plant species [13], and are believed to be abundant in nature [37].

2.6 Growth Function With Allee effect

Here a growth function with Allee effect is introduced, we first start with an equation for the per capita growth [8],

$$1 + g(N_t) = \frac{\rho N_t}{\xi + N_t^2}, \tag{2.6.1}$$

where $g(N_t)$ is the density-dependent per capita growth function and ρ, $\xi > 0$, $N \geq 0$ and $\rho, \xi, N \in \mathbb{R}$. To convert Eq. (2.6.1) into the form of the growth function compatible

with the model, we use the following difference equation for the population density

$$N_{t+1} - N_t = N_t g(N_t),$$

we then rearrange and substitute $g(N_t)$ from Eq. (2.6.1) to find

$$N_{t+1} = \frac{\rho N_t^2}{\xi + N_t^2}.$$

Using the definition for the first-order difference equation 1.1.5, we can re-write this in the more familiar notation for the growth function,

$$F(N) = \frac{\rho N^2}{\xi + N^2}. \tag{2.6.2}$$

2.7 Survival or Extinction

We now have a suitable growth function exhibiting the strong Allee effect, where the extinction-survival cases can depend on the population density as well as the growth function parameters. Firstly the conditions that lead to extinction and those that lead to survival will be investigated. One is in an unconditional-survival case if $F(N_t) > N_t$, $\forall N_t > 0$, an unconditional-extinction case if $F(N_t) < N_t$, $\forall N_t > 0$ and an extinction-survival case if $\exists N_t > 0$ where $F(N_t) > N_t$ and $\exists N_t > 0$ where $F(N_t) < N_t$. Depending on the choice of ρ and ξ, the new growth function (2.6.2) can lead to either unconditional-extinction or extinction-survival behaviour. To show this, we need to find the equilibrium solutions of (2.6.2), precisely for $N_t = F(N_t)$,

$$N_t = \frac{\rho N_t^2}{\xi + N_t^2}.$$

Rearranging and solving for N_t, one finds $N_t = 0$ is always an equilibrium solution; along with the equilibrium solutions

$$N_t = \frac{\rho \pm \sqrt{\rho^2 - 4\xi}}{2}. \tag{2.7.1}$$

Due to the application to the real world, we are only concerned with real and not complex values. Therefore, we have the condition

$$\rho^2 - 4\xi \geq 0,$$

which is precisely

$$\rho \geq 2\sqrt{\xi}.$$

From this there are three cases to consider, if $\rho < 2\sqrt{\xi}$, (2.7.1) has no real roots, if $\rho = 2\sqrt{\xi}$ (2.7.1) has one real root, and if $\rho > 2\sqrt{\xi}$ (2.7.1) has two real roots. The following condition also holds for any choice of ρ and ξ,

$$\lim_{N_t \to \infty} F(N_t) = \rho, \tag{2.7.2}$$

therefore, for unconditional-extinction it is only necessary that $F(N_t) \neq N_t$, $\forall N_t > 0$, which is precisely the case where $\rho < 2\sqrt{\xi}$; similarly, no such unconditional-survival case exists for any choice of ρ and ξ.

For an extinction-survival case, there only need exist an N_t such that $F(N_t) \geq N_t$; this is because from equation (2.7.2), it is known $F(N_t) < N_t$ always exists. There are two more cases of equation (2.7.1) still to investigate, $\rho = 2\sqrt{\xi}$, and $\rho > 2\sqrt{\xi}$. Firstly for $\rho = 2\sqrt{\xi}$, there is only one real root at $N_t = \frac{\rho}{2}$, which corresponds to $F(\frac{\rho}{2}) = \frac{\rho}{2}$, therefore, this is an extinction-survival case. However, one also has

$$F(N_t) > N_t, \ \forall\, 0 < N_t < \frac{\rho}{2},$$

if one picks $N_t = \frac{\rho}{4}$, where $0 < N_t < \frac{\rho}{2}$, one finds $\xi = \frac{\rho^2}{4}$, substituting this into $F(N_t) = N_t$,

$$F\left(\frac{\rho}{4}\right) = \frac{\rho}{5} < \frac{\rho}{4}.$$

This means the population density does not increase for any choice of N_t, and we have survival only for the point $N_t = \frac{\rho}{2}$. Now investigating $\rho > 2\sqrt{\xi}$, which has two real roots, we are in an extinction-survival case, $F(N_t) = N_t$ at the two roots. Investigating further for $F(N_t) > N$, there needs to exist an N_t such that

$$F(N_t) > N_t, \ \frac{\rho - \sqrt{\rho^2 - 4\xi}}{2} < N < \frac{\rho + \sqrt{\rho^2 - 4\xi}}{2}. \tag{2.7.3}$$

Choosing $N_t = \frac{\rho}{2}$, and substituting this into (2.6.2)

$$F\left(\frac{\rho}{2}\right) = \frac{\rho\left(\frac{\rho}{2}\right)^2}{\xi + \left(\frac{\rho}{2}\right)^2}, \tag{2.7.4}$$

we also know that $\frac{\rho^2}{4} > \xi$, substituting this into (2.7.4) one finds

$$F\left(\frac{\rho}{2}\right) > \frac{\rho}{2},$$

thus, there is a region of growth for the case when $\rho > 2\sqrt{\xi}$.

In summary, unconditional-extinction behaviour occurs for $\rho < 2\sqrt{\xi}$, with a single equilibrium solution at $\bar{N}_1 = 0$. Extinction-survival behaviour for $\rho > 2\sqrt{\xi}$ with three equilibrium solutions at $\bar{N}_1 = 0$, $\bar{N}_2 = \frac{\rho - \sqrt{\rho^2 - 4\xi}}{2}$, and $\bar{N}_3 = \frac{\rho + \sqrt{\rho^2 - 4\xi}}{2}$, and extinction-survival behaviour for $\rho = 2\sqrt{\xi}$ with two equilibrium solutions at $\bar{N}_0 = 0$ and $\bar{N}_{2,3} = \frac{\rho}{2}$.

2.8 Stability of Equilibrium Solutions

To gain further understanding of the behaviour of the growth function (2.6.2), the stability of the equilibrium solutions needs to be investigated. To do so, first the derivative of the

growth function (2.6.2) needs to be computed,

$$F'(N_t) = \frac{2\rho\xi N_t}{(\xi + N_t^2)^2}.$$

From definition 1.1, $|F'(\bar{N})|$ can be solved in order to analyse the behaviour of the equilibrium solutions. For the equilibrium solution $\bar{N}_1 = 0$,

$$|F'(0)| = 0 < 1,$$

and therefore, $\bar{N}_1 = 0$ is a locally asymptotically stable equilibrium solution. For the equilibrium solution $\bar{N}_3 = \frac{\rho+\sqrt{\rho^2-4\xi}}{2}$ when $\rho > 2\sqrt{\xi}$,

$$\left| F'\left(\frac{\rho + \sqrt{\rho^2 - 4\xi}}{2}\right)\right| = \left|1 - \frac{\sqrt{\rho^2 - 4\xi}}{\rho}\right|,$$

we also know $\rho, \xi > 0$, and $\rho > 2\sqrt{\xi}$, therefore,

$$\left| F'\left(\frac{\rho + \sqrt{\rho^2 - 4\xi}}{2}\right)\right| < 1.$$

Specifically,

$$0 < \left|1 - \frac{\sqrt{\rho^2 - 4\xi}}{\rho}\right| < 1;$$

thus, the equilibrium solution $\bar{N}_3 = \frac{\rho+\sqrt{\rho^2-4\xi}}{2}$ is locally asymptotically stable with monotonic convergence. For the equilibrium solution $\bar{N}_2 = \frac{\rho-\sqrt{\rho^2-4\xi}}{2}$ when $\rho > 2\sqrt{\xi}$,

$$\left| F'\left(\frac{\rho - \sqrt{\rho^2 - 4\xi}}{2}\right)\right| = \left|1 + \frac{\sqrt{\rho^2 - 4\xi}}{\rho}\right|,$$

we also know $\rho, \xi > 0$, and $\rho > 2\sqrt{\xi}$, therefore,

$$\left| F'\left(\frac{\rho - \sqrt{\rho^2 - 4\xi}}{2}\right)\right| > 1.$$

Specifically

$$1 + \frac{\sqrt{\rho^2 - 4\xi}}{\rho} > 1,$$

thus, the equilibrium solution $\bar{N} = \frac{\rho - \sqrt{\rho^2 - 4\xi}}{2}$ is monotonically unstable.

For the equilibrium point $\bar{N}_{2,3} = \frac{\rho}{2}$, $\rho = 2\sqrt{\xi}$, and

$$F'(\frac{\rho}{2}) = 1;$$

in order to deal with this case the following definitions [52] are required.

Definition 2.2. If $F'(\bar{N}) = 1$ then:

I. If $F''(\bar{N}) \neq 0$, $\bar{N}$ is asymptotically semi-stable from the left if $F''(\bar{N}) > 0$, and is asymptotically semi-stable from the right if $F''(\bar{N}) < 0$

II. If $F''(\bar{N}) = 0$ and $F'''(\bar{N}) < 0$, $\bar{N}$ is asymptotically stable

II. If $F''(\bar{N}) = 0$ and $F'''(\bar{N}) > 0$, $\bar{N}$ is unstable

Therefore, the second derivative is calculated

$$F''(N_t) = \frac{2\xi\rho(\xi - 3N_t^2)}{(\xi + N_t^2)^3},$$

for the case $\bar{N} = \frac{\rho}{2}$,

$$F''(\frac{\rho}{2}) = -\frac{2}{\rho} \neq 0.$$

Since $\rho > 0$, we have $F''(\frac{\rho}{2}) < 0$, and therefore, $\bar{N}_{2,3} = \frac{\rho}{2}$ is asymptotically semi-stable from the right.

2.9 A Non-Spatial Model With The Allee Growth Function

We will now investigate the speed with which the population density modelled by the difference equation with Allee growth converges to its steady state. Using the Allee growth function (2.6.2) for the model, in the same way as the analysis of the non-spatial model

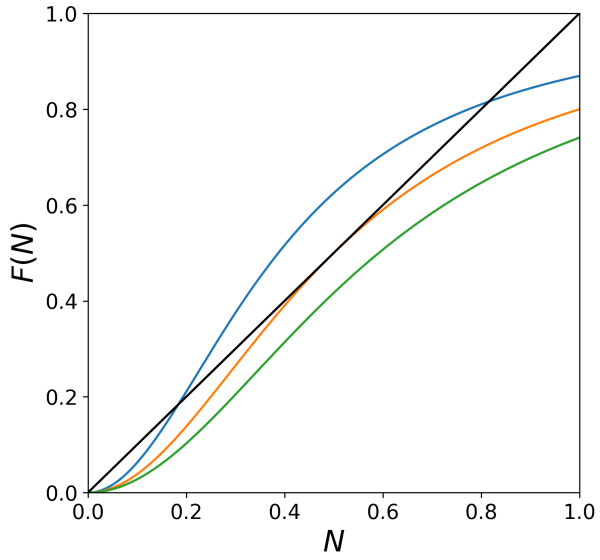

Figure 2.6: *The Allee growth function* (2.6.2) *with* $\rho = 1$*, and various values of* ξ*, where the equilibrium solutions are given by the intersection with the line* $N = F(N)$ *(solid black line). For* $\xi = 0.15$ *(solid blue line),* $\xi = 0.25$ *(solid orange line), and* $\xi = 0.35$ *(solid green line).*

for the growth function (2.1.1) conducted in section 2.1, the behaviour of how fast the population density approaches a stable equilibrium solution is investigated. Firstly, one notes that the shape of the model is unique up to linear scaling. To find the relationship between ρ and ξ under this scaling,

$$\alpha\left(\frac{\rho_1 N_t^2}{\xi_1 + N_t^2}\right) = \frac{\rho_2(\alpha N_t)^2}{\xi_2 + (\alpha N_t)^2},$$

by expanding and equating powers of N_t, the following relationships hold

$$\rho_2 = \alpha\rho_1, \tag{2.9.1}$$

and

$$\xi_2 = \alpha^2\xi_1. \tag{2.9.2}$$

In Fig. 2.6 and Fig. 2.7 one can see a representative example of the behaviour of the Allee growth function (2.6.2) for $\rho = 1$. For $\xi = 0.15$ Fig. 2.7a, $\rho < 2\sqrt{\xi}$ and, therefore, the only equilibrium solution is the stable equilibrium solution $\bar{N}_1 = 0$. In this case, the

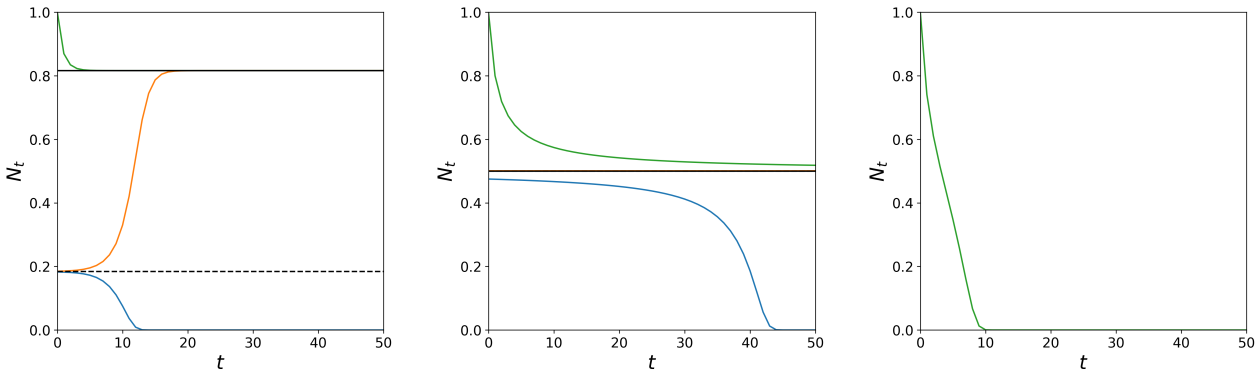

(a) $\xi = 0.15$ (b) $\xi = 0.25$ (c) $\xi = 0.35$

Figure 2.7: *The population density over time N_t given by the model* (1.1.5) *for various values of ξ, and initial population density N_0. (a) The growth parameter $\xi = 0.15$, the stable equilibrium solutions are given by the black solid line and $N_t = 0$. The unstable equilibrium solution is given by the black dashed line. (b) The growth parameter $\xi = 0.25$, the semi-stable equilibrium solution is given by the black solid line, and the stable equilibrium solution $N_t = 0$. (c) The growth parameter $\xi = 0.35$ the stable equilibrium solution is given by $N_t = 0$. See the text for full details.*

population density decays to extinction for any choice of initial population density N_0. When $\xi = 0.25$ (Fig. 2.7b), $\rho = 2\sqrt{\xi}$, in this case, there exist two equilibrium solutions the stable equilibrium solution $\bar{N}_1 = 0$, and the semi-stable equilibrium solution $\bar{N}_2 = \frac{\rho}{2} = 0.5$. If $N_0 \geq 0.5$, the population density will tend towards $\bar{N}_2$, and if $N_0 < 0.5$, the population density will tend towards $\bar{N}_1$. In the final choice of the growth parameter $\xi = 0.35$, Fig. 2.7c, $\rho > 2\sqrt{\xi}$ there are three equilibrium solutions the stable equilibrium solutions, $\bar{N}_1 = 0$ and $\bar{N}_3 = \frac{\rho+\sqrt{\rho^2-4\xi}}{2}$, and the unstable equilibrium solution $\bar{N}_2 = \frac{\rho-\sqrt{\rho^2-4\xi}}{2}$. If $N_0 < \bar{N}_2$ the population density tends to $\bar{N}_1$ over time, if $N_0 = \bar{N}_2$ the population density remains stable at $N_t = \bar{N}_t$ over time, and if $N_0 > \bar{N}_2$ the population density tends to $\bar{N}_3$ over time.

2.10 Spatio-Temporal Case

The spatio-temporal case with the growth function with Allee effects (2.6.2) will now be investigated. Due to the nature of the Allee growth function where negative growth can occur, there are three cases of behaviour that can be observed. The case that occurs

depends on the growth function parameters, the dispersal kernel parameters, and the initial condition. The first case is the survival case where over time the population density will tend towards the carrying capacity and will spread further into the spatial domain over time (see Fig. 2.8).

The second case is the extinction case where the maximum initial population density is above the unstable equilibrium point $\bar{N}_2$ but dispersal drives the population to extinction. This occurs because the strength of the dispersal kernel is greater than the growth of the population density, such that at some time after dispersal the maximum population density is now below the unstable equilibrium point $\bar{N}_2$ where negative growth now occurs everywhere in the spatial domain. This leads to the population density eventually going to extinction (see Fig. 2.9). This case is interesting as, if the dispersal were weaker, then we could be in first survival case.

The third case is the extinction case where the maximum initial population density is below the unstable equilibrium point $\bar{N}_2$. In this case, no matter the strength of the dispersal the population density experiences negative growth everywhere in the spatial domain, meaning the population density is guaranteed to go to extinction over time (see Fig. 2.10).

To explore these cases of behaviour further, we will investigate a range of growth function parameters $\rho \in (0, 1]$, and $\xi \in (0, 0.05]$, using the Gaussian dispersal kernel (2.4.3) where $\sigma = 0.1$, and the initial condition (2.4.1) where $\Phi = 0.01$, and $h = 0.1$. In Fig. 2.11a, the values of (ξ, ρ) that lead to extinction or survival are denoted by the grey solid region and black solid region, respectively. The white solid region denotes where complex solutions emerge for which we disregard the solution. In Fig. 2.11b, the values of (ξ, ρ) that go extinct in the spatio-temporal case but survive in the non-spatial case with an initial population density $N_0 = 0.1$, equal to the maximum initial population density in the spatio-temporal case $h = 0.1$ are shown. These values of (ξ, ρ) are precisely those that have case two behaviour; the maximum population density initially starts above the unstable equilibrium $\bar{N}_2$. However, in the spatio-temporal case, due to dispersal the total

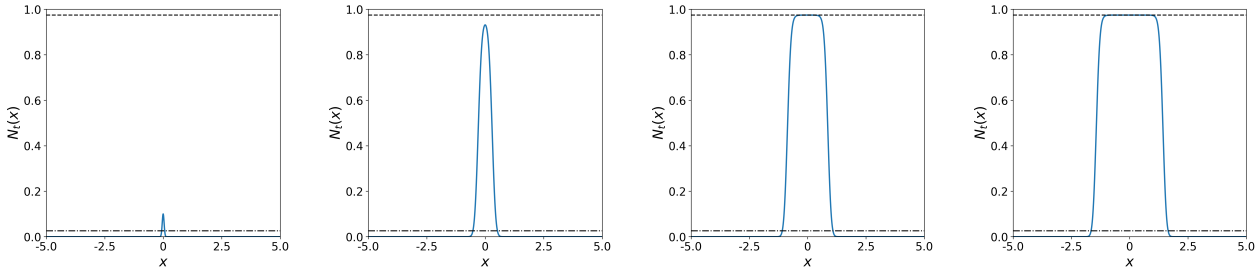

(a) $t = 0$ (b) $t = 5$ (c) $t = 10$ (d) $t = 15$

Figure 2.8: *The propagation of the invasive species using the model* (2.2.4) *with the initial condition* (2.4.1)*, dispersal kernel* (2.4.3)*, and the growth function* (2.6.2)*, where* $h = 0.1$*,* $\sigma = 0.1$*,* $\rho = 1$*, and* $\xi = 0.025$*. The non-spatial model* (1.1.5) *has the stable equilibrium solution* $\bar{N}_1 = 0$*, unstable equilibrium solution* $\bar{N}_2 = \frac{\rho - \sqrt{\rho^2 - 4\xi}}{2}$ *(black dash-dotted line), and stable equilibrium solution* $\bar{N}_3 = \frac{\rho - \sqrt{\rho^2 - 4\xi}}{2}$*.*

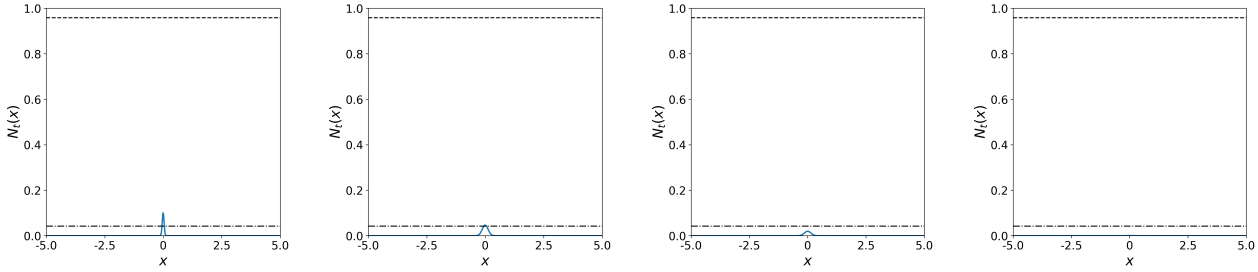

(a) $t = 0$ (b) $t = 2$ (c) $t = 4$ (d) $t = 6$

Figure 2.9: *The propagation of the invasive species using the model* (2.2.4) *with the initial condition* (2.4.1)*, dispersal kernel* (2.4.3)*, and the growth function* (2.6.2)*, where* $h = 0.1$*,* $\sigma = 0.1$*,* $\rho = 1$*,* $\xi = 0.04$*. The non-spatial model* (1.1.5) *has the stable equilibrium solution* $\bar{N}_1 = 0$*, unstable equilibrium solution* $\bar{N}_2 = \frac{\rho - \sqrt{\rho^2 - 4\xi}}{2}$ *(black dash-dotted line), and stable equilibrium solution* $\bar{N}_3 = \frac{\rho - \sqrt{\rho^2 - 4\xi}}{2}$*.*

invaded area decreases, and the species goes to extinction. In the non-spatial case, the population density tends towards the carrying capacity $\bar{N}_3$ and survival.

2.11 Propagation Speed

This section is predominantly based on the work [21].

So far, how the population density evolves in the domain and the extinction-survival cases of behaviour have been investigated. The other essential property we want to measure and understand is the propagation speed. In order to effectively control, manage,

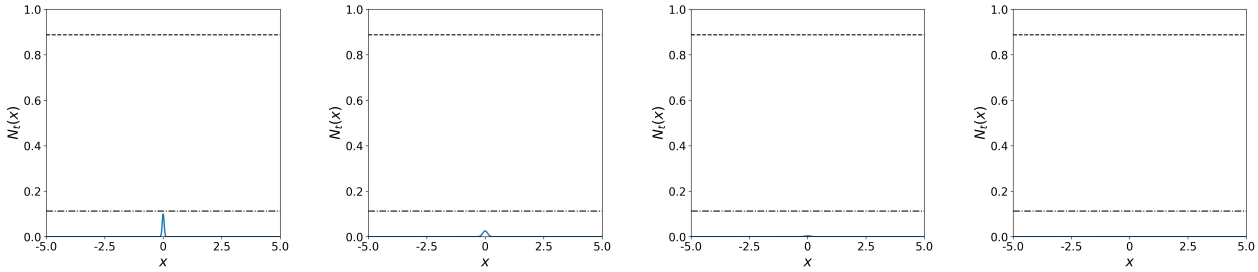

(a) $t = 0$ (b) $t = 1$ (c) $t = 2$ (d) $t = 3$

Figure 2.10: *The propagation of the invasive species using the model* (2.2.4) *with the initial condition* (2.4.1)*, dispersal kernel* (2.4.3)*, and the growth function* (2.6.2)*, where* $h = 0.1$*,* $\sigma = 0.1$*,* $\rho = 1$*,* $\xi = 0.1$*. The non-spatial model* (1.1.5) *has the stable equilibrium solution* $\bar{N}_1 = 0$*, unstable equilibrium solution* $\bar{N}_2 = \frac{\rho - \sqrt{\rho^2 - 4\xi}}{2}$ *(black dash-dotted line), and stable equilibrium solution* $\bar{N}_3 = \frac{\rho - \sqrt{\rho^2 - 4\xi}}{2}$*.*

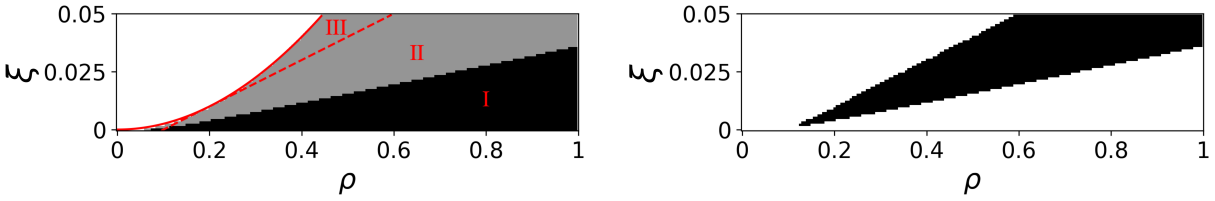

(a) (b)

Figure 2.11: *The extinction-survival cases for the Allee growth function* (2.6.2) *in the spatio-temporal model* (2.2.4)*, with the initial condition* (2.4.1) *where* $\Phi = 0.01$*,* $h = 0.1$*, and Gaussian dispersal kernel* (2.4.3) *where* $\sigma = 0.1$*. (a) The cases of* (ξ, ρ) *where extinction occurs (grey solid region) and survival occurs (black solid region). The equation* $\rho = 2\sqrt{\xi}$ *is denoted by the red solid line, and* $\bar{N}_2 = 0.1$ *is denoted by the red dashed line. (b) The cases of* (ξ, ρ) *where extinction occurs in the spatio-temporal model where survival occurs in the temporal model (black solid region).*

and predict the future distribution of invasive plant species, it is essential to understand the propagation speed of the invasive species accurately. The problem of how organisms spread in the spatial domain has long been a topic of interest [4]. The propagation speed of traveling wave solutions, once the long time behaviour has become established, in the homogeneous landscape has been investigated both analytically and numerically for a range of dispersal kernels and growth functions [27, 34, 42, 63, 71]. See section 1.1 for a general introduction of the propagation speed.

In this section the propagation speed of the model (2.2.4) will be investigated for the Gaussian dispersal kernel (2.4.3), Ricker growth function (2.1.1), and initial condition

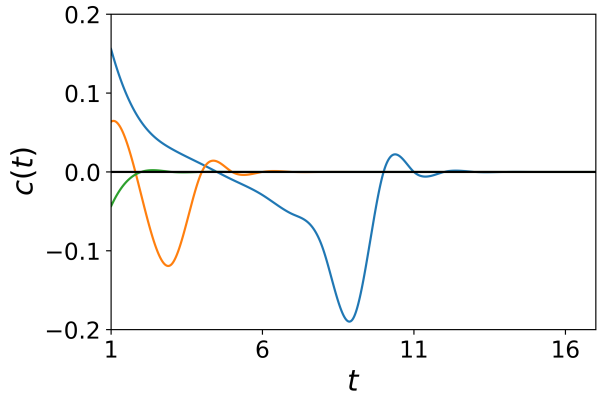

Figure 2.12: *The propagation speed $c(t)$, with the Ricker growth function* (2.1.1) *where* $A = 0.75 < 1$, *for various choices of* $\tilde{N}$. *The parameters in the problem are* $\Phi = 0.01$, $h = 0.1$, $\sigma = 0.1$. *The choices of the detection threshold are,* $\tilde{N} = 0.01h$ *(blue solid line),* $\tilde{N} = 0.1h$ *(orange solid line), and* $\tilde{N} = 0.5h$ *(green solid line).*

(2.4.1). The case of $A < 1$, where we are in an extinction case will be investigated first. This means that as long as the detection threshold $\tilde{N}$ is sufficiently low, i.e. below the maximum initial population density h, the propagation speed will initially be non-zero and then, after some time, go to zero due to extinction. An example of this can be seen in Fig. 2.12 where $A = 0.75$. It can be seen for the choices of detection threshold $\tilde{N} = 0.01h$, $\tilde{N} = 0.1h$, and $\tilde{N} = 0.5h$ (blue, orange, and green, solid lines respectively) that a non-zero propagation speed either positive or negative is observed. Then after some time the propagation speed tends towards zero, as the maximum population density decreases below the detection threshold. The higher the detection threshold the faster the propagation speed goes to zero, as it is closer to the initial maximum population density.

The survival case of behaviour when the population becomes established, i.e. $A > 1$, will now be investigated. For the Ricker growth function with the Gaussian dispersal kernel one is unable to obtain exact solutions for the propagation speed. However, we are interested in modeling the invasion of plant species and, therefore, in the propagation at low densities. In order to obtain the propagation speed, linearization of the growth function is required. The Ricker growth function (2.1.1) can be approximated by a linear

growth function with the same growth factor A,

$$F(N) = AN. \tag{2.11.1}$$

The model (2.2.4) with the linear growth function (2.11.1) and Gaussian dispersal kernel (2.4.3) then becomes,

$$N_t(x) = \int_\Omega \frac{AN_{t-1}(y)}{\sqrt{2\pi\sigma^2}} \exp\left(-\frac{|x-y|^2}{2\sigma^2}\right) dy,$$

along with the initial condition (2.4.1) an exact solution for the propagation speed can now be found everywhere in Ω. Since a convolution of a Gaussian dispersal kernel with the initial condition (2.4.1) is itself a Gaussian function (*e.g.*, see [43]), the exact solution for $t > 0$ is given by

$$N_t(x) = \frac{\Phi A^t}{\sqrt{2\pi(\sigma_0^2 + t\sigma^2)}} \exp\left(-\frac{x^2}{2(\sigma_0^2 + t\sigma^2)}\right). \tag{2.11.2}$$

By rearranging (2.11.2) for $x_t(\tilde{N})$ one finds,

$$x_t(\tilde{N}) = \sqrt{2(\sigma_0^2 + t\sigma^2) \ln\left(\frac{\Phi A^t}{\tilde{N}\sqrt{2\pi(\sigma_0^2 + t\sigma^2)}}\right)}, \tag{2.11.3}$$

where the propagation speed is given by,

$$c(t, \tilde{N}) = x_t(\tilde{N}) - x_{t-1}(\tilde{N}). \tag{2.11.4}$$

After an initial transition period, when a traveling wave front has been formed (see Fig. 2.13), the propagation speed tends towards a constant rate. The constant long time propagation speed c^* can be calculated in the following way [40] by taking $t \to \infty$,

$$c^* = \lim_{t\to\infty} \frac{x_t(\tilde{N})}{t} = \lim_{t\to\infty} \frac{\sqrt{2(\sigma_0^2 + t\sigma^2) \ln\left(\frac{\Phi A^t}{\tilde{N}\sqrt{2\pi(\sigma_0^2+t\sigma^2)}}\right)}}{t} = \sqrt{2\sigma^2 \ln(A)}. \tag{2.11.5}$$

As one can see, the long time propagation speed c^* does not depend on the values of the initial condition Φ, and σ, or of the detection threshold $\tilde{N}$. Furthermore, the asymptotic speed (2.11.5) remains the same when the model with the linear growth function (2.11.1) is compared to the model with the growth function (2.1.1).

The choice of a detection threshold in Eq. (2.11.4) requires careful consideration: when the linearly determined propagation speed is evaluated from Eq. (2.11.4) in the asymptotic regime (2.11.5) the threshold value should be taken as low as possible to provide an accurate linear approximation (2.11.1) of the growth function Eq. (2.1.1). In the direct computation of the propagation speed, the above requirement can be achieved by setting $\tilde{N} = \alpha \ln(A)$, where $\alpha \in \mathbb{R}$ and $\alpha \ll 1$. Meanwhile, the definition of a 'low threshold' is not clear in a transient regime when a travelling wave has not approached the carrying capacity yet. It can be convenient to relate the threshold density $\tilde{N}$ to the population size at time $t = 0$. Namely, the threshold value is now chosen as $\tilde{N} = \alpha h$, where the h is the height of the initial population density (2.4.2).

If accurate information about the initial population distribution (2.4.1) is available, then the requirement of a low threshold holds for $\alpha \ll 1$. However, it has been demonstrated in [53] that highly aggregated spatial distributions appearing at early stages of biological invasion may be detected with very low accuracy resulting in uncertainty when the total population size is evaluated. Therefore, all possible values of the detection threshold $0 < \tilde{N} \leq \ln(N)$ will be considered.

An example of the propagation speed is shown in Fig. 2.13a, where we compare $c(t)$ obtained from (2.11.3)–(2.11.4) with the propagation speed obtained by direct computation for the linear growth function (2.11.1). It can be seen from the figure that the result of the direct computation is in very good agreement with the analytical result, hence the accuracy of our computational method is confirmed. We then compute the propagation speed for the growth function (2.1.1), as the analytical solution is not available in the latter case. The propagation speed obtained for the Ricker function (2.1.1) very slightly differs from $c(t)$ obtained for the linear growth (2.11.1), demonstrating that the linear

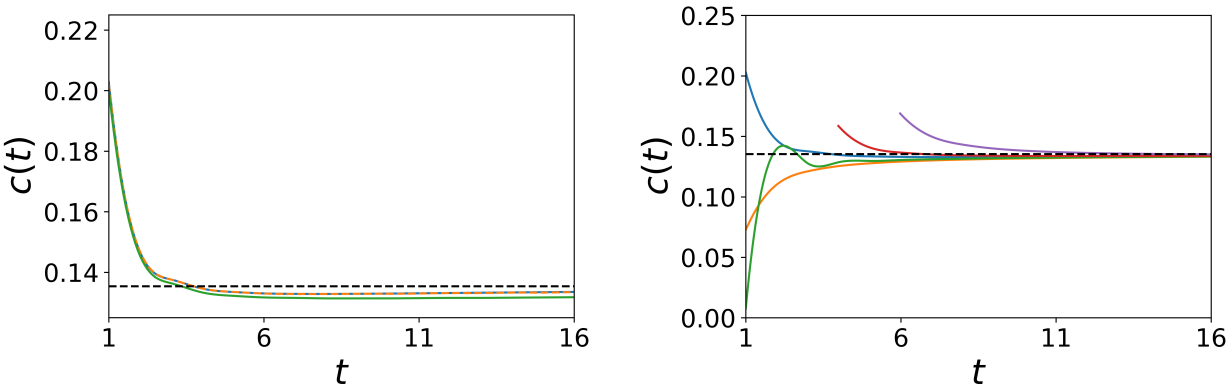

(a) (b)

Figure 2.13: *The propagation speed $c(t)$. The function $c(t)$ converges to the asymptotic propagation speed* (2.11.5) *(black dashed line in the figure), yet its behaviour at the short-time scale depends on the detection threshold. (a) Comparison between the analytical result* (2.11.3)–(2.11.4) *(blue solid line), the propagation speed obtained by direct computation for the linear growth function* (2.11.1) *(orange dashed line), and the growth function* (2.1.1) *(green solid line). The parameters are $h = 0.1$, $\Phi = 0.01$, $\tilde{N} = 0.01h$, $A = 2.5$, and $\sigma = 0.1$. (b) The propagation speed* (2.11.3)–(2.11.4) *for various choices of the detection threshold: $\tilde{N} = 0.01h$ (blue solid line), $\tilde{N} = 0.5h$ (orange solid line), $\tilde{N} = 0.9h$ (green solid line), $\tilde{N} = 2.5h$ (red solid line), $\tilde{N} = \ln(A)$ (purple solid line). The parameters are the same as in Fig. 2.13a.*

growth is a good approximation of the growth at small densities in a transient regime before the establishment of a monotone travelling wave.

One result that can be seen from Fig. 2.13a is that the invasive species decelerate before the propagation speed converges to its asymptotic value given by (2.11.5). However, the deceleration regime is not common and depends on the choice of the detection threshold $\tilde{N}$. Several examples of the propagation speed are presented in Fig. 2.13b where we vary the value of $\tilde{N}$. As the threshold density increases, the propagation speed $c(t)$ becomes first non-monotonic and then it decreases monotonically for the choice of the threshold density $\tilde{N} < h$. It is important to note that in the extreme case, $\tilde{N} > h$ detection of the high density $\tilde{N}$ only becomes possible at times $t > 3$, and we cannot compute the propagation speed at shorter times; see Fig. 2.13b.

The propagation speed either starts above or below the detection threshold once it has been detected at the detection threshold, then after some time, it tends towards the long-term analytical propagation speed c^* (2.11.5). In other words, the population density

undergoes short-term, transient, behaviour and then, after some undetermined amount of time, forms a monotone travelling wave and proceeds to invade the domain at a constant rate. Once the species is in the long-term behaviour case, the rate at which it propagates throughout the dispersal domain is predictable and changes monotonically. The long-term behaviour only depends on the dispersal parameter σ and the growth function parameter A. Even if there is some uncertainty around these parameters, a good estimation of the propagation speed at the long-term behaviour can be provided. Unlike the short-term behaviour where a small uncertainty in the detection threshold $\tilde{N}$ can lead to very different behaviour of the propagation speed. It is, therefore, useful for management and monitoring purposes to know how long this unpredictable region of transient behaviour lasts.

In order to answer this question the concept of the transition time will be introduced. The transition time t_{tran} is the time taken to converge to the constant propagation speed c^* given by (2.11.5) with certain accuracy ϵ. We have

$$\mid c(t, \tilde{N}) - c^* \mid < \epsilon, \quad \forall t \geq t_{tran}, \tag{2.11.6}$$

where the accuracy ϵ can be thought of in terms of the asymptotic speed, $\epsilon = kc^*$ with $k \ll 1$. The transition time is then defined in computation as the minimum time for which the condition (2.11.6) holds. It is immediately clear from (2.11.6) that the transition time depends on the detection threshold density $\tilde{N}$. One example of the transition time as a function of the detection threshold is presented in Fig. 2.14a. It can be readily seen from the figure that the transition time against the detection threshold is non-monotonic; for very small $\tilde{N}$ it is initially high and then proceeds to decrease with increasing $\tilde{N}$. Then after $\tilde{N} \approx 2h$, the transition time increases again. Overall, the transition time changes significantly in the graph as the detection threshold varies, and one, therefore, cannot predict or compare the propagation of the invasive species at short times before it transitions to the stable long-term behaviour. We also note that the transition time

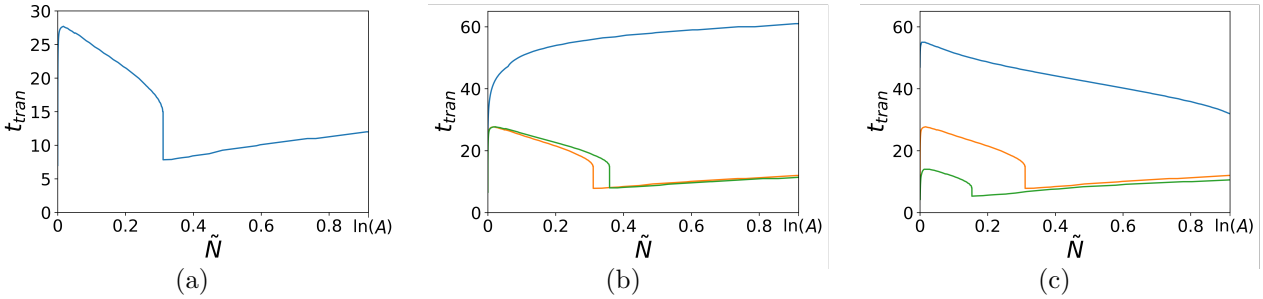

Figure 2.14: *The transition time t_{tran} given by* (2.11.6) *against the detection threshold $\tilde{N}$. (a) The transition time computed for the choice of the parameters $\Phi = 0.01$, $A = 2.5$, $\epsilon = 0.01c^*$ $h = 0.1$, and $\sigma = 0.1$. The transition time shows non-monotone behaviour as the detection threshold increases. (b) The transition time $t_{tran}(\tilde{N})$ for various choices of the height h of the initial population density: $h = 0.01$ (blue solid line), $h = 0.1$ (orange solid line), $h = 1$ (green solid line). (c) Various choices of the accuracy ϵ in the definition* (2.11.6)*: $\epsilon = 0.005$ (blue solid line), $\epsilon = 0.01$ (orange solid line), $\epsilon = 0.02$ (green solid line). The other parameters in Fig. 2.14b-c are the same as in Fig. 2.14a.*

depends on the height of the initial population h and the accuracy ϵ as demonstrated in Fig. 2.14b and Fig. 2.14c, respectively.

This means that not only is the transient propagation speed unpredictable, but so too is the length of the transition time. With all of this uncertainty around the short-term behaviour, it is important to try and work out how significant an impact it has on the short-term behaviour has on the overall spatial distribution of the population density. Therefore, one may ask: does the propagation regime at the short time scale have any lasting impact on the distance d the invasive species propagates over a given time T from the location where it was first detected?

Let the population density $\tilde{N}$ be detected at x_0 at time $t = 0$ and the same population density be observed at the location x_T at time $t = T$. Finding the distance between those points requires integration of the propagation speed,

$$d = \int_{t=0}^{t=T} c(t)dt = x(T) - x(0).$$

In the model with discrete time, the integral is replaced by the sum $d = \sum_{t=1}^{t=T} c(t)\delta t$, where

c is the propagation speed given by (2.11.4) and $t \in \mathbb{N}$. Substituting c from (2.11.4), rearranging terms and taking $\delta t = 1$ gives

$$d = \sum_{t=1}^{T}(x_t(\tilde{N}) - x_{t-1}(\tilde{N})) = x_T(\tilde{N}) - x_0(\tilde{N}) = \\ \sqrt{2(\sigma_0^2 + T\sigma^2)\ln\left(\frac{\Phi A^T}{\tilde{N}\sqrt{2\pi(\sigma_0^2 + T\sigma^2)}}\right)} - \sqrt{2\sigma_0^2 \ln\left(\frac{\Phi}{\tilde{N}\sqrt{2\pi\sigma_0^2}}\right)}. \tag{2.11.7}$$

The distance d the invasive species goes over a given time T from the point x_0 is shown in Fig. 2.15. The comparison between the distance computed from the equation (2.11.7) and the direct numerical simulation with the growth function (2.1.1) is presented in Fig. 2.15a, where the results are in very good agreement at the short times; cf. Fig. 2.13a. The distance covered by the invasive species travels over a given time T depends on the threshold density as shown in Fig. 2.15b and the graphs $d(\tilde{N})$ are shown in Fig. 2.15c for selected times T. We note from Fig. 2.15c that the function $d(\tilde{N})$ given by (2.11.7) is a monotone decreasing function of the threshold density $\tilde{N}$. In other words, the graph $d(T)$ obtained for $\tilde{N} = 0.01h$ (*i.e.*, the smallest value of the threshold density used) is the upper bound for the other graphs in Fig. 2.15b, and this result confirms the importance of taking a detection threshold density as small as possible when evaluation of the size of a spatial domain invaded over a given period of time is made.

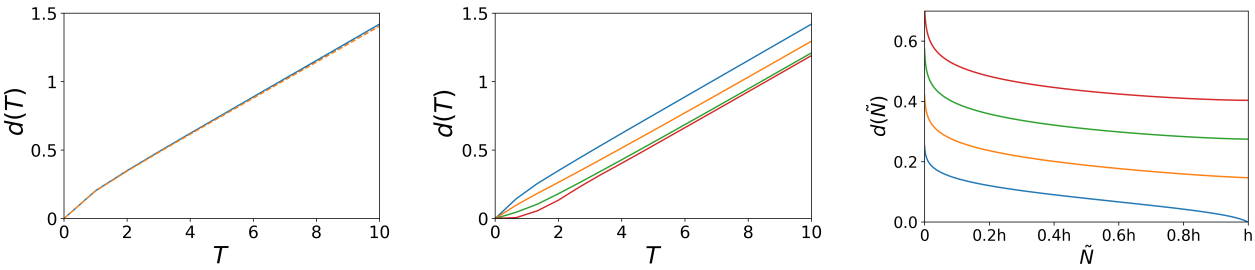

(a) (b) (c)

Figure 2.15: *The distance d covered by the invasive species over the time T from the point x_0 where it has been detected at time $t = 0$. (a) The comparison between the distance d computed from the equation* (2.11.7) *(blue solid line) and by the direct numerical simulation with the growth function* (2.1.1) *(orange dashed line). The parameters are $\Phi = 0.01$, $A = 2.5$, $\epsilon = 0.01c^*$, $h = 0.1$, $\sigma = 0.1$, and $\tilde{N} = 0.01h$. (b) The distance* (2.11.7) *for various values of the detection threshold: $\tilde{N} = 0.01h$ (blue solid line), $\tilde{N} = 0.1h$. (orange solid line), $\tilde{N} = 0.5h$ (green solid line), and $\tilde{N} = 0.9h$ (red solid line). (c) The distance $d(\tilde{N})$ for $\tilde{N} \in (0, h]$ calculated for $T = 1$ (blue solid line), $T = 2$ (orange solid line), $T = 3$ (green solid line), and $T = 4$ (red solid line). The other parameters are the same as in Fig. 2.15a.*

2.12 Summary

In this chapter, a spatio-temporal, discrete time, continuous space, integro-difference equation was introduced to model invasive plant species. Throughout this chapter, the aim was to analyse the behaviour of the population density in a homogeneous landscape. For the demographic stage, the Ricker growth function Eq. (2.1.1) and an Allee growth function Eq. (2.6.2) were investigated. The Ricker growth function has positive growth for any non-zero population density, and was chosen from an ecological perspective to represent a species in a favourable habitat, where an abundance of resources are available for the species to grow without being impeded up to the carrying capacity. The Allee growth function was chosen to represent a different ecological situation where there is negative population density growth for small population densities; representing negative environmental conditions that can impede the initial stages of establishment, i.e. competition. The Gaussian dispersal kernel (2.4.3) was used for the dispersal stage. The model for the population density was investigated both analytically and numerically. The fast Fourier transform algorithm was used for the numerical method, and the error of the numerical method was investigated in section 2.3. In the case of the Ricker growth function,

extinction-survival behaviour occurred. The survival of the species depends only on the growth function parameter and not the size of the non-zero initial population density or the dispersal parameter (see Fig. 2.3 and Fig. 2.4). Where for the Allee growth function, the cases of extinction or survival depend on both the initial condition and the dispersal parameter (see Fig. 2.11). If a species has Allee growth, it is possible to eradicate the species from the domain by reducing the local population density below the Allee threshold, without having to remove all of the population density of the species, which is the case for the Ricker growth function.

Along with the extinction-survival cases of the species' behaviour, another important property, the propagation speed, was investigated for the Ricker growth function in section 2.11. The constant long-time propagation speed 2.11.5 is a well-known result; however, here, the aim of this section was to investigate the short-time behaviour of the propagation speed as it transitioned from the initial condition to the long-time constant speed and how it depends on the detection threshold. The early stage of the invasive spread has not received a lot of attention in the literature and it is often neglected by practitioners as it is assumed that the invasive species spreads out at the long-time scale regime from the very beginning of the invasion [73]. Our results demonstrate, even here in the homogeneous environment, the propagation speed during the transition period can behave very differently to the long-time behavior (see Fig. 2.13). We also observe that the propagation speed (see Fig. 2.12) and the transition time (see Fig. 2.14) behave non-monotonically with respect to the detection threshold. This makes the prediction of the propagation speed at the short time scale and how long a period of time the transition time lasts very difficult. In particular the transition time can last for several generations (see Fig. 2.14). Long transition times suggest that assumptions about immediate establishment of the asymptotic regime of invasion need further investigation and the transition regime cannot be neglected. For a given choice of the detection threshold, accelerating and decelerating waves can be observed during the transition period, which could lead to false assumptions / predictions about the long-time behaviour of a given species in a habitat. Therefore,

this could lead to an incorrect level of priority given to management and control methods of the given species. However, the distance the species spreads over time was also investigated; the results are far more predictable with respect to the detection threshold, and the choice of detection threshold did not make a significant difference to the overall distance reached by the species (see Fig. 2.15). From an ecological perspective this means that although the behaviour of the species during the transition time, and the length of the transition time may be hard to predict and are non-monotone, which can lead to a number of management and control issues, once the species has transitioned to the long-term behaviour and continues to propagate in the domain, the choice of the detection threshold does not have a significant effect on the overall behaviour.

In Chapter 3, we investigate how the spatio-temporal behaviour observed in this chapter changes when a spatial heterogeneity is introduced into the model.

Chapter 3

Propagation of Invasive Waves in the Heterogeneous Landscape

In Chapter 2 a model of how invasive plant species growth and propagate in the homogeneous landscape was introduced. However, in the real world rarely is anything as simplistic, and for any given area many and varied landscape heterogeneities exist. As discussed in Chapter 1, first a simple mathematical model is introduced and then additional complexities are incorporated into the model to provide a more realistic representation of the real world. In any one landscape a variety of different naturally occurring and constructed landscape heterogeneities can exist. For example it has been shown that a landscape with many different heterogeneities, such as rivers, roads, construction distribution centers, and other buildings can lead to the formation of a patchy distribution of invasive species [64].

The aim of the investigation is to understand whether roads can always be thought of as corridors to facilitate propagation of the invasive species. The rate of spatial spread of the alien species is a quantity of high theoretical and practical importance, and it has been a focus of numerous studies [4, 15, 26, 28, 34, 41]. In England, the total area of woodland both publicly and privately owned as of 2020, is estimated to be 1,300,000 ha [17], and there are currently plans to increase this area over the coming years significantly. As part

of the government's 25-year environment plan, they plan to plant an additional 180,000 ha of woodland in England by 2042 [22]. Although this has significant environmental benefits, this will connect previously unconnected forest areas and create corridors for the transmission of invasive species. For example, within the plan, they commit to build forests around and alongside roads to connect forests across the country, "We will support the planting of a forest that crosses the country in a belt of trees, using the M62 corridor as its spine". It is therefore vital to understand the impact building new forests around roads could have and how this could inform future planning. It is equally important to understand the impact of already existing forest roads to inform management and prevention of invasive species. As part of England's woodland area, the National Forest Estate England is estimated to span a total area of $252,000$ ha, with an estimated 6,000 km of road through the forests giving a road density of 0.024 km ha^{-1} (estimated using data from Forest Research GIS Division [16]). From this we can see that forest roads are prevalent in England and this is only going to increase, it is therefore vital to understand the role roads play in this problem.

Section 3.1-3.2 is predominately based on the published work [20].

3.1 The Road Model

A road is incorporated into the model as a vertical rectangular strip within the dispersal domain (2.2.3),

$$\Omega_R = [x_1, x_2] \subset \Omega.$$

The no road domain consists of the remainder of the dispersal domain and is given by,

$$\Omega_{NR} = \Omega \backslash \Omega_R = [-L, x_1) \cup (x_2, L].$$

We set the width of the road to be δ. Throughout, we denote the left hand point of the road by $b \in \Omega$ and will apply the restriction $b > 0$, thus, the road subdomain becomes,

$$\Omega_R = [b, b + \delta].$$

Here the road is not considered as a 'dispersal corridor' but is modelled as a 'hostile environment' that results in an additional amount of the population density coming from the road to a spatial domain in front of the road at each time step, while the dispersal mode remains the same. To account for this behaviour of additional dispersal coming from the road, we split the the time-increment into two. From a ecological perspective, our model will deal with plant species that have distinct periods of growth and dispersal, as many plant species do. In many real-world applications, one time-increment would occur on the order of weeks to a year, where a time-increment represents one generation. Once a species has dispersed from its initial position (see Fig. 3.1a - Fig. 3.1b), most of the dispersed population i.e. seeds have reached the final location for that generation. However, the population density that has landed on the road has additional opportunities to spread off of the road. For example, seeds could get stuck in the soil, grass, or other plants, and due to the grass, plant, or tree cover, there are fewer opportunities for wind dispersal. Comparatively, on the road domain there are additional dispersal opportunities, for example by animal, human, or vehicle, and due to the lack of cover over many roads, this also allows for additional wind dispersal off of the road (see Fig. 3.1c - Fig. 3.1d). The population density that has spread off the road domain into the no road domain is then added to the rest of the population density in the no road domain (see Fig. 3.1d - Fig. 3.1e). However, at the end of this process, some population density still remains on the road domain. We then make the assumption that any population density that has remained on the road becomes unviable to propagate into a plant, i.e. the seed was eaten by an animal, crushed by a car, or frozen over winter. Therefore at the end of a generation the population density on the road domain is set to zero (see Fig. 3.1e - Fig. 3.1f). Note,

if we just set the population density over the road to zero before allowing an additional dispersal set over the road, which would avoid having to split the time-increment into two, we would not be able to take into account the additional chances of dispersal for the population density that lands on the road domain.

Mathematically, given the population density at time t, N_t, we compute the model including a region of road. Firstly we apply the integro-difference equation in the same way as in the non-road case (2.2.4) but treat this as only half a time-increment

$$N_{t+\frac{1}{2}}(x) = \int_{-L}^{L} \kappa(x,y) N_t^{gr}(y)\, dy, \tag{3.1.1}$$

next we define the population density for the region of the road,

$$N^R_{t+\frac{1}{2}}(x) = \begin{cases} N_{t+\frac{1}{2}}((x), & \text{if } x \in \Omega_R \\ 0, & \text{otherwise.} \end{cases} \tag{3.1.2}$$

We now apply an additional dispersal component to the road; since the population density does not grow on the road, we have the growth function $G(N) = 1 \cdot N = N$

$$N^R_{t+1}(x) = \int_{-L}^{L} \kappa(x,y) N^R_{t+\frac{1}{2}}(y)\, dy. \tag{3.1.3}$$

Note that this is computed across the whole domain $y \in \Omega$, by combining (3.1.1) and (3.1.3) the population density at time $t+1$ becomes

$$\hat{N}_{t+1}(x) = N_{t+\frac{1}{2}}(x) + N^R_{t+1}(x). \tag{3.1.4}$$

There is one final step at the end of the time-increment; the population density on the road dies out. We, therefore, introduce a new growth function $H(N) = 0 \cdot N = 0$, and apply this to the road. The population density across the non-road region remains the

same, and therefore we apply the growth function $G(N)$ to this region

$$N_{t+1}(x) = \begin{cases} H(\hat{N}_{t+1}(x)), & \text{if } x \in \Omega_R \\ G(\hat{N}_{t+1}(x)), & \text{otherwise,} \end{cases} \\ = \begin{cases} 0, & \text{if } x \in \Omega_R \\ \hat{N}_{t+1}(x), & \text{otherwise,} \end{cases} \tag{3.1.5}$$

obtaining the final population density for this time. See figure 3.1 for a graphical representation of the road model.

3.2 Population Density Cases of Behaviour

3.2.1 Ricker growth function - the road model

Firstly, the Ricker growth function (2.1.1) will be considered. An example of the road model with the Ricker growth function where $A = 2$, and the Gaussian dispersal kernel (2.4.3), where $\sigma = 0.1$. There are two other variables to consider, the width of the road δ and where to place the road in the domain. The choice of these needs careful consideration. In numerical simulations if we do not consider these factors carefully, the cases of extinction or survival and the overall shape of the population density can differ significantly from the solution, compared to when the road is carefully considered. The main issue arises from the shape of the population density at the edge in front of the road when becoming established. The grid accuracy Δx, has to be chosen such that it accurately represents the road width. The edges of the road fall exactly on grid points such that the computational width of the road $\delta^{comp} = \alpha \Delta x$, $\alpha \in \mathbb{Z}^+ \geq 2$. If $\alpha = 1$, there do not exist two grid nodes to represent the edges of the road, and, therefore, this would be identical to the no road case. Throughout this chapter in computations $\Delta x \leq \frac{5}{2^{10}} \approx 0.005$. Thus the difference between the computational and 'true' road width is $|\delta - \delta^{comp}| < \frac{5}{2^{10}}$.

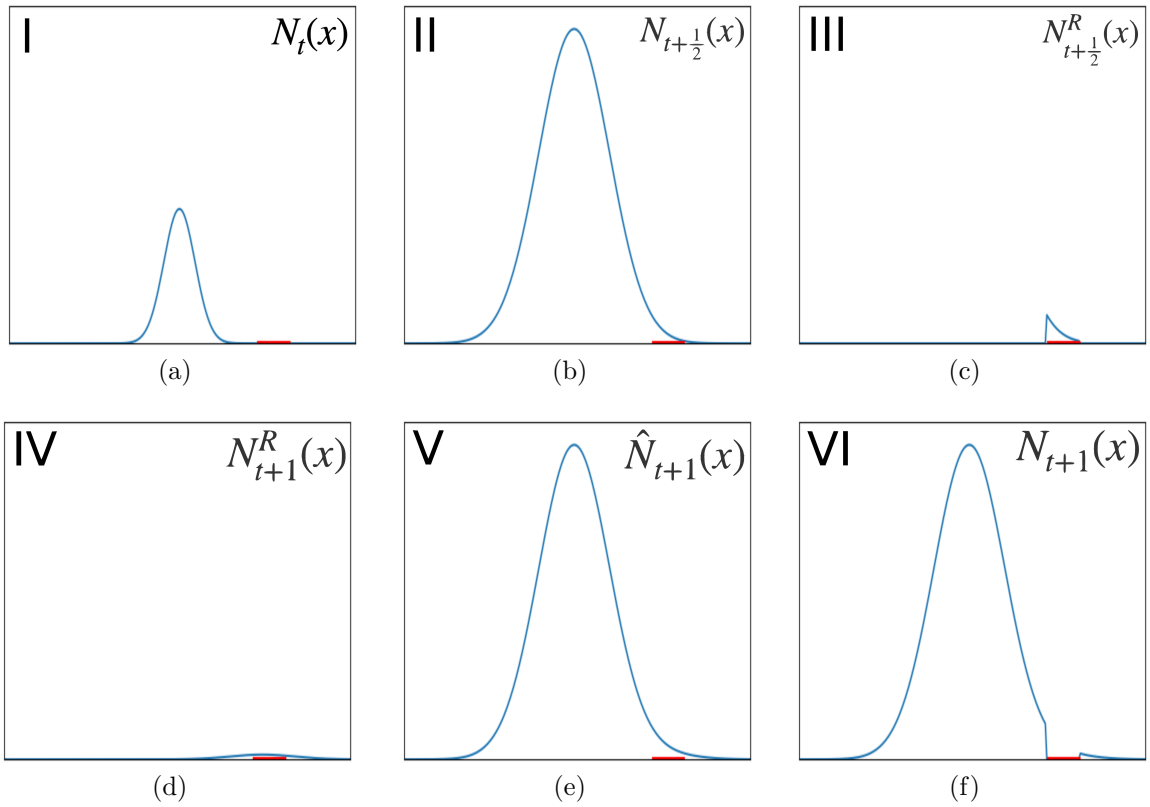

Figure 3.1: *Graphical representation of the road model, where the solid blue line corresponds to the population density and the solid red line corresponds to the road region. (a) We start with the population density at time t, $N_t(x)$, then (b) compute the population density at $t+\frac{1}{2}$ through the application of the integro-difference equation* (3.1.1). *(c) Obtaining the population density across the road* (3.1.2), *(d) we compute an additional dispersal step* (3.1.3) *calculating the road population density at $t+1$. (e) Combining the population density at $t+\frac{1}{2}$, $N_{t+\frac{1}{2}}(x)$, and the road population density at $t+1$, $N^R_{t+1}(x)$, we calculate the population density for $t+1$, $\hat{N}_{t+1}(x)$* (3.1.4). *(f) Finally, we remove the population density across the road* (3.1.5) *from the total population density across the domain obtaining the final population density at $t+1$, $N_{t+1}(x)$.*

For this example the road width is chosen to be $\delta = 0.12$, and the initial population density for the road case is a modified version of the initial population density (2.4.1),

$$N_0(x) = \begin{cases} 0, & \text{if } x \geq b, \\ \frac{\Phi}{\sqrt{2\pi\sigma_0^2}} \exp\left(-\frac{x^2}{2\sigma_0^2}\right), & \text{otherwise.} \end{cases} \tag{3.2.1}$$

The results of this example can be seen in Fig. 3.3. One can see that in this case the population density starts from the initial condition (Fig. 3.3a). Then as time progresses

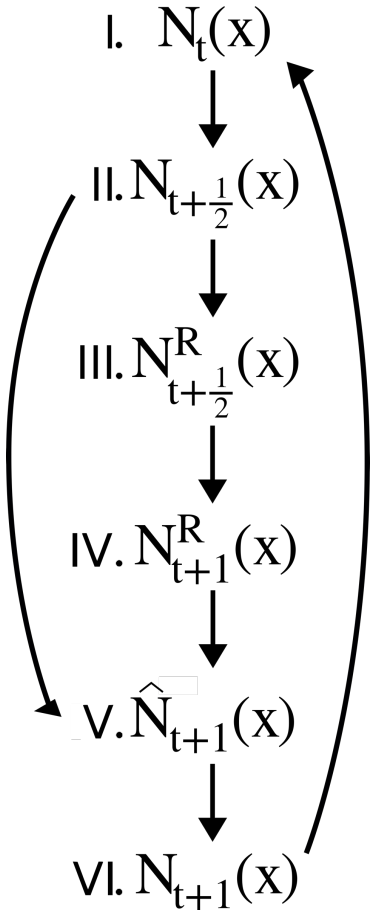

Figure 3.2: *A flow chart representation of the road model, see Fig. 3.1 for an accompanying graphical representation. In the first step I, we start with the initial population density for the time increment t. In the second step II, the growth and dispersal components are applied to the population density, see equation* (3.1.1)*. In the third step III, we isolate the population density on the road sub-domain, see equation* (3.1.2)*. In the forth step IV, additional dispersal is applied to the road population density, see equation* (3.1.3)*. In the fifth step V the population density from the second and forth step are combined, see equation* (3.1.4)*. In the sixth VI and final step any population density on the road sub domain is set to zero, see equation* (3.1.5)*. We have now achieved the final population density for this generation, the population density in VI is now used as the initial population density for the next generation.*

(Fig. 3.3b) the population density around the origin ($x = 0$) has reached the carrying capacity $\ln(A)$ where $A = 2$, and has reached and crossed over the road. As time progresses further (Fig. 3.3c) the population density then goes on to invade the left-hand and right-hand side of the domain at a constant propagation speed (2.11.5).

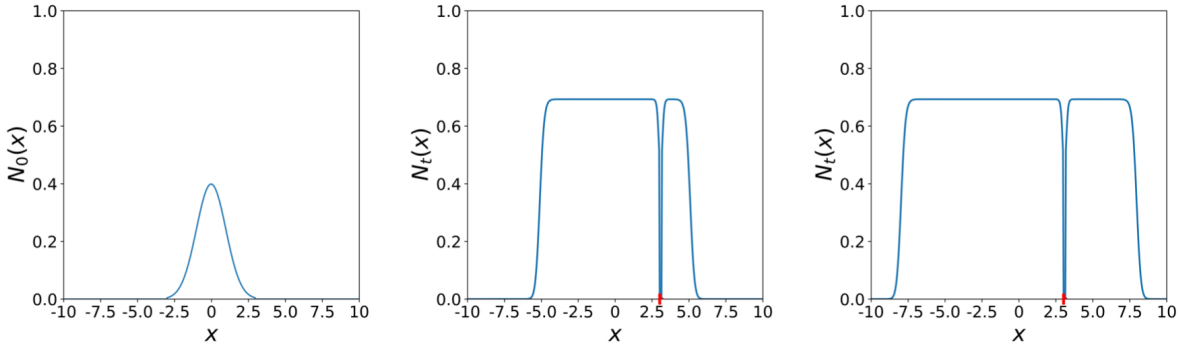

(a) (b) (c)

Figure 3.3: *Spatio-temporal dynamics of the population density $N(x,t)$ in the problem (3.1.1) - (3.1.5), with the Ricker growth function* (2.1.1)*, where $A = 2$. The road region is given by the solid red line along the x-axis, for the road width $\delta = 0.12$. (a) The initial population density (3.2.1) at time $t = 0$, (b) The population density distribution $N_t(x)$ at time $t = 25$, as the invasive species propagates in front of the road, (c) The invasive species spreads further into the space in front of the road as time progresses, $t = 50$.*

3.2.2 Invading The Domain in Front of The Road

In the example of the road model above (see Fig. 3.3) the population density reaches and then crosses over the road, however, is this the only possible case of behaviour when the population density is in the survival case? We say that the population density has invaded the domain in front of the road when some population density from one side of the road ends up in the region on the other side of the road. In figure 3.5(a), we can see that some of the population density given by the solid green line has invaded the domain in front of the road. We can see that the population density given by the solid orange line after one time-increment does not invade the domain in front of the road. However, a sufficient amount of population density has built up at the edge of the road, therefore, after two time-increments the population density given by the solid green line has invaded the domain in front of the road. The road given by the solid red line, is too wide to allow the dynamics of the population density to ever invade the domain in front of the road, no matter how much time we take. In figure 3.5(b), we see a situation where the population density is unable to invade the domain in front of the road.

In order to understand how the road can prevent the population density from invading

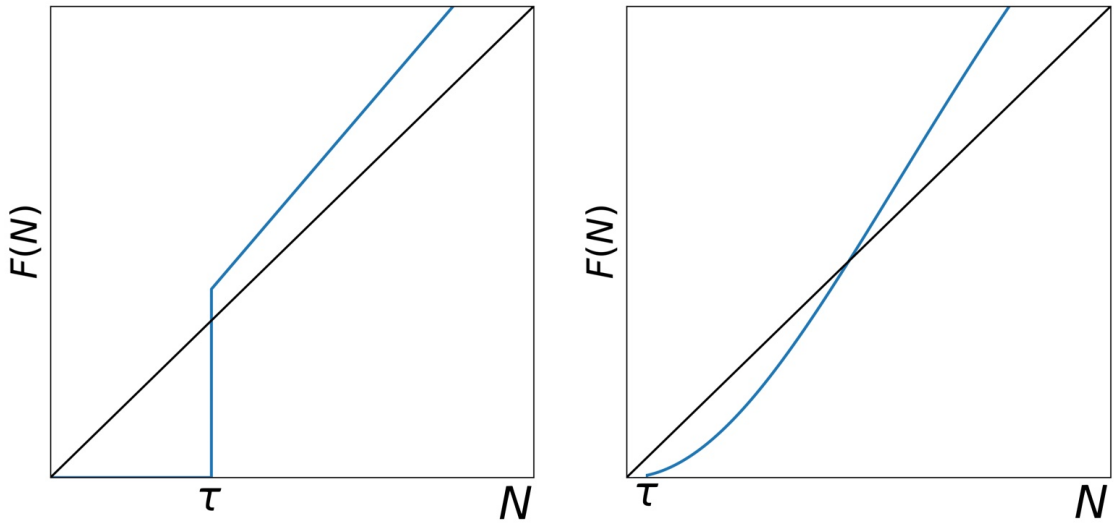

Figure 3.4: *In (a) a zoomed in example of the Ricker growth function* (2.1.1) *(solid blue line) with the cutoff τ is shown, and the line $F(N) = N$ is given by the solid black line. The Ricker growth function without the cutoff has positive growth everywhere, with the introduction of the cutoff τ, the population density is instantly set to zero if the population density is below the threshold, $N = 0$ for $N < \tau$. It is important to note that this cutoff does not introduce a region of negative non-zero growth and, therefore, still behaves fundamentally different from the Allee growth function. Comparatively in (b) an example of the Allee growth function* (2.6.2) *(solid blue line) is shown with the cutoff τ, along with the line $N = F(N)$ (solid black line). Here, we have positive growth above the Allee threshold, and then below the Allee threshold a region of negative but non-zero growth, and then zero population density below the cutoff τ. The introduction of the cutoff τ does not change the behaviour of the Ricker growth function to be equal to the Allee growth function. However, can be thought of as shifting the origin to the right, now any population density $N \in [0, \tau)$ is equal to the point $N = 0$.*

the domain in front of the road, we need to revisit the cutoff τ introduced in Section 2.3.1. From an ecological point of view, this threshold τ can be thought of as a minimum threshold for establishment, below which establishment for any growth function is not possible. In Fig. 3.4 we explore how the cutoff differs from the Allee effect observed for the Allee growth function. Note as a point of context ecologically, throughout the majority of the document $\tau = 10^{-7}$ unless specified, and the carrying capacity is around 1.

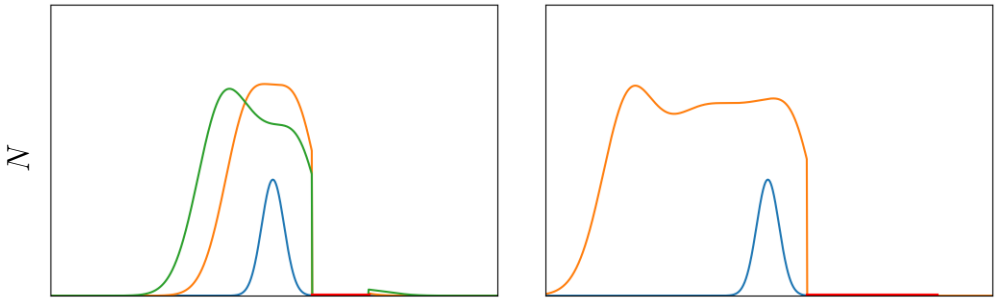

((a)) The population density can invade the domain in front of the road

((b)) The population density cannot invade the domain in front of the road

Figure 3.5: ***(a)*** *The population density at time $t = 0$ is given by the solid blue line, at time $t = 1$ is given by the solid orange line, and at time $t = 2$ is given by the solid green line. Here the population density given by the solid orange line has not invaded the domain in front of the road, but the population density given by the solid green line has invaded the domain in front of the road. In* ***(b)****, the population density for time $t = 0$ is given by the solid blue line, the population density for some time $t > 0$ is given by the solid orange line; here, for any given time, the population density does not invade the domain in front of the road.*

3.2.3 Analytical Population Density

In the Ricker growth function example, the population density invaded the domain in front of the road, however does the population density always invade the domain in front of the road if it is in the survival case?

If the population density cannot invade the domain in front of the road for all road widths, then what is the maximum road width that the population density invades the domain in front of the road? In order to answer these questions and understand the underlying behaviour it is not useful or realistic to arbitrarily compute numerical examples of the population density. Thus, this problem will be explored analytically.

Firstly, it is important to identify the situations which do not allow the population density to invade the domain in front of the road for a given time. The first situation is that the population density has not built up enough density immediately behind the road (but given enough time, the population density can be sufficiently dense) to invade the domain in front of the road, see figure 3.5(a). The second situation is that the width of the road is too great for the dynamics of the population density to spread to the domain

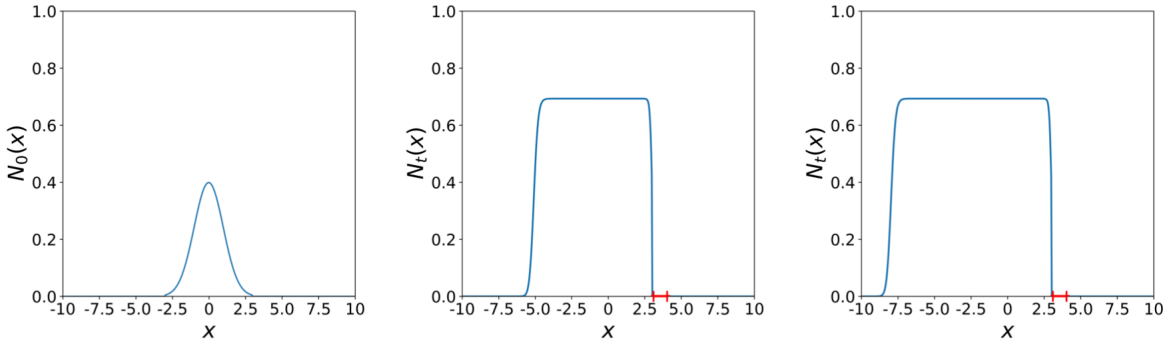

(a) (b) (c)

Figure 3.6: *Spatio-temporal dynamics of the population density $N(x,t)$ in the problem (3.1.1) - (3.1.5), with the Ricker growth function* (2.1.1)*, where $A = 2$. The road region is given by the solid red line along the x-axis, for the road width $\delta = 0.12$. (a) The initial population density (3.2.1) at time $t = 0$, (b) The population density distribution $N_t(x)$ at time $t = 25$, the population density has reached the edge of the road, however, the width of the road is sufficiently large to prevent the prevent the population density in front of the road. (c) The invasive species spreads further into the left-hand side of the road, and remains unable to cross in front of the road as time progresses, $t = 50$.*

in front of the road, see figure 3.5(b).

To explore if the population density can invade the domain in front of the road, we first want to calculate the maximum distance the population density can spread. If the maximum distance the population density can spread in the road model is less than the width of the road once it has become fully established behind the road then it cannot invade the domain in front of the road. Once the population density has become established in an area after some time the population density tends towards the carrying capacity. Thus, in order to answer this problem analytically, we will assume the population density is fully established in a region behind the road, and approximate the population density behind the road by a uniform distribution. Therefore, the population density after some time t is approximated by a uniform distribution,

$$\tilde{N}_t(x) = \begin{cases} h, & \text{if } x \in [a,b], \\ 0, & \text{otherwise.} \end{cases} \tag{3.2.2}$$

We positioned the starting population density at the edge of the road of width δ, $\Omega_R =$

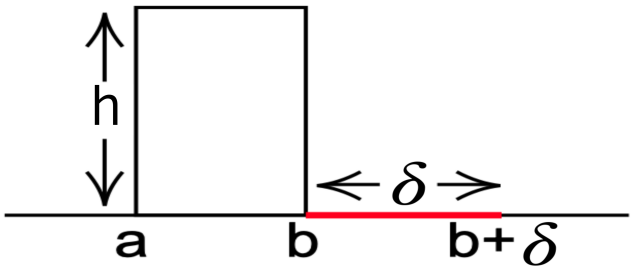

Figure 3.7: *Demonstration of the set up for the analytical results given a simple starting population density. The uniform starting distribution is given by height h and width $b-a$, b is the starting position of the road, $b+\delta$ is the end position of the road and δ is the width of the road.*

$[b, b+\delta]$, this set up is demonstrated in figure 3.7. If the population density at the leading edge of the road $N(b+\delta)$ is non-zero once the spreading speed cutoff is applied, then the population density has spread to the domain in front of the road. We will use the Gaussian dispersal kernel (2.4.3) and growth function (2.1.1), therefore, we have

$$\begin{aligned}
\tilde{N}_{t+\frac{1}{2}}(x) &= \int_{\Omega} k(x-y)F(N_t(y))dy \\
&= F(h)\int_a^b \frac{1}{\sqrt{2\pi\sigma^2}} \exp\left(\frac{-(x-y)^2}{2\sigma^2}\right)dy \\
&= F(h)\frac{1}{2}\left(\operatorname{erf}\left(\frac{(b-x)}{\sigma\sqrt{2}}\right) + \operatorname{erf}\left(\frac{x-a}{\sigma\sqrt{2}}\right)\right).
\end{aligned}$$

We now want to calculate the additional dispersal step of the population density across the road; however, the exact integral of the error function does not exist. Therefore, we use the simple approximation introduced in [67], which is valid for $x \geq 0$,

$$\operatorname{erf} x \approx 1 - \exp\left(c_1 x + c_2 x^2\right),$$

where $c_1 = -1.09599814703333$, and $c_2 = -0.75651138383854$. Making this approxima-

tion we can solve the integro-difference equation across the road,

$$\tilde{N}^R_{t+1}(x) = F(h)\frac{1}{2}\int_b^{b+\delta}\left(\left(\operatorname{erf}\left(\frac{(b-y)}{\sigma\sqrt{2}}\right)+\operatorname{erf}\left(\frac{y-a}{\sigma\sqrt{2}}\right)\right)\right.$$
$$\left.\left(\frac{1}{\sqrt{2\pi\sigma^2}}\exp\left(\frac{-(x-y)^2}{2\sigma^2}\right)\right)\right)dy, \quad (3.2.3)$$

which can be simplified to

$$\tilde{N}^R_{t+1}(x) = F(h)\frac{1}{2}\frac{1}{\sqrt{2\pi\sigma^2}}\int_b^{b+\delta}\left(\exp\left(-d_1y^2+d_2y+d_3\right)\right.$$
$$\left.-\exp\left(-d_1y^2+d_4y+d_5\right)\right)dy, \quad (3.2.4)$$

where,

$$d_1 = -\left(\frac{c_2-1}{2\sigma^2}\right),$$

$$d_2 = \left(\frac{2x+\sqrt{2}\sigma c_1-2c_2b}{2\sigma^2}\right),$$

$$d_3 = \left(\frac{-\sqrt{2}\sigma c_1b+c_2b^2-x^2}{2\sigma^2}\right),$$

$$d_4 = \left(\frac{2x+\sqrt{2}\sigma c_1-2ac_2}{2\sigma^2}\right),$$

$$d_5 = \left(\frac{-\sqrt{2}\sigma ac_1+a^2c_2-x^2}{2\sigma^2}\right).$$

Therefore, computing the integral in equation (3.2.4) one finds

$$\tilde{N}^R_{t+1}(x) = F(h)\frac{1}{4}\frac{1}{\sqrt{d_1}}\frac{1}{\sqrt{2\sigma^2}}\left(\exp\left(\frac{d_2^2}{4d_1}+d_3\right)\left(\operatorname{erf}\left(\frac{2d_1(b+\delta)-d_2}{2\sqrt{d_1}}\right)\right.\right.$$
$$\left.+\operatorname{erf}\left(\frac{d_2-2d_1b}{2\sqrt{d_1}}\right)\right)-\exp\left(\frac{d_4^2}{4d_1}+d_5\right)\left(\operatorname{erf}\left(\frac{2d_1(\delta+b)-d_4}{2\sqrt{d_1}}\right)\right.$$
$$\left.\left.+\operatorname{erf}\left(\frac{d_4-2d_1b}{2\sqrt{d_1}}\right)\right)\right), \quad (3.2.5)$$

Thus, one has the solution $\tilde{N}_{t+1}(x) = \tilde{N}_{t+\frac{1}{2}}(x) + \tilde{N}^R_{t+1}(x) = F(h)\phi(x,\delta)$, where,

$$\phi(x,\delta) = \left[\frac{1}{4}\frac{1}{\sqrt{d_1}}\frac{1}{\sqrt{2\sigma^2}}\left(\exp\left(\frac{d_2^2}{4d_1}+d_3\right)\left(\operatorname{erf}\left(\frac{2d_1(b+\delta)-d_2}{2\sqrt{d_1}}\right)+\operatorname{erf}\left(\frac{d_2-2d_1b}{2\sqrt{d_1}}\right)\right)\right.\right.$$
$$\left.\left.-\exp\left(\frac{d_4^2}{4d_1}+d_5\right)\left(\operatorname{erf}\left(\frac{2d_1(b+\delta)-d_4}{2\sqrt{d_1}}\right)+\operatorname{erf}\left(\frac{d_4-2d_1b}{2\sqrt{d_1}}\right)\right)\right)\right.$$
$$\left.+\frac{1}{2}\left(\operatorname{erf}\left(\frac{(b-x)}{\sigma\sqrt{2}}\right)+\operatorname{erf}\left(\frac{x-a}{\sigma\sqrt{2}}\right)\right)\right]. \quad (3.2.6)$$

Given uniform population density at time t and the approximation of the error function, we can calculate the population density analytically for time $t+1$.

If the population density at time $t+1$ is $N_{t+1}(x) > \tau$ for $x \in [b+\delta, L]$, the population will grow in the spatial domain in front of the road, which is precisely the corridor regime as shown in Fig. 3.3. Thus, to find the boundary between the corridor and barrier case one has to solve the equation

$$F(h)\phi(\delta) = \tau, \quad (3.2.7)$$

where the function ϕ defined by the equation (Eq. 3.2.6) is considered at the point $x = b+\delta$. This requires that $F(h) = h$, therefore, one now substitutes $h = ln(A)$ into (3.2.7) and rearranging terms to arrive at

$$A = \exp\left(\frac{\tau}{\phi(\delta)}\right). \quad (3.2.8)$$

The expression (3.2.8) defines the boundary curve separating the 'barrier' subdomain from the 'corridor' subdomain in the (A,δ)-plane. For any given value of the demographic parameter A in the growth function (2.1.1), a critical road width δ_b required to prevent propagation of the invasive species in front of the road can be calculated from Eq. (3.2.8). One notes that in the case of the Ricker growth function (2.1.1), one also has the boundary separating the extinction and survival regions. Hence, this leads to two boundary curves in the parametric plane (A,δ). The first boundary curve is the straight line $B_1 : A = 1$, the boundary separating the extinction and survival regions. The second boundary curve

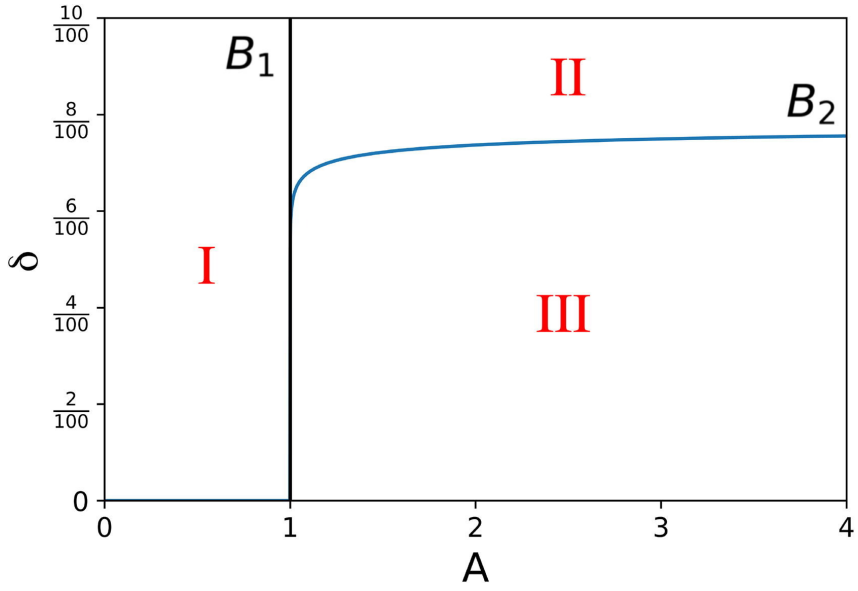

Figure 3.8: *Various propagation regimes in the road model (3.1.1) - (3.1.5) with the growth function Eq.* (2.1.1). *The road width δ is measured as a percentage of the domain size L. Region I in the parametric plane (A, δ) represents the extinction regime in the spatial domain, region III is the corridor regime, where the invasive population crosses the road and a travelling wave spreads in front of the road, and region II is the barrier region, where the road prevents propagation of the invasive species. The boundary B_2 between regions II and III determines the critical width of the road required to stop propagation of the invasive species for a given value of the growth parameter A.*

is $B_2 : \delta_b = \delta_b(A)$ which comes from solving Eq. (3.2.8) an separates the corridor and the barrier regions. The boundary curves and the regions they separate can be seen in Fig. 3.8.

It is important to note that, for the Ricker growth function, if the population density at a given point in space x is non-zero then the population density will increase (before dispersal), and due to the nature of the Gaussian dispersal kernel the population density is non-zero everywhere. Therefore, one might logically reason that for the Ricker growth function the existence of the barrier case should not be possible. The population spread results in non-zero density everywhere, so once in the survival case we should always be in the survival case, and this should not depend on the road width δ. However, one must remember the existence of the threshold density τ. Thus, the barrier regime only exists in the case of the Ricker growth function because of τ. Now that it is clear that the existence

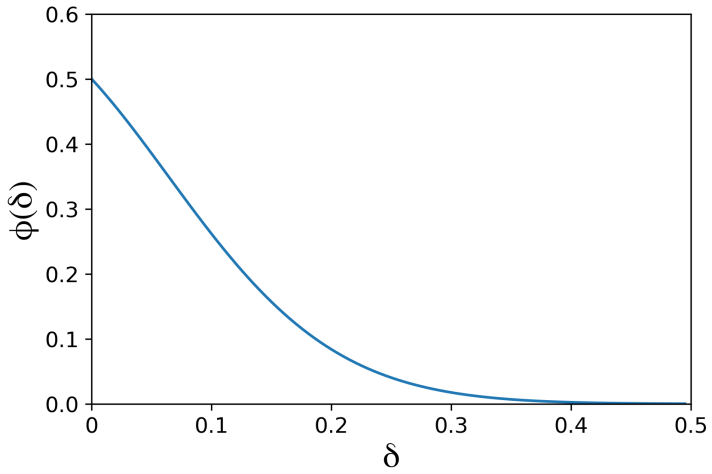

Figure 3.9: *The function $\phi(x, \delta)$ defined by (3.2.6) and considered at the right edge x_r of the road, $x_r = b + \delta$, is a decreasing function of the argument δ.*

of the barrier regime depends on τ, one might consider what will happen if the threshold τ increases. An increasing threshold could represent harsher growth conditions in front of the road for example. To consider this let the original threshold density be $\tau = \tau^*$, and the new higher threshold density be $\tau^{**} > \tau^*$. Consider a point $P = (A, \delta_b^*)$ at the boundary B_2 obtained for the threshold τ^*. Given the same value of A, the position of this point P will change when the new value of τ^{**} is implemented in the problem. It follows from Equation (3.2.8) that

$$A = \exp\left(\frac{\tau^*}{\phi(\delta_b^*)}\right) = \exp\left(\frac{\tau^{**}}{\phi(\delta_b^{**})}\right),$$

where δ_b^{**} is the road width for which $P = (A, \delta_b^{**}) \in B_2$ when $\tau = \tau^{**}$. Rearranging terms we obtain

$$\frac{\tau^{**}}{\tau^*} = \frac{\phi(\delta_b^{**})}{\phi(\delta_b^*)},$$

and, since $\tau^{**}/\tau^* > 1$, we have $\phi(\delta_b^{**}) > \phi(\delta_b^*)$.

In order to understand how the boundary curves behave from the above equations one must understand the behaviour of the function $\phi(\delta)$. The graph of the function $\phi(\delta)$ is shown in Fig. 3.10. It can be seen from the graph that $\phi(\delta)$ is a decreasing function of

its argument and therefore $\delta_b^{**} < \delta_b^*$, *i.e.,* the point P moves down along the vertical axis in Fig. 3.8. Hence, if the threshold density τ increases, the boundary B_2 will go down in the parametric plane (A, δ) to increase the area of the barrier region. In other words, if environmental conditions become harsher in front of the road, a more narrow road can still prevent propagation of the invasive species. Conversely, for smaller values of τ, the boundary B_2 will go up to make the corridor regime region larger in the parametric plane.

Having investigated how our solution depends on the threshold density, it is also important to investigate how the solution depends on the other, until now fixed, parameters in the problem. So far the dispersal parameter of the dispersal kernel (2.4.3) σ, has been fixed at the value $\sigma = 0.1$. It will now be discussed how the critical value δ_b of the road width responsible for the transition from the corridor regime to the barrier regime depends on the dispersal parameter σ in the dispersal kernel. Let us fix the parameters A and τ and vary σ in Eq. (3.2.7). The function ϕ defined by Eq. (3.2.6) at the point $x = b + \delta$ becomes a function of variables σ and δ only, and Eq. (3.2.7) can be solved to obtain the curve $B_\sigma : \delta = \delta(\sigma)$ defining the boundary between the corridor and barrier regime. The boundary curve B_σ is shown in Fig. 3.10. We note that the semi-analytical approach used to obtain the curve B_σ, as explained above, does not require any upper bound for variables δ and σ in the definition of the function ϕ Eq. (3.2.6). However, the choice of a large dispersal parameter $\sigma \gg 1$ results in a degenerate dispersal kernel, i.e., the dispersal is so weak that any road width can be considered as a barrier; see Fig. 3.10a. Hence, we also show a fragment of the boundary curve B_σ obtained for small σ in Fig. 3.10. It can be seen from the figure that an increase in σ within the interval $\sigma \in [0, 1]$ results in a linear growth of the corridor domain, *i.e.*, we have $\delta = k\sigma$, where the slope k of a straight line in the figure can be approximated as $k \approx 7.38$ for $\tau = 10^{-7}$ and $A = 3$ used in computation.

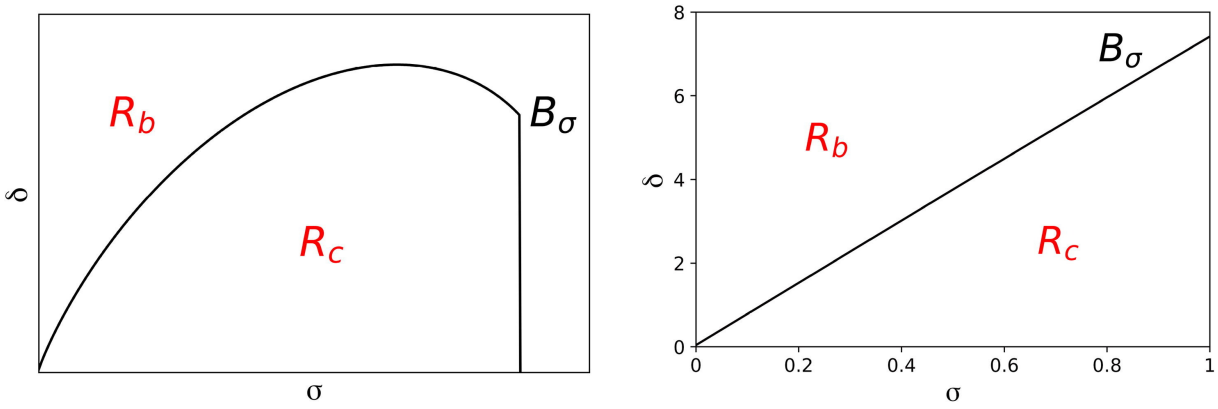

Figure 3.10: *The propagation regimes in the road model* (3.1.1) - (3.1.5) *with the growth function* (2.1.1) *shown in the* (σ, δ)*-plane. The region* R_c *represents the corridor regime in the spatial domain, the region* R_b *represents the barrier regime. (a) The boundary* B_σ *between regions* R_b *and* R_c *determines the critical width of the road* δ_b *required to stop propagation of the invasive species for any given value of the parameter* σ *in the dispersal kernel* (2.4.3)*; see further explanation in the text. (b) The boundary* B_σ *shown for* $\sigma \in [0, 1]$*. The boundary curve can be approximated by a linear function* $B_\sigma : \delta = k\sigma$*, where the slope of the straight line has been computed as* $k \approx 7.38$ *for* $\tau = 10^{-7}$ *and* $A = 3$*.*

3.2.4 The road model with the Allee effect growth function

So far the behaviour of the Ricker growth function has been analysed with the results showing, if we are in the survival case then we fall into either the barrier or the corridor regime. However, as we have already seen from Chapter 2, the behaviour is more complex for the Allee growth function (2.6.2), with negative growth for at small densities. Thus one might have the question, do we get the same set of possible barrier or corridor regime behaviours when we are in the survival case for the Allee growth function? When this question was investigated we did still observe the barrier and corridor regimes for the Allee growth function (2.6.2). The overall shape of the wave pattern that the population density produces is very similar to those of the Ricker growth function (see Fig. 3.3 and Fig. 3.6). However, upon further investigation a new regime of the spatio-temporal dynamics was observed. This new regime is labelled as the 'beachhead' regime, an example of the beachhead regime can be seen in Fig. 3.11. The beachhead regime differs from the corridor regime. In the beachhead regime once the population density crosses over the

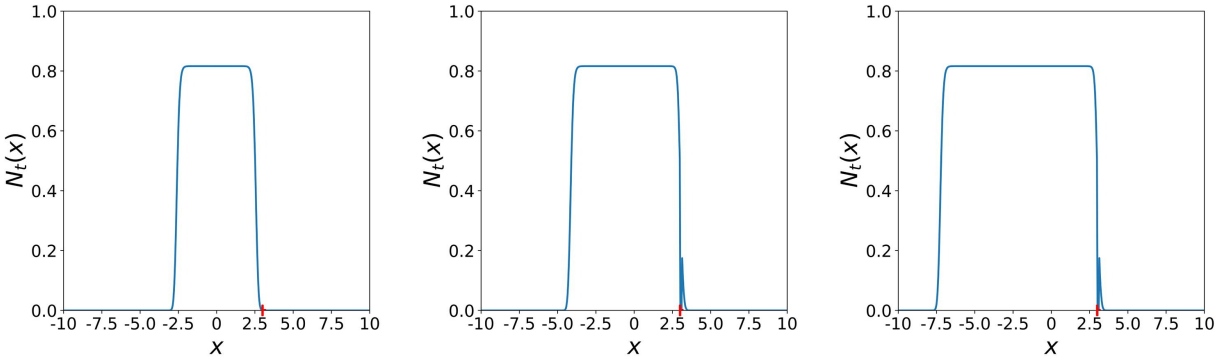

(a) (b) (c)

Figure 3.11: *The beachhead regime in the problem (3.1.1) - (3.1.5) with the Allee growth function (2.6.2). The parameters are* $\xi = 0.15$, $\rho = 1.0$. *The road width is* $\delta = 0.12$ *and the road region is shown in red on the x-axis. (a) A travelling wave approaches the road at time* $t = 50$, *(b) The population density distribution* $N_t(x)$ *at time* $t = 100$. *The beachhead region in front of the road has been invaded, yet the invasive species does not propagate further into the space, (c) The population density distribution* $N_t(x)$ *in front of the road remains the same at time* $t = 200$ *as in earlier times (cf. Fig. 3.11b).*

road and spreads into the domain in front of the road, it does not continue to invade further into the domain with time.

This new regime can be seen in numerical examples (Fig. 3.11), however, this needs to be investigated further to confirm that it is, in fact a new regime. To investigate the existence of the beachhead, the propagation speed c and the width W of the domain occupied by the species in front of the road are calculated as functions of the road width δ. The results can be see in Fig. 3.12. One can see by comparison of the graphs in Fig. 3.12a and Fig. 3.12b that the beachhead spatio-temporal dynamics appears in the problem when the road width is $\delta \in [\delta_1, \delta_2]$. The left boundary δ_1 is shown in the graph $c(\delta)$ in Fig. 3.12a. It can be defined as the minimum road width that prevents further propagation of the population wave, *i.e.,* $c(\delta_1) = 0$ and $c(\delta) > 0$ for any $0 < \delta < \delta_1$. The right boundary δ_2 is shown in the graph $c(\delta)$ in Fig. 3.12b. It can be defined as the minimum road width that results in the population extinction in front of the road, *i.e.,* $W(\delta) = 0$ for any $\delta \geq \delta_2$. When the road width is $\delta \in [\delta_1, \delta_2]$, the propagation speed in the right-hand direction is zero, meaning the population density in front of the road is either stable or zero. Furthermore, the width of the population density in front of the

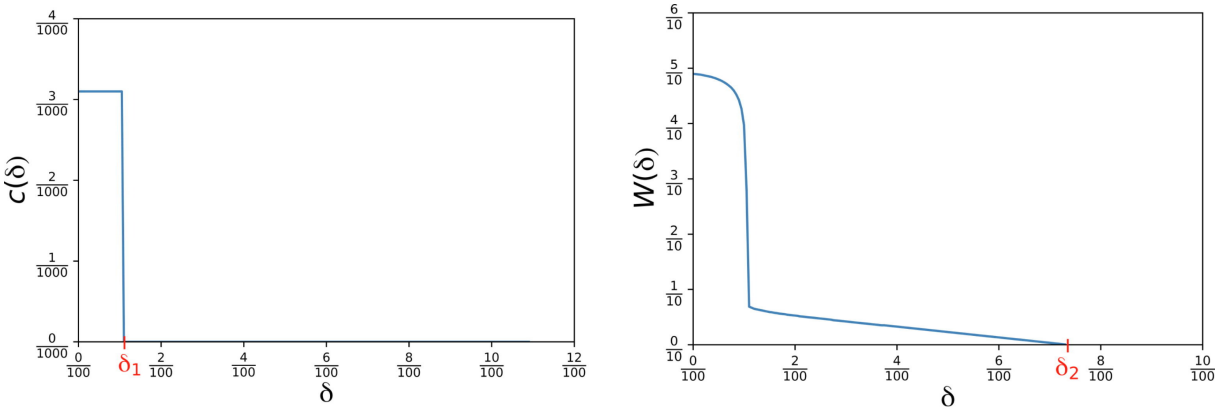

(a) (b)

Figure 3.12: *The problem (3.1.1) - (3.1.5) with the growth function (2.6.2). The rate of spread c and width W of the domain occupied by the population in front of the road are shown as functions of the road width δ measured as percentage of the domain size L. The parameters are $\xi = 0.15$, $\rho = 1.0$. (a) For any road width $\delta > \delta_1$, the population does not spread in front of the beachhead region. (b) For any road width $\delta > \delta_2$, the road acts as a barrier that the invasive population cannot cross.*

road is non-zero. This means that there is a stable non-zero population density in front of the road; which is precisely the beachhead regime.

It is noted that, for a given road width δ, the size W of the beachhead spatial region in front of the road depends also on the parameters ξ and ρ of the growth function; see Fig. 3.14. Hence, our next step is to identify the beachhead regime in the parametric plane. This is in line of the analysis conducted for the Ricker growth function (see Fig.3.8). Let us fix ξ in the definition of the growth function (2.6.2) and vary another demographic parameter ρ in (2.6.2) and the road width δ. The graph should look similar to that observed with the Ricker growth function (see Fig.3.8), where several regions were observed in the (ρ, δ)-plane, however, there should also exist a new region representing the beachhead regime.

The curve that separates the extinction region in the (ρ, δ)-plane from the other regimes is defined directly from the analysis of the growth function (2.6.2), *i.e.,* we require that the population density behind the road is given by the stable steady state $\bar{N}_2$ in section 2.5 which only exists when $\rho \geq 2\sqrt{\xi}$. Thus, we define a boundary B_1 of the extinction region in the parametric plane as $L_1 : \rho = 2\sqrt{\xi}$ for all values of δ. The straight

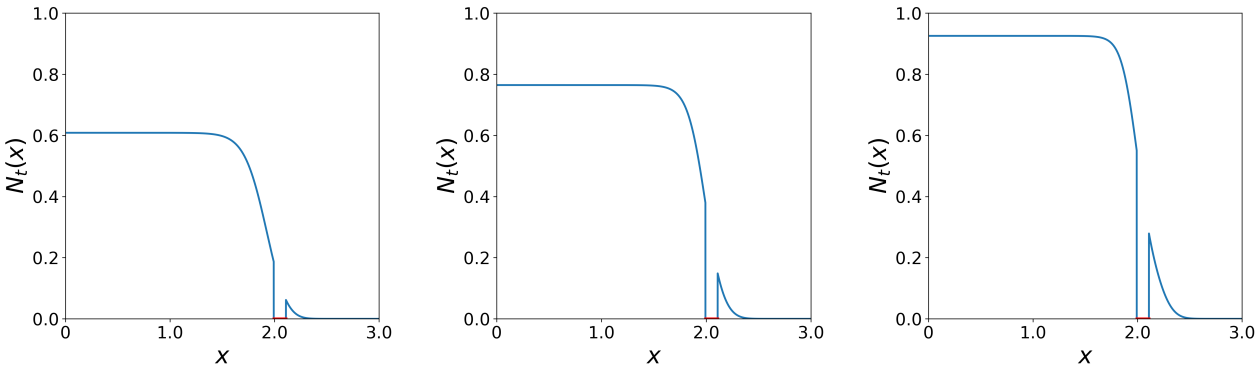

(a) (b) (c)

Figure 3.13: *The population density distributions $N_t(x)$ at time $t = 100$ after the beachhead region has been invaded in front of the road. For the given road width $\delta = 0.12$, the size of the beachhead region depends on the parameters of the growth function (2.6.2). (a) The parameters are $\xi = 0.15$, $\rho = 0.855$, (b) $\xi = 0.18$, $\rho = 1.0$, (c) $\xi = 0.18$, $\rho = 1.12$. Only the spatial subdomain $x \in [0, 3]$ is shown in the figure for the sake of better visualisation of the beachhead region.*

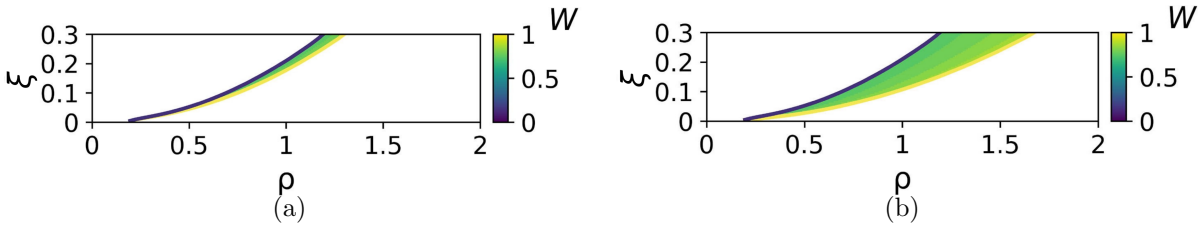

(a) (b)

Figure 3.14: *The spatial width of the beachhead region W as a function of the parameters ρ and ξ in the growth function (2.6.2). (a) The road width is $\delta = 0.12$, (b) the road width is $\delta = 0.19$.*

line B_1 is shown in Fig. 3.15a where it separates the extinction region I from the other regimes.

Consider now $\rho > 2\sqrt{\xi}$ and let the population density brought to the front of the road from behind the road be below the threshold density τ. It follows from our discussion of the Ricker growth function (2.1.1) in the previous section, that the invasive species will not spread in front of the road, *i.e.,* we have the barrier regime. The boundary B_2 of the barrier region is given by the same condition (3.2.7) as for the Ricker growth function. For the growth function (2.6.2), the condition (3.2.7) written at the stable steady state $\bar{N}_2$ becomes

$$\frac{\rho + \sqrt{\rho^2 - 4\xi}}{2}\phi(\delta) = \tau,$$

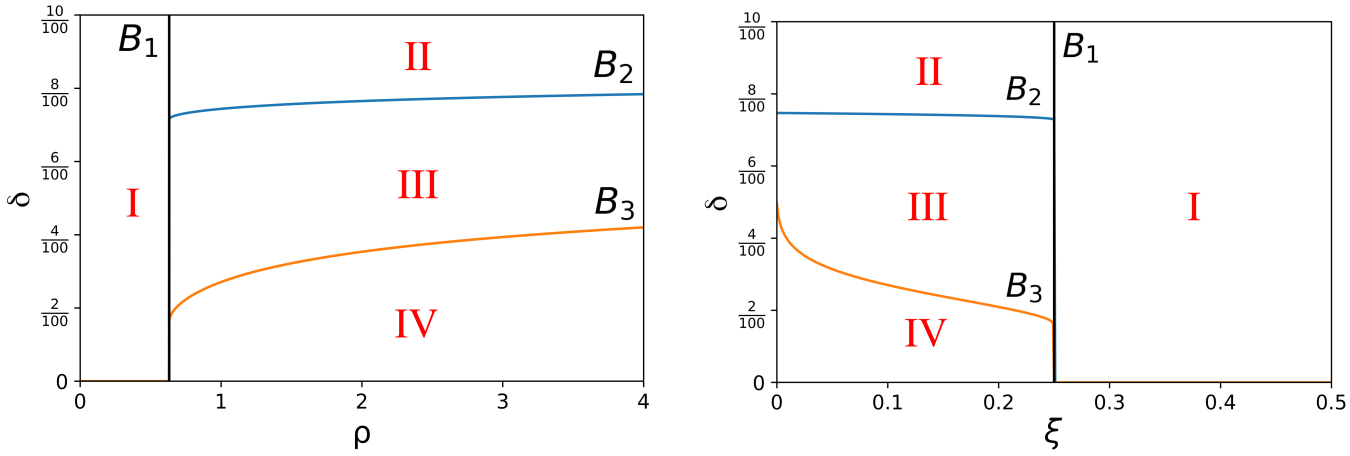

Figure 3.15: *Various spatio-temporal dynamics regimes in the road model (3.1.1) - (3.1.5) with the growth function (2.6.2). (a) The parametric plane (ρ, δ). Region I represents the extinction regime in the spatial domain. Region II is the barrier regime, where the road prevents propagation of the invasive species. Region III is the beachhead regime, where the population invades a spatial beachhead region in front of the road without further propagation. Region IV is the corridor regime, where the invasive population crosses the road and a travelling wave spreads in front of the road to invade the entire domain as time progresses.(b) The parametric plane (ξ, δ). The notation used to mark different regions is the same as in Fig. 3.15a.*

which we can rearrange for ρ to give the equation of the boundary curve B_2 in the parametric plane,

$$B_2 : \ \rho = \frac{\xi\phi^2(\delta) + \tau^2}{\phi(\delta)\tau}. \tag{3.2.9}$$

The curve B_2 shown in Fig. 3.15 bounds the region II which corresponds to the barrier regime in the spatial domain.

Let us now investigate the beachhead regime where the population density brought to the region in front of the road is fully compensated by the negative growth at the demographic stage. In our further analysis, we approximate the beachhead case by the following condition

$$N_{t+1}(b+\delta) = N_t(b+\delta), \quad \text{for } \tau < N < \bar{N}_2, \tag{3.2.10}$$

i.e., we require that the population density remains constant at the edge of the road in

the beachhead regime.

The population density at time $t+1$ can be presented as

$$N_{t+1} = N_t + \Delta N,$$

where the increment ΔN is brought to the edge of the road over the dispersal stage. Since the travelling wave given by Eq. (3.2.2) has constant height h behind the road, the increment ΔN in the population density remains constant at any time t for a given road width $\delta > 0$, yet its value depends on δ. This increment is then compensated by the negative growth occurring between $\tau < N < \bar{N}_2$ at the growth stage to meet the condition (3.2.10). It follows from the above consideration that the beachhead regime is entirely related to the Allee effect, *i.e.*, the negative growth at the interval $N \in [\tau, \bar{N}_2]$. This conclusion is further illustrated in Fig. 3.11 where the growth function $F(N)$ given by (2.6.2) is shown as a black solid line and a dashed line is the equilibrium line $F(N) = N$. Let us draw a new growth function $F(N) + \Delta N$, where $\Delta N = const$, *i.e.*, we move the graph of the function $F(N)$ along the y-axis by the distance ΔN. For relatively small ΔN, this transformation results in a new stable steady state, *i.e.*, formation of the beachhead regime; see curve ξ in the figure, where $\Delta N_1 < \Delta N_{cr}$ and the new stable steady state is shown as a blue dot on the line $F(N) = N$. As δN increases, the new steady state defining the beachhead regime moves closer to the steady state $\bar{N}_2$ along the equilibrium line $F(N) = N$, and the two steady states coincide when $\delta N = \delta N_{cr}$ (curve B in the figure). For any $\Delta N_2 > \delta N_{cr}$, we have the corridor regime only, as $F(N) + \Delta N > N$ and the population grows in front of the road (curve C).

The increment ΔN_{cr} defines the transformation of the beach-head regime to the corridor regime. Since ΔN depends on the road width, $\Delta N = \Delta N(\delta)$, the boundary B_3 between the beachhead region and the corridor region in the parametric plane (ρ, δ) can be found from the condition,

$$F(N^*) + \Delta N_{cr}(\delta) = N^*, \tag{3.2.11}$$

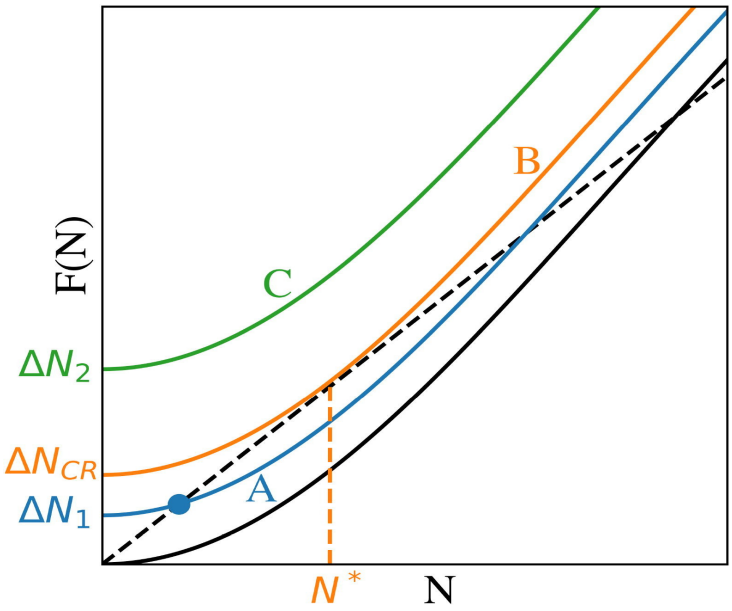

Figure 3.16: *The beachhead regime is produced by the Allee effect. The original Allee growth function* 2.6.2 *(black solid line) has the only point of intersection* $N = \bar{N}_2$ *with the line* $F(N) = N$ *(dashed line) in the interval* $N \in [\tau, \bar{N}_2]$*. Another point of intersection appears when* $F(N)$ *is raised by the value* $\Delta N < \Delta N_{cr}$ *(curve* ξ*, blue solid line). The new stable steady state shown as a blue dot in the figure corresponds to the beachhead distribution of the population density in the spatial domain. As* ΔN *increases, the new steady state goes up along the line* $F(N) = N$*, while the unstable steady state* N_2 *goes down along the curve. At* $\Delta N = \Delta N_{cr}$*, the beachhead steady state coincides with the unstable steady state; see curve* B *(orange solid line) in the figure. For any* $\Delta N > \Delta N_{cr}$*, the condition* $F(N) + \Delta N > N$ *holds and provides the corridor regime (curve* C*, green solid line).*

where N^* is defined from the requirement that the line $F(N) = N$ is the tangent line for the function $F(N)+\Delta N$ at point N^*, *i.e.*, we have $F'(N) = 1$ at $N = N^*$. Differentiating $F(N)$ and rearranging terms we arrive at

$$N^4 + 2\xi N^2 - 2\xi\rho N + \xi^2 = 0, \tag{3.2.12}$$

where we require $\rho > 2\sqrt{\xi}$ and $\tau < N < \bar{N}_2$. Let us fix the parameter ξ in the growth function (2.6.2). The Eqs. (3.2.4) and (3.2.4) are then solved for any given value of ρ to find the curve $\delta = \delta(\rho)$. The boundary $B_3 : \delta = \delta(\rho)$ is shown in Fig. 3.15. The position of the boundary curves in the parametric plane is defined by parameters in equation (3.2.9) and equation (3.2.4). Consider, for example, the boundary B_2 shown in Fig. 3.15, where

the curve B_2 is defined from Eq. (3.2.9) for some baseline value of the threshold density $\tau = \tau^*$. The boundary B_2 will move down to make the barrier region larger and the beachhead region narrower when τ increases to $\tau^{**} > \tau^*$; see a dash-dotted line in Fig. 3.17. Furthermore, it follows from the analysis in Fig. 3.17 that the beachhead region between the boundaries B_2 and B_3 will completely disappear in the extreme case $\tau > N^*$, where N^* is defined by equation (3.2.4). Conversely, the boundary B_2 will move up to decrease the size of the barrier region when τ decreases to some $\tau^{***} > \tau^*$ (see the dashed line in Fig. 3.17). It also follows from equation (3.2.4) and (3.2.4) that the boundaries B_1 and B_3 do not move when we vary the threshold density τ. Consider now the boundary B_3 that corresponds to the baseline value of the demographic parameter $\xi = \xi^*$ as shown in Fig. 3.17. Let us decrease ξ to some new value $\xi^{**} < \xi^*$. The boundary B_1 will move to the left when ξ decreases, while the boundary B_3 will move up to increase the size of the corridor domain in the parametric plane (see dash-dotted lines in the figure). Conversely, let the new parameter value be $\xi^{***} > \xi^*$. It can be seen from Fig. 3.17 that the corridor domain will shrink as the boundary B_1 moves to the right and the boundary B_3 moves down (see dashed lines in the figure). These conclusions are similar to the case of the Ricker growth: if environmental conditions become harsher in front of the road, a more narrow road will be able to prevent propagation of the invasive species.

3.3 Invasion at the short-time scale in the heterogeneous landscape

This section is predominantly based on the work [21].

In the previous section, a model that allows one to take into account different dispersal and growth behaviours of invasive plant species when a road is introduced into the dispersal domainwas developed and the possible behaviour were classified. In this section the transient propagation speed in front of the road for the corridor regime and Ricker growth is investigated. This analysis is designed to be comparable to that undertaken for invasion in the no road case (2.11).

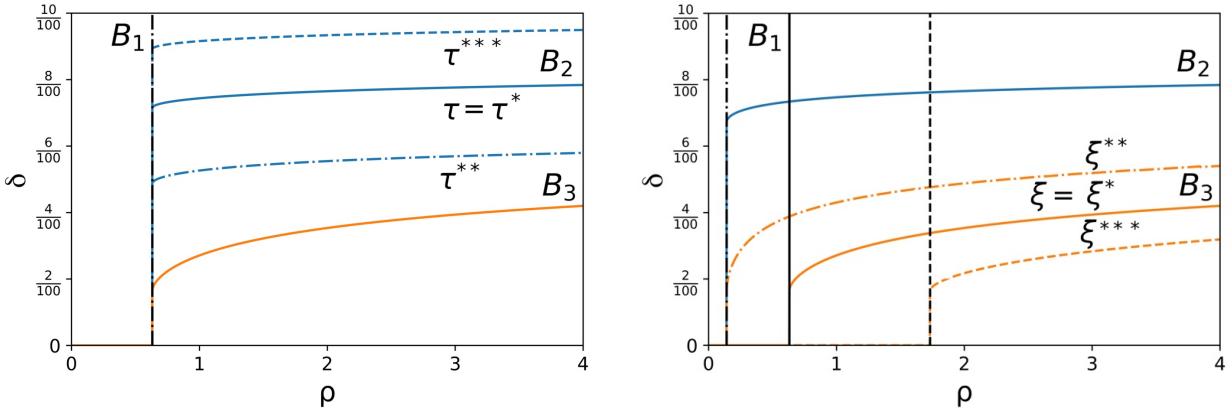

(a) (b)

Figure 3.17: *The Allee growth function (2.6.2): domains in the parametric plane (ρ, δ) corresponding to different spatio-temporal dynamics regimes when problem parameters are varied. (a) The size of the barrier domain defined by the position of the boundary B_2 increases when the value of the threshold density τ increases from τ^* (the solid line B_2 in the figure) to $\tau^{**} > \tau^*$; a new position of the boundary B_2 is shown as a dash-dotted line in the figure. Conversely,the size of the barrier domain decreases when the threshold density τ decreases from τ^* to $\tau^{***} < \tau^*$ (a dashed line in the figure). (b) The size of the corridor domain defined by the position of the boundaries B_1 and B_3 increases when the value of the demographic parameter ξ decreases from ξ^* (the solid lines B_1 and B_3 in the figure) to $\xi^{**} < \xi^*$; new boundaries B_1 and B_3 are shown as dash-dotted lines in the figure. Conversely, the size of the corridor domain decreases when the value of ξ increases from ξ^* to $\xi^{***} > \xi^*$ (dashed lines in the figure).*

As we are interested in investigating the propagation at short time scales in front of the road, we first assume that the population density has become established and has formed a traveling wave behind the road (see Fig. 3.18), thus,

$$N_t(x) = \ln(A), \text{ for } x \leq b. \tag{3.3.1}$$

A small amount of the population density is then brought in front of the road, which evolves over time into the same travelling wave as behind the road. To make a comparison between the no road and road cases, we have to introduce a definition of the 'initial condition' in the road model. In particular, we need to mathematically describe the population density in front of the road when a propagating front crosses the road, ensuring compatibility with the initial condition (2.4.1).

We assume that the population density behind the road is given by Eq. (3.3.1) for all

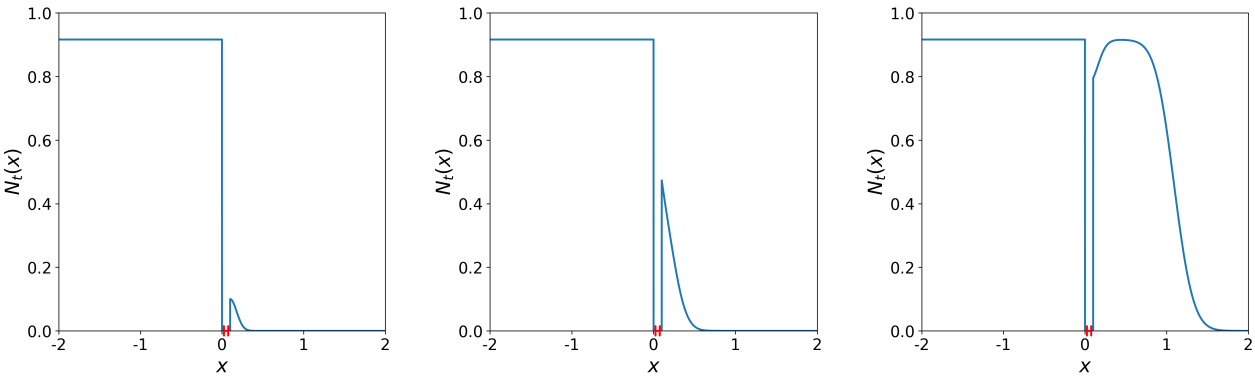

(a) $t = 0$ (b) $t_1 > 0$ (c) $t_2 > t_1$

Figure 3.18: *The propagation of the invasive species in the heterogeneous environment given by the model* (3.1.1)–(3.1.5). *The left edge of the road is positioned at* $b = 0$. *The parameters used in computation are* $\Phi = 0.01$, $h = 0.1$, $\sigma = 0.1$, $\Psi \approx 0.016$, *and* $A = 2.5$. *(a) The initial population density in front of the road is given by* (3.3.2). *A travelling wave has already been established behind the road. (b) After some time* $t_1 > 0$ *the population density in front of the road grows and spreads further into the spatial domain, (c) At a later time* $t_2 > t_1$ *the population density in front of the road continues to grow and spread into the domain. The same propagating wave as behind the road will be formed in front of the road as time progresses.*

times $t \geq 0$. The initial population density $N_0(x)$ in front of the road is approximated at $t = 0$ as

$$N_0(x) = \Phi \frac{\sqrt{2}}{\sqrt{\sigma_0^2 \pi}} \exp\left(-\frac{|x - (b + \delta)|^2}{2\sigma_0^2}\right) \text{ for } x \geq b + \delta. \tag{3.3.2}$$

The initial condition (3.3.2) in front of the road requires definition of the unknown dispersal parameter σ_0. Hence, the initial total population density in front of the road Φ and the height h of the population density at the edge of the road $x = b + \delta$ needs to be the same as in the initial condition (2.4.1) in order to make (3.3.2) compatible with the no road short-time propagation investigation. The dispersal parameter σ_0 is computed as

$$\sigma_0 = \frac{\Phi\sqrt{2}}{h\sqrt{\pi}},$$

for a given Φ and h.

The model then proceeds as follows. The initial condition (3.3.2) is transformed into

a normal distribution

$$N_0^{normal}(x) = \Phi \frac{1}{\sqrt{2\pi\sigma_0^2}} \exp\left(-\frac{|x-(b+\delta)|^2}{2\sigma_0^2}\right).$$

The linear growth function (2.3.5) is now applied and the population density is dispersed, using the Gaussian dispersal kernel (2.4.3) with dispersal variable σ, to obtain

$$N_{\frac{1}{2}}^{normal}(x) = \Phi A \frac{1}{\sqrt{2\pi(\sigma_0^2+\sigma^2)}} \exp\left(-\frac{|x-(b+\delta)|^2}{2(\sigma_0^2+\sigma^2)}\right).$$

After the dispersal, the population density is transformed back into the form of a half-normal distribution,

$$N_{\frac{1}{2}}(x) = (\Phi A) \frac{\sqrt{2}}{\sqrt{\pi(\sigma_0^2+\sigma^2)}} \exp\left(-\frac{|x-(b+\delta)|^2}{2(\sigma_0^2+\sigma^2)}\right) \text{ for } x \geq b+\delta.$$

Finally, the population density $\Psi = \Psi(\delta, \sigma)$ brought over from behind the road at time $t = 1$ is added to the population density in front of the road

$$N_1(x) = (\Phi A + \Psi) \frac{\sqrt{2}}{\sqrt{\pi(\sigma_0^2+\sigma^2)}} \exp\left(-\frac{|x-(b+\delta)|^2}{2(\sigma_0^2+\sigma^2)}\right) \text{ for } x \geq b+\delta. \tag{3.3.3}$$

The computation of the quantity Ψ is provided in Appendix A. It is important to emphasise here that the amount of the population density brought over from behind the road depends on the road width δ and the dispersal strength σ, yet it does not depend on time as the population density behind the road is given by the fixed condition (3.3.1). Once the population density Ψ has been computed for $t = 1$, it can then be used for any further $t > 1$.

The expression (3.3.3) gives the population density at the time $t = 1$. To calculate the population density at any time $t > 0$, the above procedure is implemented to the population density at time $t-1$. Hence, an exact form for the population density in front

of the road for any $t > 0$ is given by

$$N_t(x) = (\Phi A^t + \Psi \sum_{i=0}^{t-1} A^i) \frac{\sqrt{2}}{\sqrt{\pi(\sigma_0^2 + t\sigma^2)}} \exp\left(-\frac{|x-(b+\delta)|^2}{2(\sigma_0^2 + t\sigma^2)}\right) \text{ for } x \geq b+\delta. \quad (3.3.4)$$

This now gives one an analytical expression (3.3.4) for the population density at any time increment. Therefore, we can now define a spatial location $x_t(\tilde{N}) > b + \delta$ in front of the road where the population density $\tilde{N}$ is detected at time t. For $t = 0$, we solve $N_0(x_0) = \tilde{N}$ to find x_0, where the population density distribution N_0 is given by the initial condition (3.3.2). In the road case we have

$$x_0(\tilde{N}) = b + \delta + \sqrt{2\sigma_0^2 \ln\left(\frac{\Phi\sqrt{2}}{\tilde{N}\sqrt{\sigma_0^2\pi}}\right)}.$$

Similarly, we solve $N_t(x_t) = \tilde{N}$ to find a spatial location x_t for any $t > 0$, where N_t is given by Eq. (3.3.4),

$$x_t(\tilde{N}, \Psi) = b + \delta + \sqrt{2(\sigma_0^2 + t\sigma^2) \ln\left(\frac{(\Phi A^t + \Psi \sum_{i=0}^{t-1} A^i)\sqrt{2}}{\tilde{N}\sqrt{\pi(\sigma_0^2 + t\sigma^2)}}\right)}. \quad (3.3.5)$$

The propagation speed $c = \dfrac{\delta x}{\delta t}$ is then calculated in the same way as in the homogeneous environment Eq. (2.11.4). We have

$$c(t, \tilde{N}, \Psi) = x_t(\tilde{N}, \Psi) - x_{t-1}(\tilde{N}, \Psi), \quad (3.3.6)$$

where $x_t(\tilde{N}, \Psi)$ is defined from (3.3.5).

The propagation speed computed by using Eq. (3.3.6) is shown in Fig. 3.19a where it is compared with the propagation speed obtained when the population density is computed by solving the model (3.1.1)-(3.1.5) with the growth function (2.1.1) numerically. It can be seen from the figure that, although approximation (3.3.2) of the population density in front of the road results in a slight difference between analytical and numerical results, the qualitative behaviour of the propagation speed is the same in both cases.

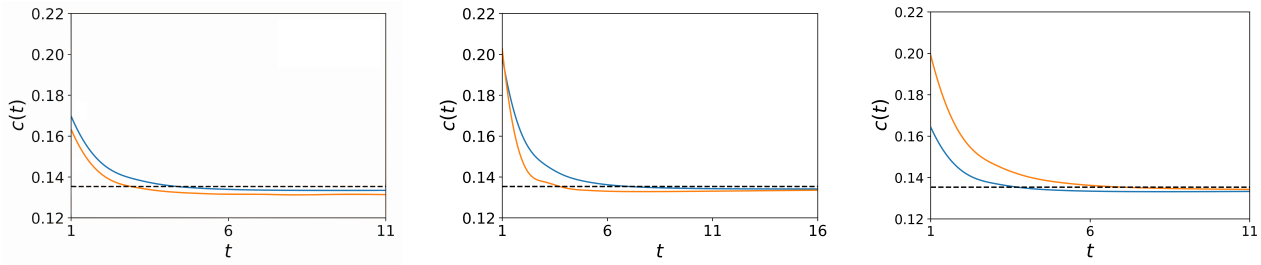

Figure 3.19: *The propagation speed $c(t)$ when the invasive plant begins spreading in front of the road. (a) The comparison of the propagation speed $c(t)$ obtained from Eq.* (3.3.6) *(blue solid line) with $\Psi = 0.005$ and by numerical computation with the growth function* (2.1.1) *(orange solid line). (b) The comparison of the propagation speed in the road model* (3.3.6) *for $\Psi = \Psi_{max}$ (blue solid line) and the no road model* (2.11.4) *(orange solid line). (c) The propagation speed* (3.3.6) *for $\Psi \to 0$ corresponding to the road width $\delta \to \infty$ (blue solid line), and $\Psi = \Psi_{max} \approx 0.037$ corresponding to the road width $\delta \to 0$ (orange solid line). The other parameters are $\Phi = 0.01$, $h = 0.1$, $\tilde{N} = 0.01$, $\sigma = 0.1$, and $A = 2.5$.*

We then consider the extreme case of the road width $\delta \to 0$ in order to imitate the homogeneous environment. The investigation of this case is provided in the Appendix A, where the amount of the population density $\Psi_{max} = \Psi_{max}(\sigma)$ brought from behind an infinitely narrow road is defined by the formula (A.2.1). The comparison between the no road model and the road model (3.3.6) for $\Psi = \Psi_{max}$ is presented in Fig. 3.19b. It can be concluded from the graphs in the figure that the extreme case of an infinitely narrow road in the model, Eq. (3.1.1)–(3.1.5) is not equivalent to the homogeneous environment: adding a constant amount of the population density to the population in front of the road results in a different propagation speed at the short-time scale. The difference, however, diminishes as time progresses and the initial population density evolves into a travelling wave propagating at the constant asymptotic speed (2.11.5).

Another extreme case is given by a very wide road, *i.e.*, the road width $\delta \to \infty$, where the additional population density brought from behind the road is negligible. The population density obtained in the road model can then be used by setting $\Psi = 0$ in the formula (3.3.4); see Appendix A for further explanation. The comparison between the road model (3.3.6) for $\Psi \to 0$ and $\Psi = \Psi_{max}$ is presented in Fig. 3.19c. It is readily seen from the graphs that the invasive population spreads faster in the case of a very narrow

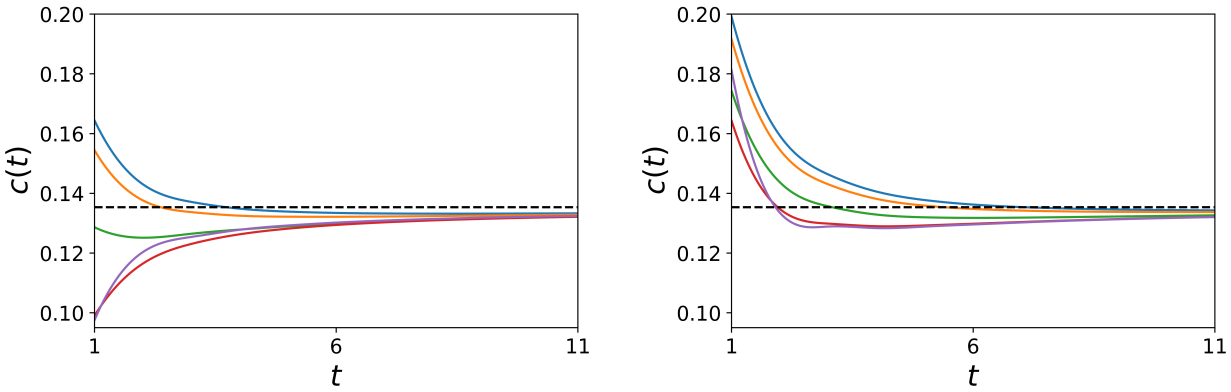

Figure 3.20: *The propagation speed $c(t)$ for various values of $\tilde{N}$, where the population density brought over the road is (a) $\Psi \to 0$ corresponding to $\delta \to \infty$ and (b) $\Psi = \Psi_{max} \approx 0.037$ corresponding to $\delta \to 0$. The threshold density values are $\tilde{N} = 0.01h$ (blue solid line), $\tilde{N} = 0.02h$ (orange solid line), $\tilde{N} = 0.1h$ (green solid line), $\tilde{N} = 0.5h$ (red solid line), and $\tilde{N} = 0.9h$ (purple solid line). The other parameters are $\Phi = 0.01$, $h = 0.1$, $\sigma = 0.1$, and $A = 2.5$.*

road $\delta \to 0$.

The examples of the propagation speed $c(t)$ for various values of the detection threshold $\tilde{N}$ are shown in Fig. 3.20. We first vary $\tilde{N}$ when $\Psi \to 0$ (a wide road) where the results are provided in Fig. 3.20a. Although not identical, the underlying behaviour of the propagation speed against the detection threshold remains the same. The propagation speed is then computed for the same choice of $\tilde{N}$ but with population density $\Psi = \Psi_{max}$ (a narrow road); see Fig. 3.20b. It is seen from the figure that decreasing the road width makes the behaviour of the propagation speed more predictable as we now have $c(t) > c^*$ at small times, no matter what the value of $\tilde{N}$ is.

Let us now calculate the propagation speed $c(\tilde{N})$ as a function of the detection threshold at various times. Again, we consider the extreme cases of $\Psi \to 0$ (infinitely wide road) and $\Psi = \Psi_{max}$ (infinitely narrow road) where the results are shown in Fig. 3.21a and Fig. 3.21b respectively. The results in the figure suggest that a rapid transition to the asymptotic regime occurs in the case of a narrow road in a spatial domain, while the propagation speed depends heavily on the detection threshold density as time progresses in the wide road environment.

Next, we compare the transition time (2.11.6) in the no road case and when the road

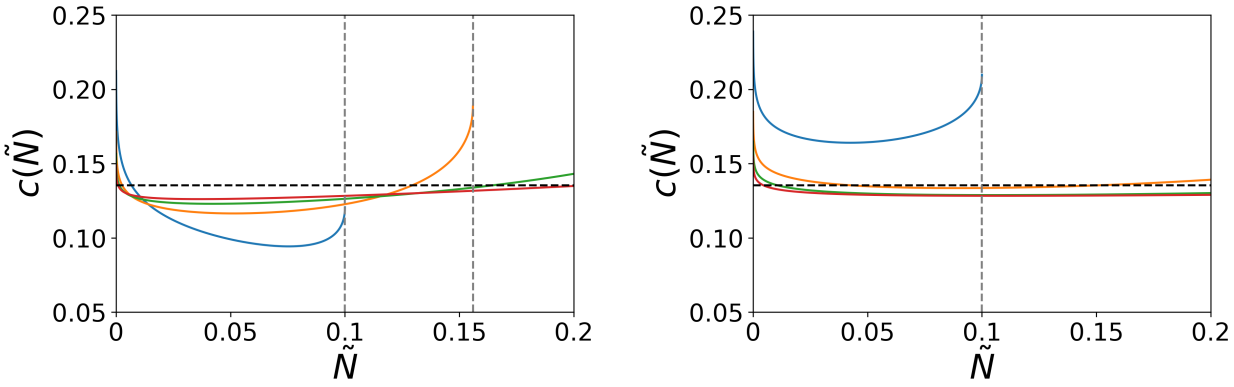

Figure 3.21: *The propagation speed $c(\tilde{N})$ for various values of t, and asymptotic propagation speed* (2.11.5) *(black dashed line), where the population density brought over the road is (a) $\Psi \to 0$ corresponding to $\delta \to \infty$ and (b) $\Psi = \Psi_{max} \approx 0.037$ corresponding to $\delta \to 0$. The time increments are $t = 1$ (blue solid line), $t = 2$ (orange solid line), $t = 3$ (green solid line), and $t = 4$ (red solid line). The other parameters are $\Phi = 0.01$, $h = 0.1$, $\sigma = 0.1$, and $A = 2.5$.*

width $\delta \to 0$ in Fig. 3.22a. It is readily seen from the figure that the transition time is not the same in both cases as we have a different propagation speed at the short-time scale, as discussed earlier. The transition time depends now on the quantity Ψ as well as the detection threshold $\tilde{N}$, and the transition time as a function of the threshold density $\tilde{N}$ is shown in Fig. 3.22b for various values of Ψ. It can be seen from the figure that changing Ψ results in the minimum and maximum transition times, as does the transition time for a given threshold. However, it is worth noting here that the overall behaviour of the transition time with increasing $\tilde{N}$ remains the same as in the no road case (cf. Fig. 2.14). We also demonstrate how the transition time changes when we decrease the road width (*i.e.*, the amount of the population density Ψ is increased) in Fig. 3.22c where a very different behaviour of the transition time is observed for different threshold values.

Finally, we investigate the distance d the invasive species travels from the road edge over a given time T from the road edge $x = b + \delta$. The graphs $d(T)$ are presented in Fig. 3.23a where we compare the case of a narrow road ($\delta \to 0$, $\Psi = \Psi_{max}$) and a wide road ($\delta \to \infty$, $\Psi \to 0$). The detection threshold density is selected as $\tilde{N} = 0.01h$ in line with the discussion of $d(T)$ in chapter 2. It is seen from the graphs that at any time T, the size of an invaded domain is for a very wide road than for a very narrow road.

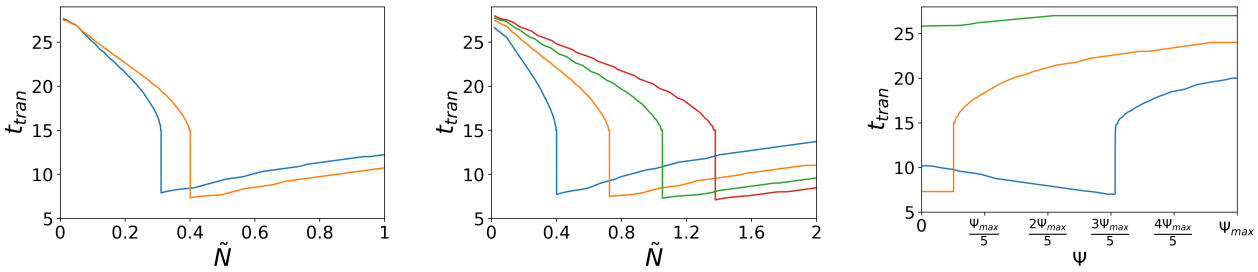

(a) (b) (c)

Figure 3.22: *The transition time t_{tran} given by Eq.* (2.11.6) *in the heterogeneous environment. The parameters used in computation are $\Phi = 0.01$, $A = 2.5$, $\epsilon = 0.01c^*$, $h = 0.1$, and $\sigma = 0.1$ (cf. Fig. 2.14). (a) The no road case (blue solid line) vs the road case as the road width $\delta \to 0$, i.e., $\Psi = \Psi_{max} = 0.037$ (orange solid line). (b) The transition time against the detection threshold density $\tilde{N}$ for various values of Ψ: the infinitely narrow road $\Psi = \Psi_{max} = 0.037$ (red solid line), $\Psi = 2\Psi_{max}/3$ (green solid line), $\Psi = \Psi_{max}/3$ (orange solid line), and the infinitely wide road $\Psi \to 0$ (blue solid line). (c) The transition time against the amount of the population density Ψ for various values of the detection threshold density $\tilde{N}$: $\tilde{N} = 10h$ (blue solid line), $\tilde{N} = 5h$ (orange solid line), and $\tilde{N} = h$ (green solid line).*

Let us introduce the invasion ratio $r(T)$ as

$$r(T) = \frac{d(T, \delta_1)}{d(T, \delta_2)}, \tag{3.3.7}$$

for two roads of width $\delta_1 \to \infty$ and $\delta_2 \to 0$, respectively. The function $r(T)$ is shown in Fig. 3.23b, where the relative size of the invaded region remains $r(T) < 1$ for any $T > 0$. This result agrees with our previous conclusions: while the asymptotic propagation speed does not depend on the road width, propagation in a transient regime is slower in the presence of a wide road when a smaller the population density is brought from behind the road at each time step. Hence, the construction of a wide road slows down invasion in the spatial domain in front of the road.

3.4 Summary

In this chapter, we have developed a novel model that allows one to take into account different dispersal and growth behaviour of invasive plant species when a road is presented in a spatial domain. A stage-structured population has been considered in the model

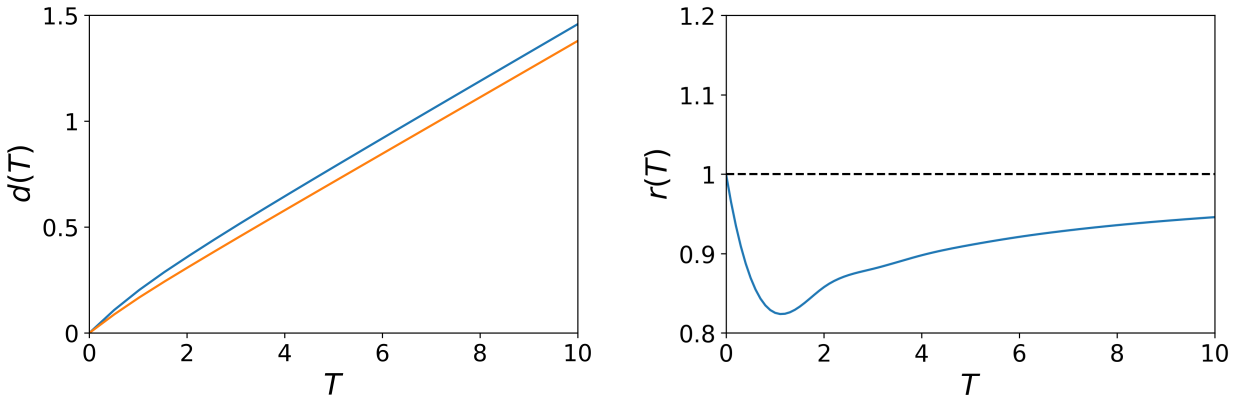

(a) (b)

Figure 3.23: *(a) The distance d covered by the invasive species over the time T from the point x where it has been detected at time $t = 0$. The amount of population density brought over from behind the road is given by $\Psi \to 0$ (blue solid line) and $\Psi = \Psi_{max}$ (orange solid line). The other variables are $\tilde{N} = 0.01h$, $\Phi = 0.01$, $A = 2.5$, $h = 0.1$, and $\sigma = 0.1$. (b) The relative size of the invaded domain $r(T)$ given by* (3.3.7) *when the road width $\delta_1 \to \infty$ and $\delta_2 \to 0$. The other parameters are the same as in Fig. 3.23a.*

where the condition of no growth in the road sub-domain has been implemented at the growth stage, and the dispersal stage has included clearing the population from the road.

The results obtained demonstrate that, in the case of the short-distance dispersal, the growth function is the dominant factor determining how the species propagates. In particular, the choice of growth function determines which behaviour regimes can occur. As for Ricker growth, the barrier and corridor regimes were observed for the Allee growth function. However, in the Allee growth case, a third regime emerges in the problem, the beachhead regime. This occurs due to negative growth at low population densities. Furthermore, when the growth and dispersal parameters in the problem are fixed, the propagation regime depends solely on the road width δ. We have shown that that there exists a threshold value of the road width δ, that separates the barrier and corridor regimes. If one is in the barrier regime, where the population density is unable to cross over the road and invade the domain in front of the road, and decrease the road width δ below this threshold value, one moves to the corridor regime where the population density goes on to invade the domain in front of the road. Conversely if one is in the corridor regime and increased the road width δ, one moves from the corridor regime to the barrier

regime.

When the Allee growth function was investigated, more complex behaviour emerged in the problem. For the Allee growth function both the barrier and corridor regime as in the case of the Ricker growth function was observed. However, due to negative growth for small population densities, in the case of the Allee growth function a third new regime emerges in the problem, the beachhead regime. In the beachhead regime some small population density has spread to the domain in front of the road, however, once the growth function has been applied, the population density in front of the road decreases. This back and forth between population density being brought from behind the road to in front of the road, and then the population density decreasing, leads to non-zero population density being present in front of the road which does not go on to invade further into the domain as time progresses. The beachhead regime can be thought of as the transition between the corridor and barrier regimes. Unlike the barrier regime, some population density can spread from behind to in front of the road,but not enough to invade the rest of the domain, as in the corridor case.

We have shown that a small change in conditions of the environment favouring the invasive species, for example, due to climate change, can change the propagation regime, allowing the invasive species to invade the domain in front of the road where it previously could not spread.

Having investigated the spatial temporal distribution of the population density in the heterogeneous domain, we then moved our attention towards the problem of the propagation speed at the short time scale for the Ricker growth function. We have demonstrated that even in this relatively simple case, where the propagation speed is asymptotically constant, non-linear spatio-temporal dynamics appear at short times where conclusions about the propagation regime depend on the detection threshold density in the heterogeneous landscape. Depending on the detection threshold, we have shown that the propagation speed at short time scales can be greater than or less than its long-time constant behaviour. It is, therefore, not possible to predict, from measuring the propagation speed at

the beginning of invasive spread, whether the rate of invasion will increase or decrease or the time it will take the invasive species to become established in the dispersal domain.

Another factor to take into account is the population density brought over the road, and that quantity also contributes to the non-linear behaviour of the propagation speed and the transition time at the short-time scale. This adds another layer of uncertainty to the problem, where, apart from the changes in the detection threshold density, small changes in this population density can also lead to different values of the transition time.

Meanwhile, the population density brought across the road depends on the road width, and that parameter alone can be used to control the propagation of the invasive species in the spatial domain. The distance the invasive species propagates over a given time from the location where it has been first detected in front of the road depends on the road width, and invasion slows down in the presence of a wide road.

Chapter 4

The 2-D Problem

In Chapters 2 and 3, we introduced and investigated the one-dimensional model. In this chapter the two-dimensional problem will be investigated. The one-dimensional model is interesting in its own right and allowed us to gain significant insight into the problem within a simplified setting. However, the two-dimensional problem is more realistic to the real world problem. Although this is the case, one will see that many of the results and insights gained in the one-dimensional problem can be directly applied to the two-dimensional problem when the strength of dispersal is the same in all directions. Therefore, the results in the one-dimensional case will help to inform the results and directions of investigation in the two-dimensional case. However, certain dynamics and interactions of the problem are only possible if we consider the two-dimensional model. This understanding of the two-dimensional problem is needed to apply the insights gained to a real-world problem; however, it is important to understand the potential scale of the problem. The case where the dispersal is the same in all directions will be considered first.

4.1 Isotropic Dispersal

We are now working in two-dimensional space, where x, and y are chosen to be the two spatial dimensions. A position in two-dimensional space is denoted by $\mathbf{r} = (x, y)$. The dispersal domain will be a square domain defined as follows,

$$\Omega = \{(x, y) : -L \leq x \leq L, -L \leq y \leq L\}. \tag{4.1.1}$$

The demographic stage is defined by the growth function, this was also the case in the one-dimensional model (2.2.1). However, here the spatial location is given by $\mathbf{r}$, thus the two-dimensional demographic stage is defined by,

$$N_t^{gr}(\mathbf{r}) = F(N_t(\mathbf{r})).$$

Next, the dispersal stage is required and is defined by the dispersal kernel, the dispersal kernel was first defined in the one-dimensional case (2.2.2). The two-dimensional version gives the probability of moving from position $\mathbf{r}^* = (x^*, y^*) \in \Omega$ to position $\mathbf{r} = (x, y) \in \Omega$, given by $k(\mathbf{r}, \mathbf{r}^*)$. The dispersal domain (4.1.1) is closed and, therefore, none of the population density can escape,

$$\int_\Omega k(\mathbf{r}, \mathbf{r}^*) d\mathbf{r}^* = \int_\Omega k(\mathbf{r}, \mathbf{r}^*) d\mathbf{r} \equiv 1.$$

In the one-dimensional case we explored both the Ricker growth function (2.1.1) and the Allee growth function (2.6.2), we will also explore both of these functions in two-dimensions. The growth functions' behaviour is the same in the two-dimensional case because they only depend on the population density at a point in space. The only difference is that they will depend on a point in two-dimensional space, where the two-dimensional Ricker growth function is given by,

$$F(N_t(\mathbf{r})) = AN_t(\mathbf{r}) \exp(-N_t(\mathbf{r})), \tag{4.1.2}$$

and the two-dimensional Allee growth function is given by,

$$F(N_t(\mathbf{r})) = \frac{\rho N_t^2(\mathbf{r})}{\xi + N_t^2(\mathbf{r})}. \tag{4.1.3}$$

Then after the dispersal stage the population density for the next generation is given by,

$$N_{t+1}(\mathbf{r}) = \int_\Omega k(\mathbf{r}^*, \mathbf{r}) N_t^{gr}(\mathbf{r}^*) d\mathbf{r}^*. \tag{4.1.4}$$

Initially, the dispersal kernel considered will be the two-dimensional normal distribution,

$$k(|\mathbf{r} - \mathbf{r}^*|) = \frac{1}{2\pi\sigma^2} \exp\left(-\frac{|\mathbf{r} - \mathbf{r}^*|^2}{2\sigma^2}\right). \tag{4.1.5}$$

We will also consider a road-model with a rectangular road domain. The total dispersal domain is defined by

$$\Omega = \{(x, y) : -L \leq x \leq L, -L \leq y \leq L\},$$

where the road domain in two dimensions is given by

$$\Omega_R = \{(x, y) : x_1 \leq x \leq x_2, -L \leq y \leq L\},$$

and, therefore, the no road domain is defined to be $\Omega_{NR} = \Omega \backslash \Omega_R$. The population density over the road can now be defined,

$$N^R(\mathbf{r}) = \begin{cases} N(\mathbf{r}), & \text{if } x \in \Omega_R \\ 0, & \text{otherwise.} \end{cases} \tag{4.1.6}$$

To define the two-dimensional model with the road, firstly the integro-difference equation is applied in the same way as in the no road model (4.1.4), however this is treated as half

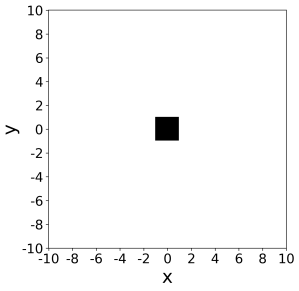

Figure 4.1: *Initial population density* $N_0(\boldsymbol{r})$.

a time increment,

$$N_{t+\frac{1}{2}}(\mathbf{r}) = \int_{\Omega} k(\mathbf{r}, \mathbf{r}^*) N_t^{gr}(\mathbf{r}^*)\, d\mathbf{r}^*, \tag{4.1.7}$$

then the additional dispersal kernel for the road is applied using the growth function $G(N) = N$

$$N_{t+1}^{R}(\mathbf{r}) = \int_{\Omega} k(\mathbf{r}, \mathbf{r}^*) N_{t+\frac{1}{2}}(\mathbf{r})\, d\mathbf{r}^*. \tag{4.1.8}$$

Next, combining (4.1.7) and (4.1.8) the population density at time $t+1$ is obtained before the road clearing is applied,

$$\hat{N}_{t+1}(\mathbf{r}) = N_{t+\frac{1}{2}}(\mathbf{r}) + N_{t+1}^{R}(\mathbf{r}).$$

Finally, the remaining population density across the road is removed by applying the growth functions $H(N) = 0$ and $G(N)$

$$\begin{aligned} N_{t+1}(\mathbf{r}) &= \begin{cases} H(\hat{N}_{t+1}(\mathbf{r})), & \text{if } \mathbf{r} \in \Omega_R \\ G(\hat{N}_{t+1}(\mathbf{r})), & \text{otherwise,} \end{cases} \\ &= \begin{cases} 0, & \text{if } \mathbf{r} \in \Omega_R \\ \hat{N}_{t+1}(\mathbf{r}), & \text{otherwise,} \end{cases} \end{aligned} \tag{4.1.9}$$

the final population density for the two-dimensional road model has been obtained.

Throughout, the initial population density will consist of a square of constant popu-

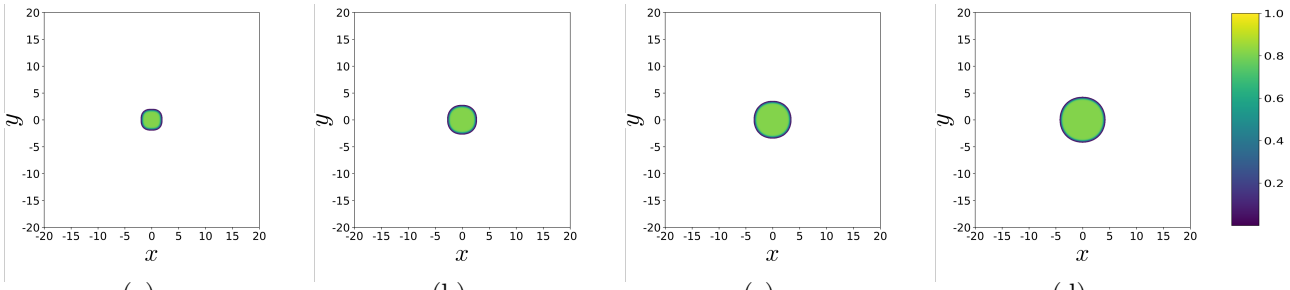

Figure 4.2: *The no road model: a traveling wave solution* $N(\boldsymbol{r}, t)$ *for the problem* (4.1.4), (4.1.10) *with the growth function* (4.1.3). *The parameters are* $\xi = 0.15$, $\rho = 1$, *and* $\sigma = 0.1$. *(a) The population density distribution* $N_t(\boldsymbol{r})$ *at* $t = 25$. *(b) The invasive species spreads further into the space as time progresses,* $t = 50$, *(c, d) This spread continues with time,* $t = 75$, *and* $t = 100$.

lation density

$$N_0((x-y)) = \begin{cases} \alpha, & \text{if } x \in [a,b] \text{ and } y \in [c,d], \\ 0, & \text{otherwise,} \end{cases} \tag{4.1.10}$$

unless specified $a = c = -1$, $b = d = 1$, giving $x \in [-1, 1]$, and $y \in [-1, 1]$ (see Fig. 4.1). The computational cutoff will be fixed at $\tau = 10^{-7}$ throughout.

From one-dimension to two-dimensions

Many of the results in the 1-D case can be transferred to the 2-D case in both the no road case and the road case, with a road of uniform width spanning the y-axis and using the Gaussian dispersal kernel. In the 1-D no road model, for the survival case a traveling wave solution was observed, the same is true here for the 2-D case. Using the parameters $\rho = 1$, $\xi = 0.15$ for the growth function (4.1.3), how the population density evolves with time in the no road case can be seen in figure 4.2.

As long as the population density becomes established and does not go to extinction, a similar picture with varying rates of spread will be obtained for any choice of parameters in the no road case.

Next, we will investigate the impact of including a rectangular road in the domain. As in the 1D case, three distinct cases of behaviour were observed for the Allee growth

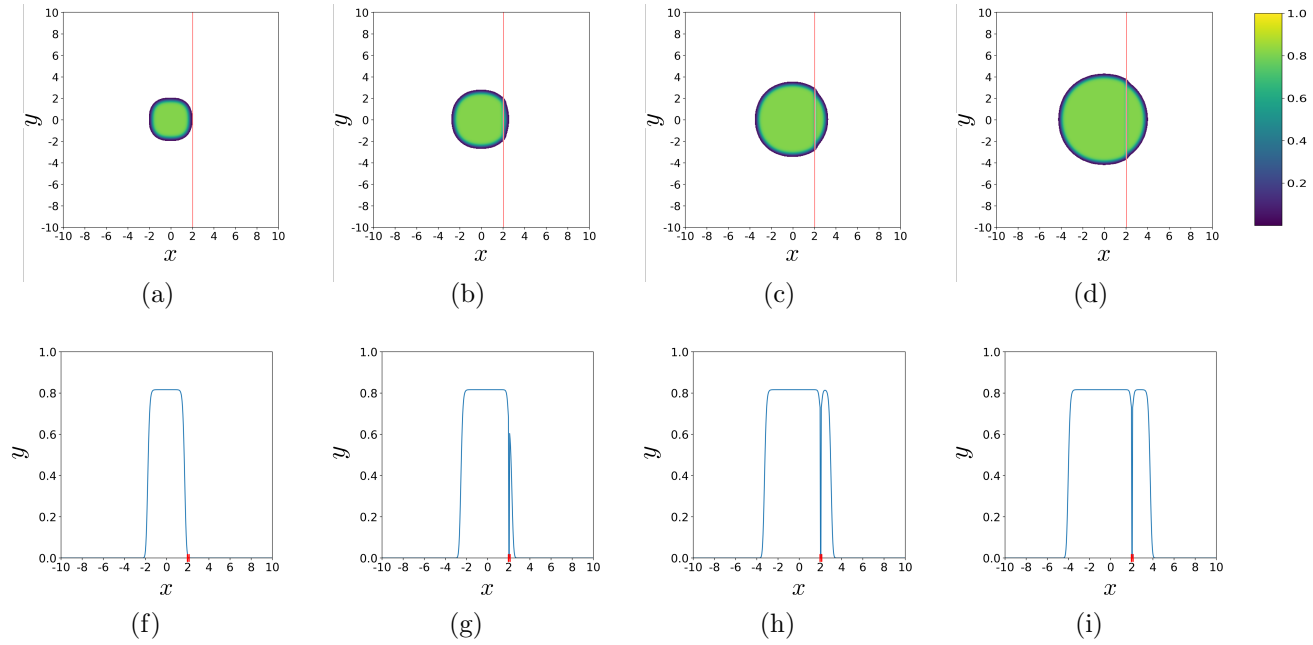

Figure 4.3: *Corridor Regime: spatio-temporal dynamics of the population density* $N(\boldsymbol{r}, t)$ *in the problem* (4.1.7)-(4.1.9) *with the growth function* (4.1.3)*, where* $\xi = 0.15$*,* $\rho = 1$*. The road region is shown in red, where the road width* $\delta = 0.12$ *in the* x*-axis results in the corridor case. (a) The population density distribution* $N_t(x)$ *at time* $t = 25$*, the invasive species reaches the road, (b) The invasive species propagates in front of the road,* $t = 50$*, (c, d) The invasive species spreads further into the space, t=75, t=100.*

function, the barrier, beachhead, and corridor cases. All three cases of behaviour are also obtained in the two-dimensional case. For a demonstration of the behaviour of each of these cases in the 2-D domain see Fig. 4.3, 4.4, and 4.5.

4.1.1 Analytical results

So far similar behaviour has been observed in the 1 and 2 dimensional cases. The possible cases for the population density have now been explored for the Allee growth function in the 2-D domain with a simple rectangular road domain spanning the y-axis. The same set of possible regimes for the invasive species in front of the road have been obtained as in the 1-D case. The question remains can we apply the results and understanding gained in the 1-D case to the 2-D case? In order to truly compare the 1-D and 2-D results and demonstrate that the results obtained in 1-D can be directly applied to the 2-D case, it

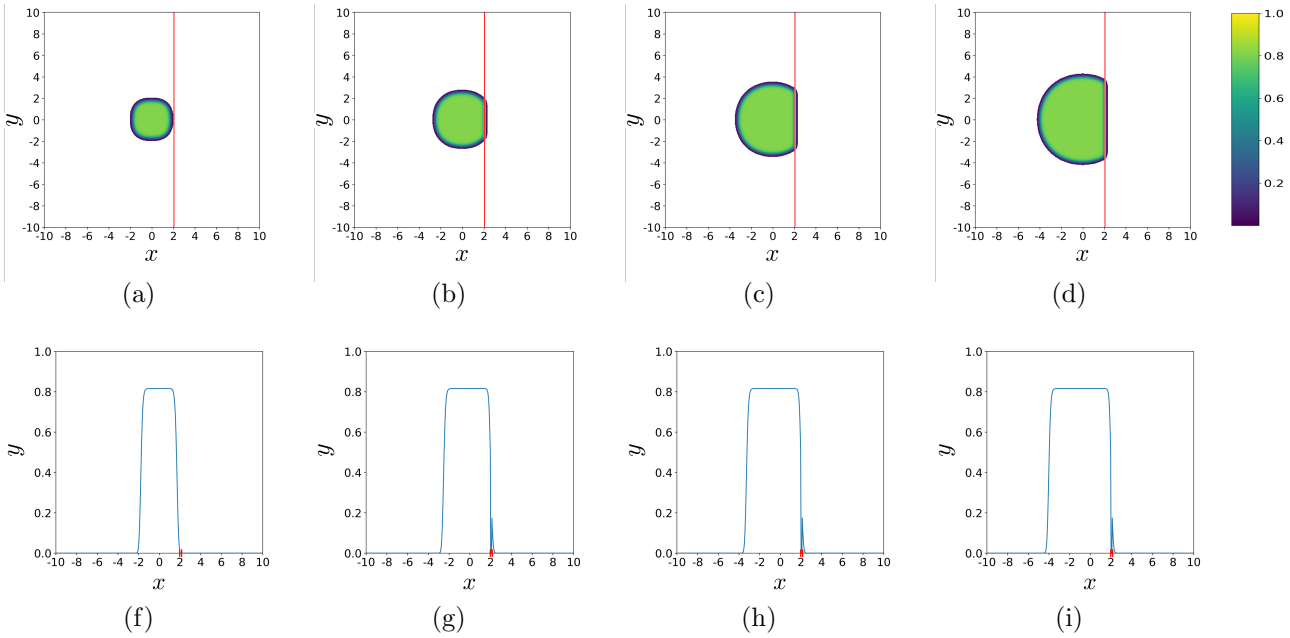

Figure 4.4: *The beachhead regime in the problem* (4.1.7)-(4.1.9) *with the growth function* (4.1.3). *The road with is* $\delta = 0.16$, *the other parameters are the same as in Fig. 4.3. (a) The population density distribution* $N_t(x)$ *at time* $t = 25$, *the invasive species reaches the road, (b) The invasive species propagates in front of the road,* $t = 50$, *(c) As time progresses the population density remains in front of the road, however, the invasive species does not continue to invade in the* x*-axis,* $t = 75$, *(d) The maximum distance reached in the* x*-axis in front of the road remains stable as time progresses,* $t = 100$.

is necessary to show that the cases of behaviour in front of the road are comparable for a large range of variables. This can be done by obtaining analytical results in-line with the analytical results obtained in the 1-D case.

In the 2-D case an additional parameter needs to be considered in the Gaussian dispersal kernel. The dispersal parameter σ in both the x and y directions can now be altered. Firstly, for the analytical results the 2-D Gaussian dispersal kernel the x and y components are independent and therefore it can be split into its x, and y components,

$$k((x,y)-(\tilde{x},\tilde{y})) = \left(\frac{1}{\sqrt{2\pi\sigma_x^2}}\exp\left(\frac{-(x-\tilde{x})^2}{2\sigma_x^2}\right)\right)\left(\frac{1}{\sqrt{2\pi\sigma_y^2}}\exp\left(\frac{-(y-\tilde{y})^2}{2\sigma_y^2}\right)\right). \tag{4.1.11}$$

Analytical results can, thus, be obtained in-line with the 1-D results by treating the dispersal kernel as the product of two 1-D Gaussian dispersal kernels.

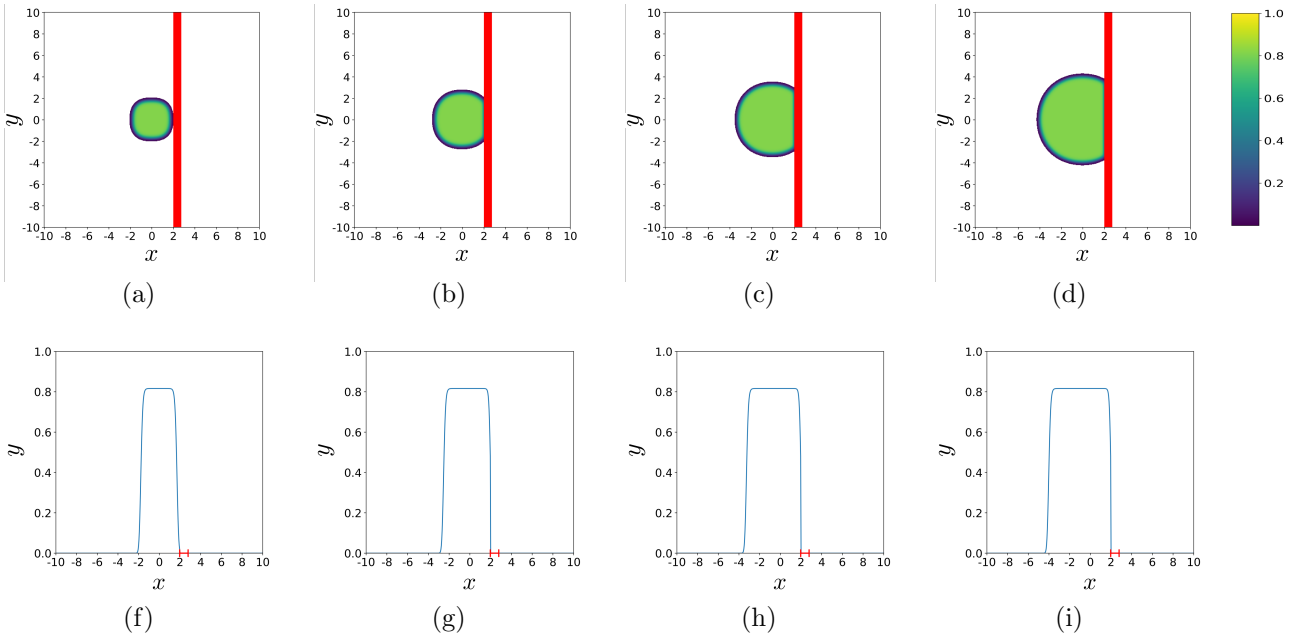

Figure 4.5: *The barrier regime in the problem* (4.1.7)-(4.1.9) *with the growth function* (4.1.3). *The road with is* $\delta = 0.78$, *the other parameters are the same as in Fig. 4.3. (a) The population density distribution* $N_t(x)$ *at time* $t = 25$, *the invasive species reaches the road, (b) At* $t = 50$ *the invasive species has not spread in front of the road, (c, d) As time progresses* $t = 75$, $t = 100$, *the invasive species remains blocked by the road as it acts as a barrier, preventing the species spreading in front of the road. This remains the case for all future time.*

The analytical result is found to be

$$\tilde{N}_1^R(x, y) = F(\alpha)\phi(x, \delta), \tag{4.1.12}$$

where the function $\phi(x, \delta)$ is given by given in the Appendix B.

Then

$$\tilde{N}_{\frac{1}{2}}(x, y) = F(\alpha)\frac{1}{4}\left(\text{erf}\left(\frac{(b-x)}{\sigma_x\sqrt{2}}\right) + \text{erf}\left(\frac{x-a}{\sigma_x\sqrt{2}}\right)\right)\left(\text{erf}\left(\frac{(n-y)}{\sigma_y\sqrt{2}}\right) + \text{erf}\left(\frac{y-m}{\sigma_y\sqrt{2}}\right)\right),$$

where

$$\tilde{N}_1(x, y) = \tilde{N}_{\frac{1}{2}}(x, y) + \tilde{N}_1^R(x, y).$$

4.1.2 Comparison to The 1D Case: When $\mathbf{y = 0}$

Now the analytical result has been obtained in 2-D, the overall behaviour can be explored in more detail. Firstly, how the 2-D results compare to those obtained in 1-D will be explored. In order for this to happen the cases of behaviour in front of the road will be compared. It is known that the x and y components are independent in the 2-D Gaussian dispersal kernel. Because we are only interested in the behaviour in front of the road, and, therefore, only interested in the x-direction, we can fix $y = 0$. This means that all of the y components are constant and the following relationship to the 1-D case is obtained

$$\tilde{N}_1(x, y) = \alpha(\tilde{N}_{\frac{1}{2}}(x) + \beta\tilde{N}_1^R(x)), \tag{4.1.13}$$

where $\alpha, \beta > 0$.

If $\alpha = 1$, and $\beta = 1$, we would have the exact same values for the population density at the edge of the road as in the 1-D case. The values of α and β depend on the size of the initial population density. It is thus important to understand how α and β change when the size of the initial population density is adjusted in the y-direction and for what size of population density do α and β approach 1.

Due to analysing the behaviour at $y = 0$, the population density width is set to be the same in either direction $c = -d$. Then one can ask the question how does α and β depend on the width $2c$. Note that the width will also depend on σ_y, which will be fixed at $\sigma_y = 0.1$. The results can be seen in Fig. 4.6.

As the width of the initial population density is increased, so do α and β, approaching $\alpha = \beta = 1$ even before an initial population density width of 1 in the y-direction is reached. The initial width in the y-direction used throughout is 2. Thus, the 2-D results will be in agreement on the population density values at the edge of the road from the analytical results with the 1-D results.

This is important because the analysis in the 1-D case of the various spatio-temporal dynamics regimes and the conclusions made in the 1-D case can be directly transferred

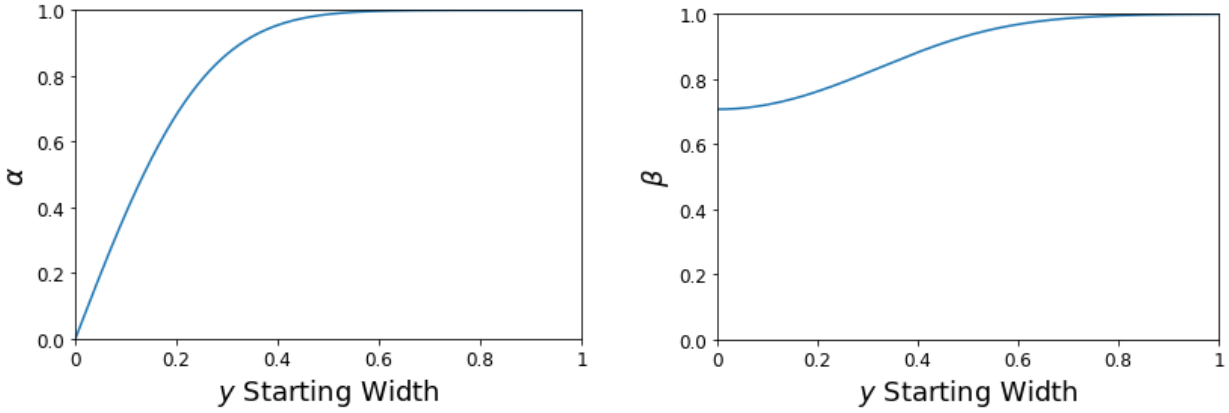

(a) (b)

Figure 4.6: *How the 2-D analytical case tends to the 1-D analytical case for increasing starting population density width. As α and β approach 1, the regimes in the 2-D case approximate the regimes in the 1-D case.*

to the 2-D case for a road of uniform width spanning the y-axis.

4.2 Comparison of the Ricker and Allee growth functions

The beachhead case is due to the region of decay in the Allee growth function when $N - F(N) < 0$. This is between $\bar{N}_0 = 0$, and $\bar{N}_1 = (\rho - \sqrt{\rho^2 - 4\xi})/2$. The left boundary at $N = 0$ does not change and depends on the growth function parameters. Thus, $\bar{N}_1$ is the only equation that needs to be considered. For any given $\rho > 0$ fixed, if $\xi \to 0$, then $\bar{N}_1 \to 0$. As ξ decreases $\bar{N}_1$ also decreases and, therefore, the decay region decreases. The population density values that lead to a decrease subsequently reduce with this, so does the maximum decay. Thus, the cases that lead to a beachhead and subsequently the beachhead region also declines. If $\bar{N}_1 < \tau$ then no beachhead region exists. If this occurs then the Ricker growth function approximates a special case of the Allee growth function.

In order to make comparisons between the Ricker and the Allee growth function, the stable positive steady state is equated and the overall behaviour (the cases that the population density leads to) should be the same. To demonstrate how the Ricker growth function can be viewed as a particular case of the Allee growth function, the Ricker growth

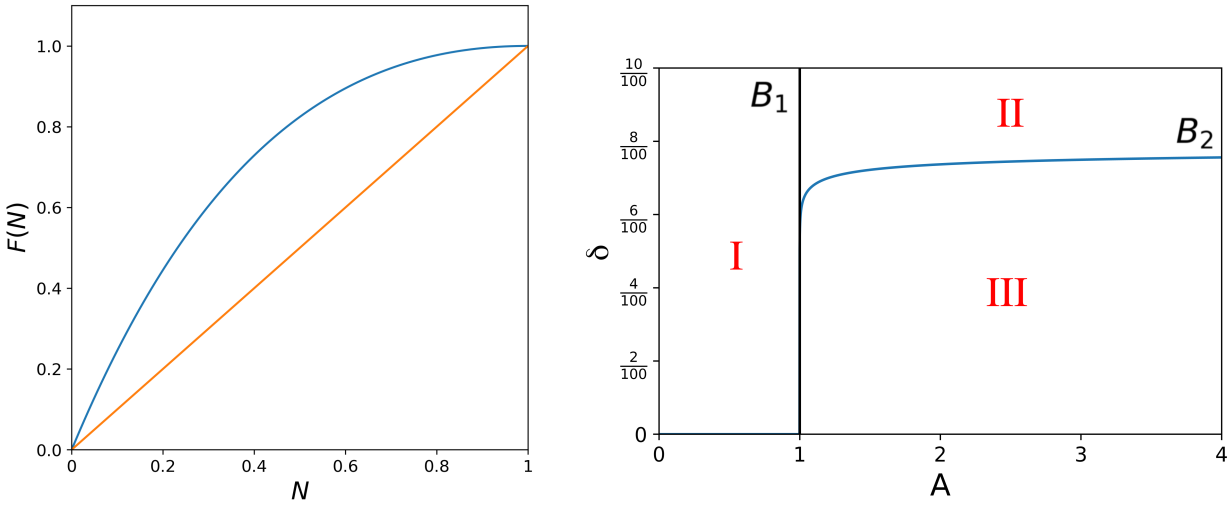

(a) (b)

Figure 4.7: *Ricker growth function: (a) Growth function where* $A = e$, $\bar{N}_1 = 1$, *(b)* (A, δ) *– plane.*

function with $A = e$ along with the (A, δ)-plane can be seen in figure 4.7. In figure 4.8 both the Allee growth function where $\rho = 1$ for decreasing ξ, and the corresponding (ρ, δ)-plane for the given ξ are plotted. It can be seen as ξ decreases the Allee growth function approximates the Ricker growth function where the beachhead case does not exist.

4.3 Directional dispersal

It has been shown that the 1-D results can be applied to the 2-D case as set up above when the starting population density is of a sufficient but small width in the y-direction. However, there are new things to consider in the 2-D case that cannot be solved by directly applying the results and understanding in the 1-D case. Namely we can have directional dispersal, this is where the rate of dispersal in x-direction differs from the rate of dispersal in the y-direction. In the 1-D case it was only possible to consider dispersal in one direction, and in order to apply the 1-D results to the 2-D case we set $\sigma_x = \sigma_y$.

Here it is investigated how the population density changes when $\sigma_x \neq \sigma_y$. The no road case will first be analysed to act as a comparison for the road case. Given a simple starting population density, as long as the species does not go to extinction, given a

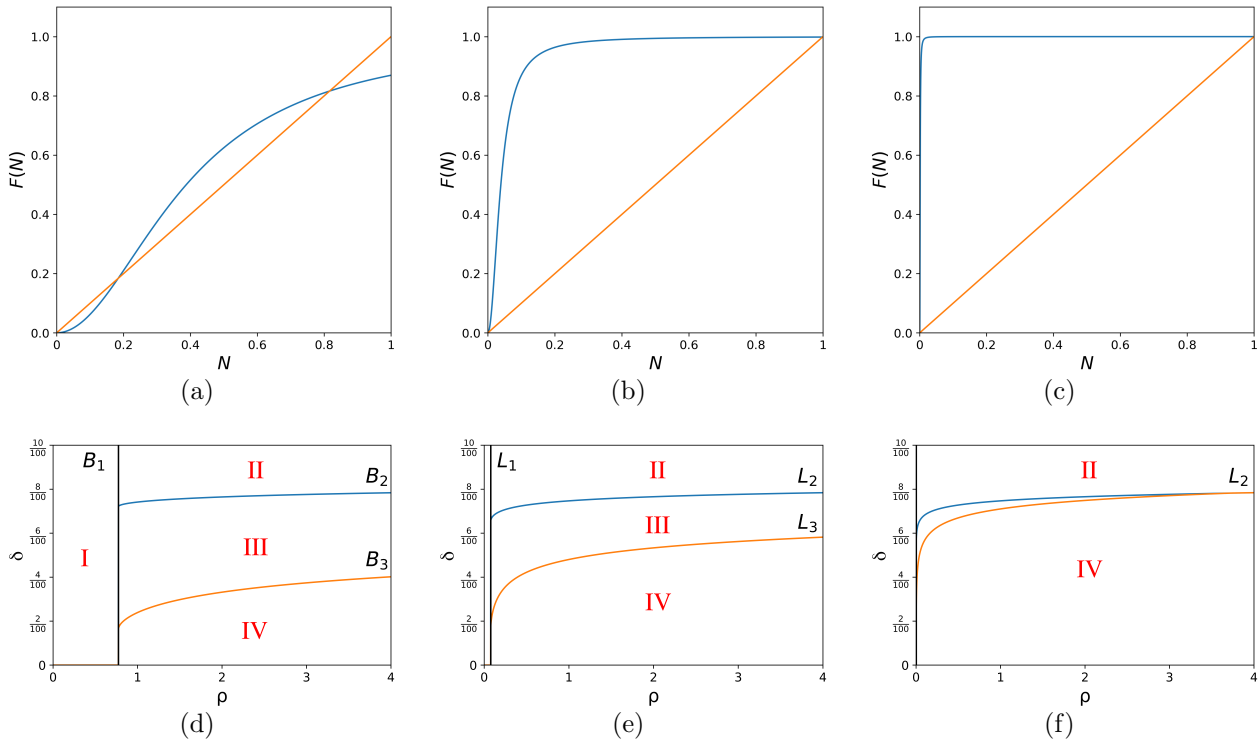

Figure 4.8: *Allee growth function for decreasing values of ξ: (a, b, c) The Allee growth function where $\rho = 1$, for $\xi = 1.5 \times 10^{-1}$, $\xi = 1.5 \times 10^{-3}$, and $\xi = 1.5 \times 10^{-6}$ respectively. As ξ decreases the unstable steady state tends to 0, and the stable steady state tends to 1. When this occurs the behaviour of the Allee growth function approximates the Ricker growth function where there is no region of population density decline, (d, e, f) The (ρ, δ)-plane for $\xi = 1.5 \times 10^{-1}$, $\xi = 1.5 \times 10^{-3}$, and $\xi = 1.5 \times 10^{-6}$ respectively. Region I represents the extinction regime, II the barrier regime, III the beachhead regime, and IV the corridor regime. As ξ declines to 0, the beachhead region reduces, approaching the Ricker growth function where for survival cases we have either the barrier or the corridor case.*

sufficient amount of time it will take the shape of the directional Gaussian dispersal kernel (see Fig. 4.9).

4.3.1 The road case

The behaviour in the no road case remains simple and can be described by a traveling wave with different rates of dispersal in the x-, y-directions. The road case will now be investigated, here the cases of the population density in front of the road will be considered. Firstly, the behaviour will be investigated when σ_y is changed but σ_x is kept fixed. From the analytical results it has been shown that the x and y components can

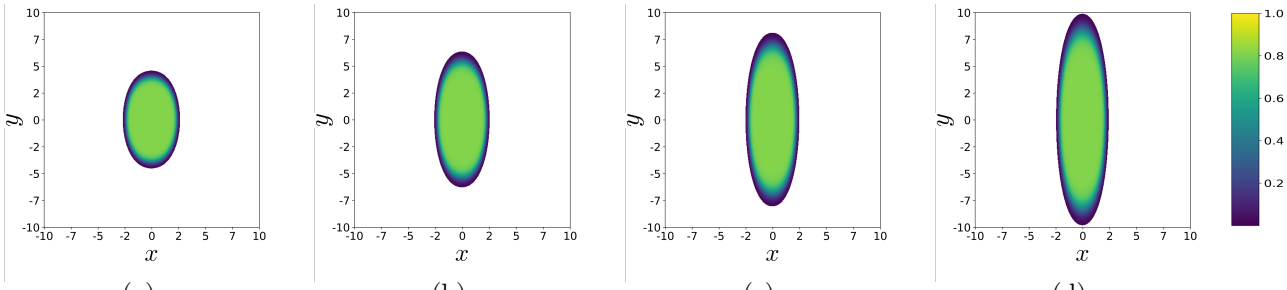

Figure 4.9: *The no road model, $\sigma_x \neq \sigma_y$: for the problem* (4.1.4), (4.1.10) *with the growth function* (4.1.3). *The parameters are $\xi = 0.15$, $\rho = 1$, $t = 50$, $\sigma_x = 0.1$, and $\sigma_y = 0.2, 0.3, 0.4$, and 0.5 for (a), (b), (c), and (d) respectively. Given a sufficient amount of time, the population density takes on the shape of the directional Gaussian dispersal kernel.*

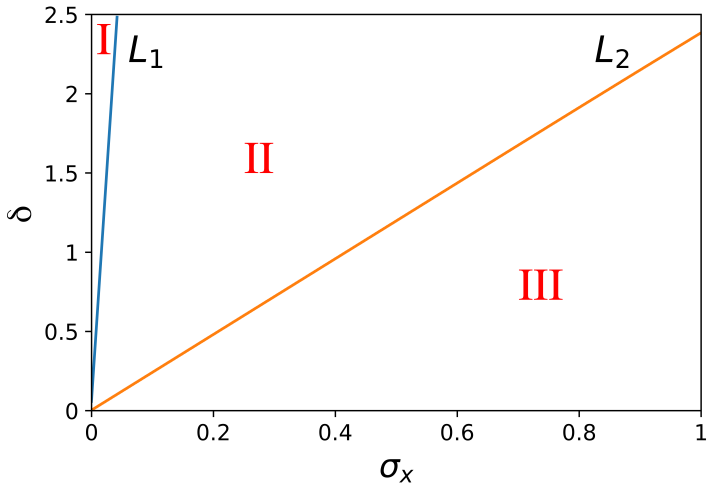

Figure 4.10: *Propagation regimes in the road model* (4.1.7)-(4.1.9) *with the growth function* (4.1.3), *where $\sigma_y = 0.1$ and σ_x is varied. As σ_x is varied we move from the barrier regime, to the beachhead regime, and finally to the corridor regime. The value σ_x for a particular regime and the increase required to move from one regime to another increases with δ.*

be treated separately. Therefore, again when $y = 0$, for a sufficiently large initial starting population density the same results as in the 1-D case will be obtained.

Now the behaviour can be investigated when $\sigma_y = 0.1$ is fixed, and σ_x is changed (see Fig. 4.10). It can be seen for a given road width as σ_x is increased, the invasive species moves from the barrier regime, to the beachhead regime, and then to the corridor regime. The amount σ_x is required to increase for this to happen, increases as the road width δ increases.

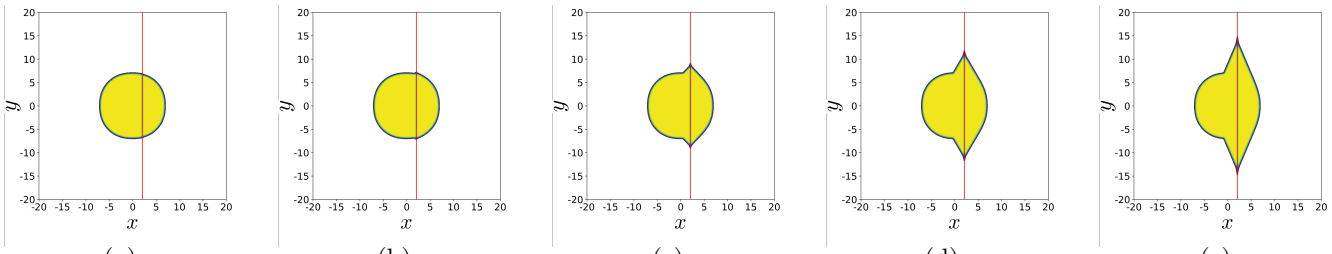

Figure 4.11: *Increased rate of dispersal along the road for varying* σ_y^R*: population density distributions* $N_t(\boldsymbol{r})$ *at time* $t = 50$ *with the Allee growth function* (4.1.3)*. The parameters are* $\xi = 0.02$*,* $\rho = 1$*,* $\delta = 0.2$*,* $\sigma = 0.1$*, and* $\sigma_y^R = \sigma, 2.5\sigma, 5\sigma, 7.5\sigma$*, and* 10σ*, for (a), (b), (c), (d), and (e) respectively.*

4.3.2 Increased σ_y^R along the road compared to the no road domain

So far in 2-D we have explored the no road case both when $\sigma_x = \sigma_y$, and when $\sigma_x \neq \sigma_y$, we have also explored the road case for when $\sigma_x = \sigma_y$, and $\sigma_x \neq \sigma_y$ across the whole dispersal domain. However, in the road case one can vary the behaviour on the road compared to off the road. To account for the behaviour of the invasive species on the road an additional dispersal step is employed, and then the road is cleared at the end of each generation. Up until now we have treated this additional dispersal step as identical to the one chosen in the no road section of the dispersal domain. In this section the impact of choosing a different dispersal kernel for the road domain will be investigated, be that the same dispersal kernel with different parameter choices, or a different dispersal kernel entirely.

In order not to introduce too many variables and to allow one to compare results, the Gaussian dispersal kernel (4.1.5) were $\sigma_x = \sigma_y = 0.1$ will be used for the no road dispersal domain throughout. For conciseness we set $\sigma = 0.1$, to represent this dispersal parameter in both the x, and y directions.

Firstly, we will keep the Gaussian dispersal kernel (4.1.5) for the additional road dispersal step, and also keep $\sigma_x^R = \sigma$, only varying σ_y^R. A comparison of results can be seen in Fig. 4.11.

As σ_y^R is increased the distance the invasive species spreads into the domain in the

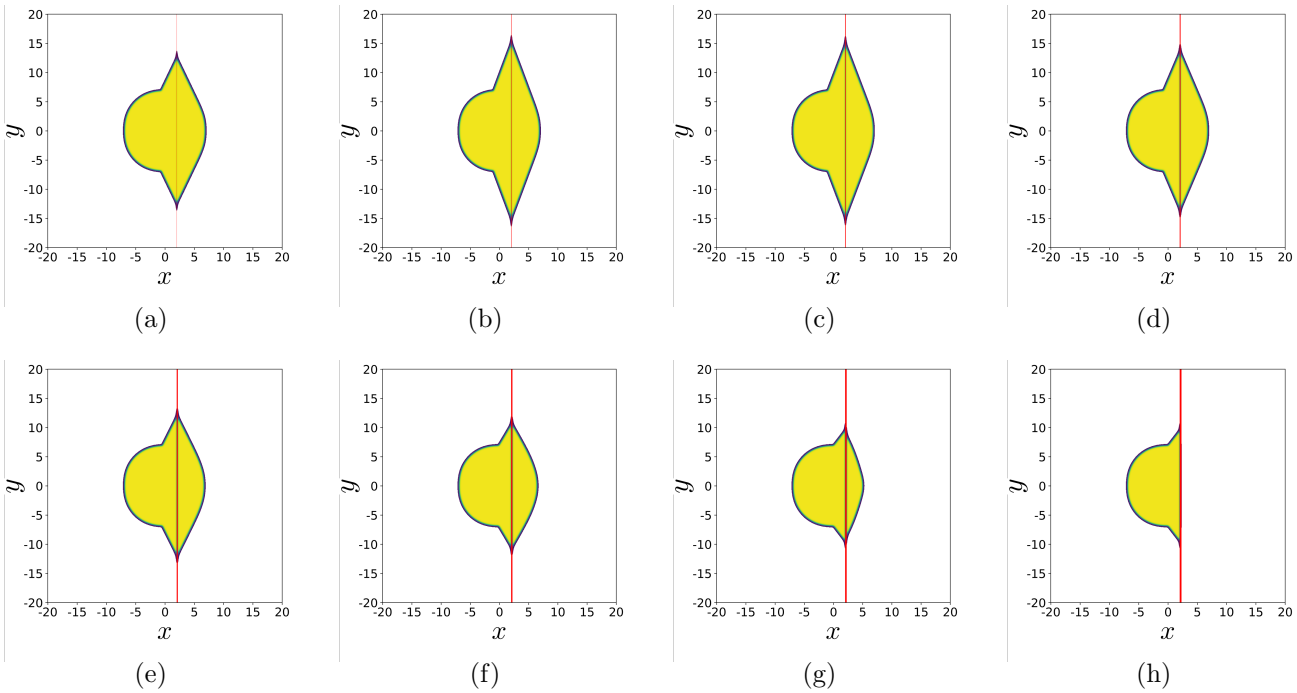

Figure 4.12: *Differing invasion distances in the direction of the road for varying road widths: population density distributions* $N_t(\boldsymbol{r})$ *at time* $t = 50$ *with the Allee growth function* (4.1.3). *The parameters are* $\xi = 0.02$, $\rho = 1$, $\sigma = 0.1$, $\sigma_y^R = 1$, *and* $\delta = 2\upsilon$, 3υ, 4υ, 5υ, 6υ, 7υ, 8υ, *and* 9υ, *where* $\tau = 5/2^7$, *for (a), (b), (c), (d), (e), (f), (g), (h), and (f) respectively. The distance the invasive species spreads into the domain in the* y*-direction initially increases with increasing road width. However, as the width of the road continues to increase the species reaches a maximum distance of spread. This then continues to decline, suggesting that there is an ideal road width for the species.*

y-direction increases.

In Fig. 4.12 the effects of altering the road width on an anisotropic dispersal kernel are investigated. It can be seen that as the road width is increased, we increase the invasion in the y-direction. However, as the road width continues to increase, there is a point the invasion in the y-direction decreases. This suggests that there is an 'ideal' road width for the invasive species given every other parameter is fixed in the problem.

To investigate this further, for a range of road width and rate of dispersal along the road is computed. The difference for the total distance traveled in the direction of the road for $t = 50$, can be seen in Fig. 4.13. However, more importantly in Fig. 4.14 we compare the rate of spread for the different cases computed. Finally, to observe the overall effect of this increased rate of spread on the total population density in the domain, the

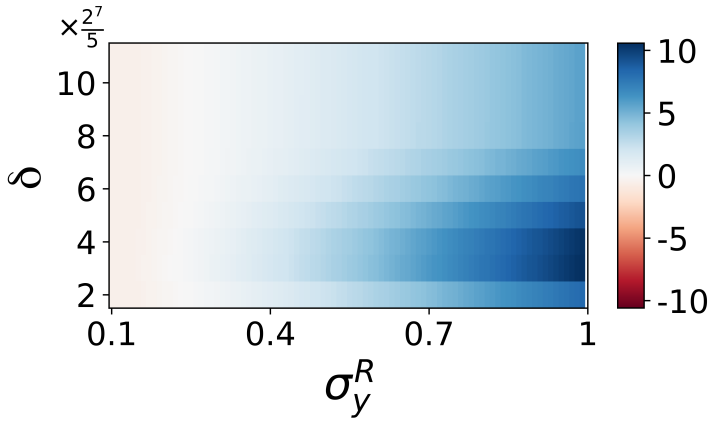

Figure 4.13: *Comparison of the distance traveled in the direction of the road compared to the isotropic case $\sigma_y^R = \sigma$, calculated at time $t = 50$ with the Allee growth function* (4.1.3). *The parameters are $\xi = 0.02$, $\rho = 1$, with varying δ, and σ_y^R. As σ_y^R increases the distance traveled increases. However, as the road width increases, the distance traveled initially increases, reaches a maximum, and then decreases.*

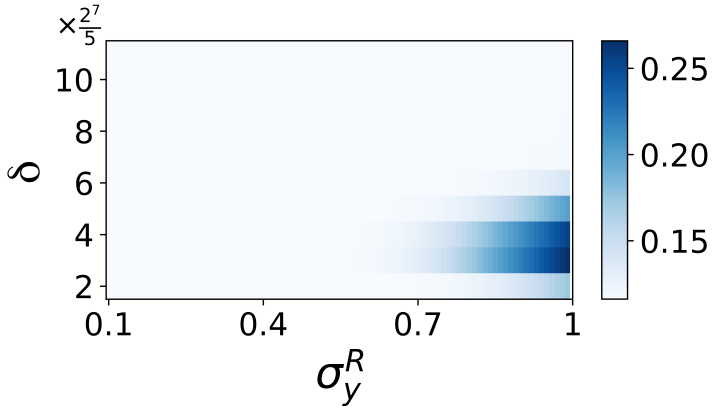

Figure 4.14: *Rate of spread in the dispersal domain in the upward y-direction (equal to the rate of spread in the downward y-direction), calculated at time $t = 50$ with the Allee growth function* (4.1.3). *The parameters are $\xi = 0.02$, $\rho = 1$, with varying δ, and σ_y^R.*

difference as a fraction of the population density of the initial case is plotted in Fig. 4.15.

4.4 Long distance dispersal

Above we investigated the effects of varying the parameters of the Gaussian dispersal kernel along the road. Although some interesting effects were observed in this case, the

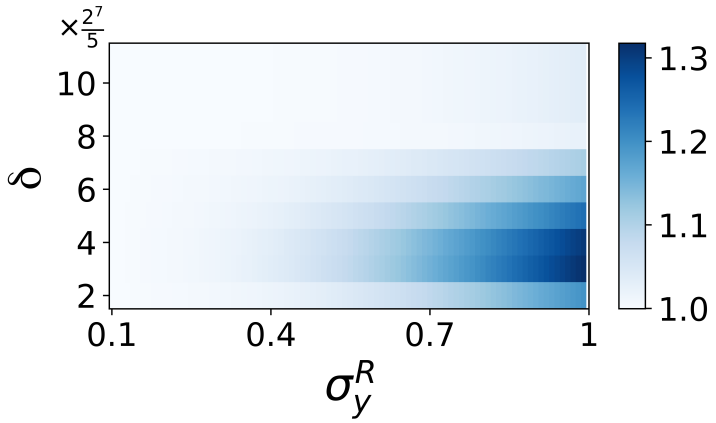

Figure 4.15: *The overall population density compared to the isotropic case* $\sigma_y^R = \sigma$*, calculated at time* $t = 50$ *with the Allee growth function* (4.1.3)*. The parameters are* $\xi = 0.02$*,* $\rho = 1$*, with varying* δ*, and* σ_y^R*.*

Gaussian dispersal kernel is considered to be a short range dispersal kernel. However, there is some evidence that suggests that the geometry and structure of the road leads to long distance dispersal [69, 48, 36]. Therefore, in this section a different long distance dispersal kernel for the additional dispersal step over the road is implemented, the Gaussian dispersal kernel for the no road domain remains.

It has been shown that long distance dispersal events can have a significant impact on the overall population density, both its size and shape. In order to consider this in the model a power-law based dispersal kernel is introduced. The dispersal kernel of choice will be the Cauchy based dispersal kernel. In the 1-D case the Cauchy based dispersal kernel is given by,

$$k(x, x^*) = \frac{\gamma}{\pi((x - x^*)^2 + \gamma^2)}.$$

Unlike the Gaussian based dispersal kernel, the extension from the 1-D case to the 2-D case is not trivial and there exist multiple definitions. The 2-D Cauchy based dispersal kernel proposed in [29] will be implemented

$$k(|(x, y) - (\tilde{x}, \tilde{y})|) = \frac{\gamma}{\pi(\gamma + |(x, y) - (\tilde{x}, \tilde{y})|)^3}. \tag{4.4.1}$$

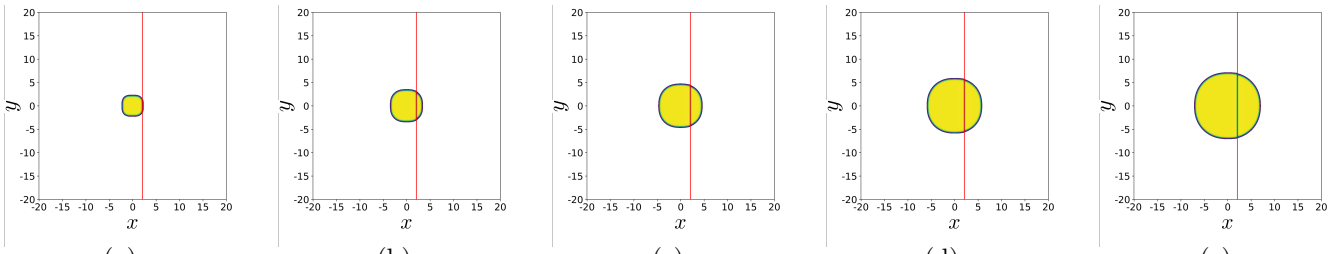

Figure 4.16: *Long distance dispersal along the road: population density distributions* $N_t(\boldsymbol{r})$ *with the Allee growth function* (4.1.3)*, Gaussian dispersal kernel in the no road domain* (4.1.5)*, and the Cauchy dispersal kernel in the road domain* (4.4.1)*. The parameters are* $\delta = 0.2$*,* $\xi = 0.02$*,* $\rho = 1$*,* $\sigma_x = \sigma_y = 0.1$*, and* $\gamma = 0.049$*. Calculated for time* $t = 10$*, 20, 30, 40, and 50, for (a), (b), (c), (d), and (e) respectively. One can see that employing a long-distance dispersal kernel over the road alone does not lead to an increased dispersal for the invasive species.*

In [57], in order to compare any results gained using the Cauchy kernel to the results using the Gaussian kernel, they set the radius to encompass half the probability of the species dispersing to be,

$$\gamma = \sigma(2 - \sqrt{2})\sqrt{\ln 2} \approx 0.4877\sigma.$$

Due to the nature of long range dispersal, a comparatively larger domain than that used for the Gaussian kernel is required (e.g. $L = 80$, compared to $L = 10$).

This symmetric long-distance dispersal Cauchy does not result in an increased rate of invasion along the road. This holds for a range of parameters Fig. 4.16. Thus, the use of a long-distance dispersal kernel is not, by itself, enough to produce an increased rate of invasion.

4.4.1 Anisotropic Cauchy kernel

When the Gaussian kernel is considered, it can be separated into the x and y components, then when the anisotropic dispersal is considered one can simply adjust the dispersal variable σ in the independent x or y direction. However, with the Cauchy kernel, and many other dispersal kernels, the kernel cannot be split into the x and y components. In these

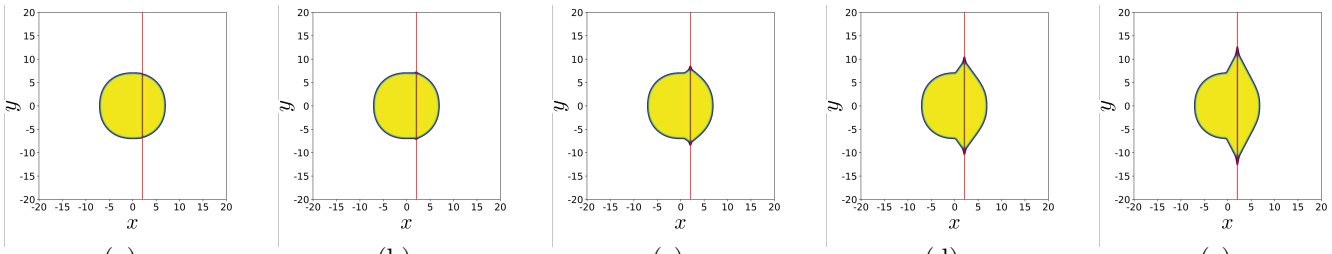

Figure 4.17: *Anisotropic Cauchy dispersal kernel along the road: population density distribution* $N_t(\boldsymbol{r})$ *with the Allee growth function* (4.1.3)*, Gaussian dispersal kernel in the no road domain* (4.1.5)*, and the Cauchy dispersal kernel in the road domain* (4.4.2)*. The parameters are* $\delta = 0.2$*,* $\xi = 0.02$*,* $\rho = 1$*,* $\sigma_x = \sigma_y = 0.1$*, and* $\gamma = 0.049$*. With varying* $\beta = 1$*, 2.5, 5, 7.5, and 10, for (a), (b), (c), (d), and (e) respectively.*

cases it is not trivial to go from the isotropic dispersal kernel to the anisotropic dispersal kernel. Nevertheless, there do exist methods of transforming the isotropic Cauchy kernel into an anisotropic one, from doing so mechanistically [60], to applying a von Mises distribution [25]. Here the framework outlined in [56] will be followed. Putten et al. provide a method where an anisotropic dispersal kernel can be derived by modifying the probability density function. Following this framework, to begin with the dispersal kernel needs to remain centered around the origin, and remain symmetric around the lines $x = 0$, and $y = 0$, the isotropic Cauchy dispersal kernel (4.4.1), therefore, becomes

$$k(|(x,y) - (\tilde{x},\tilde{y})|) = \frac{\gamma}{\pi\beta\left(\gamma + \left|(x-\tilde{x}) + \frac{(y-\tilde{y})}{\beta}\right|\right)^3}, \tag{4.4.2}$$

where β is the shape parameter.

In Fig. 4.17 the Gaussian dispersal kernel is applied to the no road domain, and the anisotropic Cauchy dispersal kernel is applied to the road domain. It can be seen that in this case, an increased rate of invasion is achieved. In Fig. 4.18, we also see a maximum rate of spread is achieved for a particular road width. If the road width is increased or decreased from this 'optimum' road width, the maximum rate of dispersal is decreased.

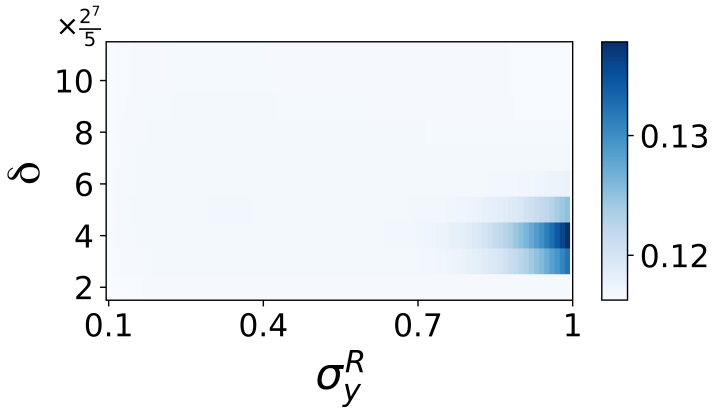

Figure 4.18: *Rate of spread in the dispersal domain in the upward y-direction (equal to the rate of spread in the downward y-direction), calculated at time $t = 50$ with the Allee growth function* (4.1.3)*, Gaussian dispersal kernel in the no road domain, and Cauchy dispersal kernel in the road domain. The parameters are $\xi = 0.02$, $\rho = 1$, with varying δ, and β.*

4.5 Summary

In this chapter we have extended the one-dimensional problem in both the homogeneous and heterogeneous dispersal domains, introduced in Chapter 2, and Chapter 3 respectively to the two-dimensional dispersal domain. When the dispersal kernel parameters are the same in all directions of the dispersal domain, the results and understanding from these previous chapters can be carried over and applied to the 2-D problem. Thus, in the case of isotropic dispersal for the no road case the population density propagates into the domain equally in all directions. When the Ricker (4.1.2) growth function is applied we are in the survival case as long as $A > 1$, and when the Allee (4.1.3) growth function is applied extinction survival case is observed. For the road model with isotropic dispersal the same propagation regimes are observed in the problem as in the 1-D model. For the Ricker growth function, the corridor and barrier regimes, and for the Allee growth function the corridor, beachhead, and barrier regimes are observed. Moreover, as is the case in the 1-D problem, the introduction of a road in the domain in this case, does not lead to an increased rate of dispersal of the population density in the domain.

However, due to now working in two dimensions, the dispersal parameters in the x-axis, and y-axis directions can be chosen to be different, that is to obtain anisotropic

dispersal. In the no road case the behaviour remains the same and the population density forms an ellipse instead of a circle in the dispersal domain after sufficient time is given to transition from the initial condition. However, in the road case, depending on the strength of the dispersal in the y-axis compared to the x-axis, and the road width, an increase in the rate of invasion in the direction along the road can occur. This increase in the rate of invasion is not just confined to the immediate vicinity around the road, but also spreads out to a larger region around the road, leading to an increase in the overall population density in the domain. Interestingly we find that for a given set of growth and dispersal parameters, there exists an optimal road width which leads to the maximum rate of dispersal along the road and to the maximum amount of population density in the dispersal domain for a given time increment.

Chapter 5

Additional Effects in the Heterogenious Landscape

5.1 The Edge Problem

In Chapter 3 we introduced a landscape heterogeneity in the form of a road in the dispersal domain. Where the rest, the non-road portion, of the domain is treated as homogeneous. However, there is evidence to suggest that the make up and conditions in the region of the dispersal domain around the edge of the road is different from the dispersal domain further away from the edge of the road. Depending on the plant species, these 'edge effects' of the road could have either a negative or positive effect on the population density. Here, we therefore investigate the problem of both negative and positive edge effects in the dispersal domain.

5.1.1 Negative Edge Effects

Firstly, the case where the edge effects negatively impact the invasive species will be investigated. The road is of width δ, the edge effects of the road will be applied a distance of $\eta = \hat{\eta}\delta$ from either edge of the road.

Here it is investigated how the propagation of plants in the presence of a road is altered

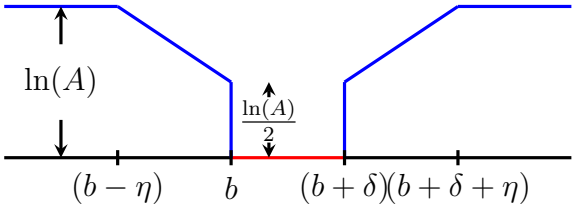

Figure 5.1: *Negative edge effects growth function parameter.*

by incorporating edge effects of the road into the model. It will be investigated both how edge effects that positively and negatively affects the plant species change the overall behaviour of the species. The edge region will not affect the dispersal kernel or dispersal parameters, instead it will affect the carrying capacity in the growth function. The region of the domain which is not in the road or edge regions is called the landscape region. The Ricker growth function Eq. (2.1.1) is considered. The effect of the edge will decrease the carrying capacity over the edge region, compared to the homogeneous landscape region where the carrying capacity is constant,

$$A(x) = \begin{cases} 0, & \text{if } x \in \Omega_R, \\ A(x), & \text{otherwise.} \end{cases}$$

In the case with negative edge effects we assume that the carrying capacity declines linearly until it reaches half its value at the edge of the road compared to the rest of the domain (Fig. 5.1),

$$A(x) = \begin{cases} A, & \text{if } x \in [-L, b-\eta) \cup (b+\delta+\eta, L], \\ \exp\left(\ln\left(A\right)\left(\frac{b-x}{2\eta} + \frac{1}{2}\right)\right), & \text{if } x \in [b-\eta, b], \\ \exp\left(\ln\left(A\right)\left(\frac{x-(b+\delta)}{2\eta} + \frac{1}{2}\right)\right), & \text{if } x \in [b+\delta, b+\delta+\eta], \\ 0, & \text{otherwise,} \end{cases} \tag{5.1.1}$$

i.e. the non-road portion, was treated as homogeneous.

In Fig. 5.2, an example of the spatio-temporal dynamics of the population density

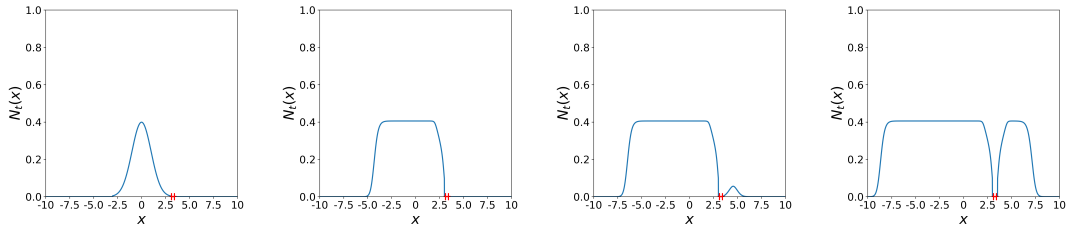

Figure 5.2: *Negative edge effects: spatio-temporal dynamics of the population density $N(x,t)$, with the growth function Eq.* (2.1.1) *where the growth function parameter is given by Eq.* (5.1.1), *and road width $\delta = 0.55$. (a) Initial population density $t = 0$, (b) as the population builds up behind the road $t = 25$ the population density declines in the edge region towards the road, (c) as time progresses $t = 50$ the population density starts to establish in front of the road. However, this process is delayed due to the negative edge effects, (d) $t = 75$ the population density then continues to invade the domain in front of the road and does so at the same rate as the landscape region.*

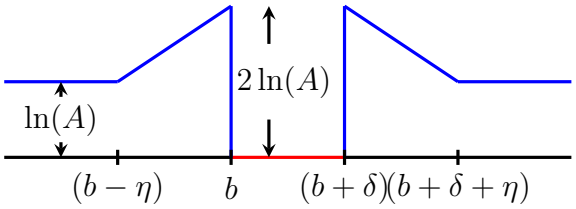

Figure 5.3: *Positive edge effects growth function parameter.*

with negative edge effects is provided.

5.1.2 Positive Edge Effects

In the case with positive edge effects the carrying capacity increases linearly until it reaches $2\ln(A)$ at the edge of the road (Fig. 5.3),

$$A(x) = \begin{cases} A, & \text{if } x \in [-L, b-\eta) \cup (b+\delta+\eta, L], \\ \exp\left(\ln(A)(\frac{x-b}{\eta} + 2)\right), & \text{if } x \in [b-\eta, b], \\ \exp\left(\ln(A)(\frac{(b+\delta)-x}{\eta} + 2)\right) & \text{if } x \in [b+\delta, b+\delta+\eta], \\ 0, & \text{otherwise.} \end{cases} \tag{5.1.2}$$

In Fig. 5.4 an example of the spatio-temporal dynamics of the population density with

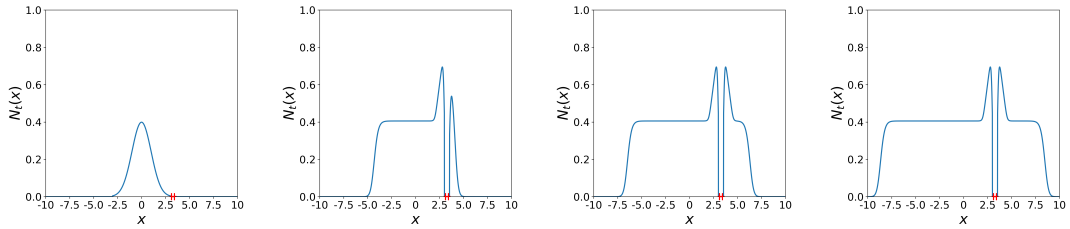

Figure 5.4: *Positive edge effects: spatio-temporal dynamics of the population density* $N(x,t)$*, with the growth function Eq.* (2.1.1) *where the growth function parameter is given by Eq.* (5.1.2)*, and road width* $\delta = 0.55$*. (a) Initial population density* $t = 0$*, (b) as the population builds up behind the road* $t = 25$ *the population density increases in the edge region towards the road compared to the landscape region. Due to the increased carrying capacity the species establishes itself in front of the road at an accelerated pace. (c, d) as time progresses* $t = 50$*,* $t = 75$ *the population density then continues to invade the domain in front of the road and does so at the same rate as the landscape region.*

negative edge effects is provided.

5.1.3 Analytical Results

We will explore how the change of the growth function parameter near the edge of the road changes which barrier, corridor, or beachhead regime we obtain for a given set of parameters. Given a sufficient amount of the time (in the survival case) the population density behind and sufficiently far away from the road will tend towards the carrying capacity. However, near the road the population density will be near to but not equal to the carrying capacity, due to loss from dispersal and the road itself (the road is cleared at the end of a generation). Note this is true even in the no edge effect case, though the analytical solution was approximated by a step function of uniform density equal to the carrying capacity of the invasive species. In the edge effect case, we also have population density spill over from the domain not affected by the road which may result in the population density in the edge domain being above the carrying capacity for this area.

As with the no edge effect case for the analytical solution a simplification of the population density behind the road was required, the same will be true for the edge effect

case. We will first look at the case where the edge negatively impacts the species. The population density will be set to the carrying capacity for the growth function,

$$N_t(x) = \begin{cases} h, & \text{if } x \in [a, b-\delta), \\ h(\frac{b-x}{2\eta} + \frac{1}{2}), & \text{if } x \in [b-\eta, b], \\ 0, & \text{otherwise.} \end{cases}$$

We will assume that this population density will stay constant for any time t. One key detail that this neglects is what happens when the population density in front of the road is brought to the domain behind the road, increasing the population density at the edge of the road which we assume to be constant. However, with the analytical results we are solely interested in the cases of behaviour in front of the road. The aforementioned behaviour will only occur when the population density is of sufficient density in front of the road and thus in the corridor case. Therefore, for the purpose of this investigation, this behaviour can be ignored.

Because no growth occurs on the road we can consider the model for both components separately. It is now possible to find the analytical result,

$$N_{t+1}(x) = F(h)\phi_{edge}(x, \delta), \tag{5.1.3}$$

where ϕ_{edge} is given by Eq. (C.0.4), for the Ricker growth function we have survival for $A > 1$ (for full details see Appendix C).

A similar analysis for the positive edge effects can be conducted using the equivalent stable population density,

$$N_t(x) = \begin{cases} h, & \text{if } x \in [a, b-\delta), \\ h(\frac{x-b}{\eta} + 2), & \text{if } x \in [b-\eta, b], \\ 0, & \text{otherwise.} \end{cases}$$

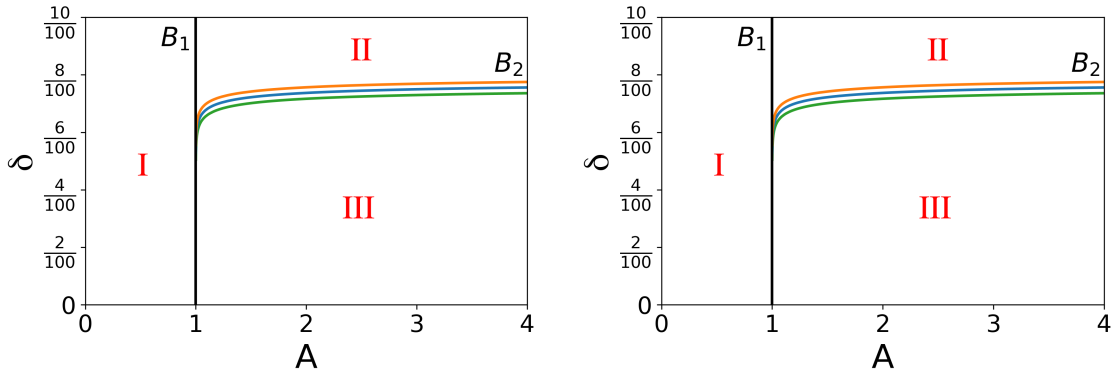

Figure 5.5: *Various spatio-temporal dynamics regimes for various landscape dynamics (a) $\eta = \delta$, and (b) $\eta = 5\delta$: region I represents the extinction regime, II the barrier regime, and III the corridor regime. The lines B_2 represent the boundary between the corridor and barrier region, the no edge effect model is given by the solid blue line, the negative edge effect model by the solid green line, and the positive edge effect model is given by the solid orange line. The negative edge effects reduces the size of the corridor regime and increase the size of the barrier regime compared to the no edge effect regime, where the positive edge effect regime increase the size of the corridor regime and reduces the size of the barrier regime.*

We can now plot the (A, δ)-plane for the no edge effect, negative edge effect, and positive edge effect cases for two different values of η (see Fig. 5.5). It can be observed that the cases do not differ significantly between the three situations, and for the different values of η. More precisely the value of the B_2 line at $\rho = 2.5$ for the no edge effect case is α, in comparison the value for the negative edge effect case is 0.97α and for the positive edge effect case 1.03α, a difference of only 3% compared to the no edge effect case. This means that the effect of the edge being positive or negative for the species and the size that the edge effects occurs over does not have a significant impact on altering the final case of the population density, even though the population density within the edge region is significantly different. This stability of the population density can be viewed as a positive. For example, if a native species was negatively effected by the edge domain region it is unlikely to go into the barrier case if it was in the corridor case without the edge effects being present.

5.1.4 Rate of Spread

From the spatio-temporal dynamics of the population density it can be visually observed that there is significant difference between the edge effect cases. However, it has been shown that the corridor, barrier cases are largely stable under change of the edge effects. A natural question then might be, is the rate of propagation changed by the effects of the edge. The rate of spread to the right for a given t is given by

$$c(t) = x_r(t) - x_r(t-1),$$

where $x_r(t) = \max(x)$ s.t. $N_t(x) \geq 0.1h$, and h is the carrying capacity (see Fig. 5.6). The population density initially starts in the landscape domain and the rate of spread in the landscape region is constant and the same for all three cases. Then as the population density approaches the edge domain the rate of spread differs in all three cases. In the no edge effect case the rate of spread remains constant until the population density reaches the edge of the road where it is reduced due to the cleaning that occurs over the road. In the negative edge effect case the rate of spread declines and continues to do so as it approaches the road. Comparatively in the positive edge effect case the rate of spread increases and continues to do so until it reaches near the edge of the road and then declines as in the no edge effect case. The time taken for the population density to be above the spreading speed cut off also changes based on the domain layout and the size of the edge region. In the negative edge effect case, it takes longer for the population density to overcome the road and become established in front of the road compared to the no edge effect case, the time this takes increases when η increases. The converse is true in the positive edge effect case, the time taken to become established in front of the road is reduced and decreases with increasing η. After the population density has become established in front of the road in all three cases a temporary increase in c is observed, this is both due to the additional population density behind the road and the properties of the growth function.

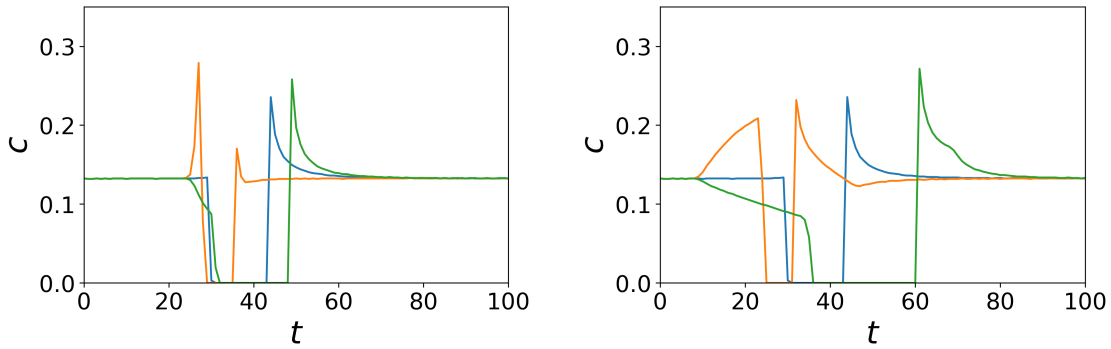

Figure 5.6: *Rate of spread with time in the direction of the road, for* $A = 2.5$, $\delta = 0.55$ *and various values of* η *(a)* $\eta = \delta$*, and (b)* $\eta = 5\delta$*: the no edge effect model is given by the solid blue line, the negative edge effect model by the solid green line, and the positive edge effect model is given by the solid orange line. See text for further explanation.*

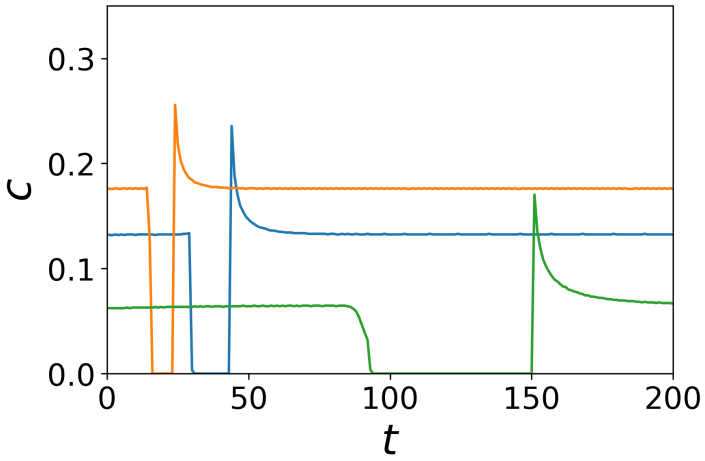

Figure 5.7: *Rate of spread with time in the direction of the road, no edge effect case: for* $\delta = 0.55$ *and various values of* A *where* $A_0 = 2.5$*,* $A = A_0$ *given by the solid blue line,* $A = 2A_0$ *given by the solid orange line, and* $A = 0.5A_0$ *given by the solid green line.*

5.1.5 Rate of spread explanation

When $\eta \gg \sigma$, then the simple rate of spread approximation for integro-difference equations provides a good estimate for the rate/shape of spread leading up to the road. However, the behavior for small η, or the behaviour in the edge region in front of the road is more complex, and cannot be explained/approximated in this way.

The rate of spread for long term behaviour[1] can be approximated by linearising the growth function when the Ricker growth function is being used. We then arrive at the following approximation for the rate of spread when using the Ricker growth function,

$$c^* = \sqrt{2\sigma^2 \ln(A)}, \tag{5.1.4}$$

see [40] for full details.

Here we want to analytically show the trend of increased rate of spread that occurs initially when the population density spreads to the domain in front of the road as observed in numerical simulations (see Fig. 5.6). To do so we treat the population density behind the road by the uniform population density equal to the carrying capacity for the species as previously calculated $\phi(x, \delta)$ is given by (3.2.6).

This gives us a constant population density that is added from behind the road to in front of the road at every time increment. In order to semi-analytically calculate the rate of spread a number of approximations and changes need to be made to the model. The well-known analytical result for the rate of spread when using a Gaussian dispersal kernel [40], relies on carefully choosing initial conditions and then calculating the t-fold convolution of the Gaussian PDF which itself is Gaussian. The same cannot be applied when the front of the traveling wave is near the road.

For the initial condition we approximate $\phi(x, \delta)$ by the half normal distribution,

$$f(x, \sigma) = \frac{\sqrt{2}}{\sigma\sqrt{\pi}} \exp\left(-\frac{x^2}{2\sigma^2}\right), \text{ for } x > 0,$$

with two conditions the height of the population density at the edge of the road and the total population density in front of the road are preserved. The height of the population density at the edge of the road is given by $\phi(b + \delta, \delta)$. For the total population density

[1] We can think of being in the long term behaviour stage when the size and shape of the population density within a small region behind where you are trying to approximate is not sufficiently different from the size of the population density where you are trying to approximate.

being preserved we need to first find the total population density,

$$F(h)\int_{b+\delta}^{\infty}\phi(x,\delta)\approx\Phi(x,\delta,h)\,dx,$$

where Φ is given in Appendix C.

From this we have the area of the constant population density brought over in front from behind the road. The population density can now be estimated by the half normal distribution,

$$f(x,\sigma)=\frac{\sqrt{2}}{\sigma\sqrt{\pi}}\exp\left(-\frac{|x-(b+\delta)|^2}{2\sigma^2}\right),$$

Then the population density over the road is given by the initial condition,

$$N_0(x)=\Phi\frac{\sqrt{2}}{\sqrt{\sigma^{*2}\pi}}\exp\left(-\frac{|x-(b+\delta)|^2}{2\sigma^{*2}}\right)\text{ for }x\geq b+\delta, \tag{5.1.5}$$

where

$$\sigma^*=\frac{\Phi\sqrt{2}}{\phi\sqrt{\pi}}.$$

The method is then as follows, the half normal is transformed into a normal distribution conserving total population density

$$N_0^{normal}(x)=\Phi\frac{1}{\sqrt{2\pi\sigma^{*2}}}\exp\left(-\frac{|x-(b+\delta)|^2}{2\sigma^{*2}}\right),$$

a linear growth factor R is then applied and the population density disperses using the Gaussian dispersal kernel with dispersal variable σ,

$$N_1^{normal}(x)=\Phi R\frac{1}{\sqrt{2\pi(\sigma^{*2}+\sigma^2)}}\exp\left(-\frac{|x-(b+\delta)|^2}{2(\sigma^{*2}+\sigma^2)}\right).$$

The population density is then transformed back into a half normal distribution conserving population density and then the amount of population density brought over from behind

the road Φ is added to obtain the final population density

$$N_1(x) = \Phi(R+1)\frac{\sqrt{2}}{\sqrt{\pi(\sigma^{*2}+\sigma^2)}}\exp\left(-\frac{|x-(b+\delta)|^2}{2(\sigma^{*2}+\sigma^2)}\right) \text{ for } x \geq b+\delta. \tag{5.1.6}$$

The equation (5.1.6) can now be generalised for any time increment t,

$$N_t(x) = \Phi(\sum_{i=0}^{t} R^i)\frac{\sqrt{2}}{\sqrt{\pi(\sigma^{*2}+t\sigma^2)}}\exp\left(-\frac{|x-(b+\delta)|^2}{2(\sigma^{*2}+t\sigma^2)}\right) \text{ for } x \geq b+\delta. \tag{5.1.7}$$

For the rate of spread the maximum distance $x(t,\tilde{N})$ at which the population density has reached a given threshold density $\tilde{N}$ can be found by rearranging (5.1.7),

$$x(t,\tilde{N}) = (b+\delta) + \sqrt{-2(\sigma^{*2}+t\sigma^2)\ln\left(\frac{\tilde{N}\sqrt{\pi(\sigma^{*2}+t\sigma^2)}}{\Phi(\sum_{i=0}^{t} R^i)\sqrt{2}}\right)}. \tag{5.1.8}$$

Then the rate of spread at time t for $t > 0$ is given by $c = x(t,\tilde{N}) - x(t-1,\tilde{N})$.

For large time when the leading edge of the population density is sufficiently far away from the road, the rate of spread is equal to the rate of spread in the no road case. For a linear growth function and Gaussian dispersal this is given by the following [43]

$$c_l = \sqrt{2\sigma^2\ln(R)}, \tag{5.1.9}$$

this is the same as the large time rate of spread using the Ricker growth function (2.1.1) where $R = A$.

One can now compute an example using the semi analytical formulation (5.1.8). From Fig. 5.8 the analytical based result is shown agreeing with the trend of an initial increased rate of dispersal as the population density spreads into the domain in front of the road, and then concavely decreases to the constant rate of spread in the domain when not interacting with the road. This agrees with the numerical results that display the same behaviour when invading the domain in front of the road.

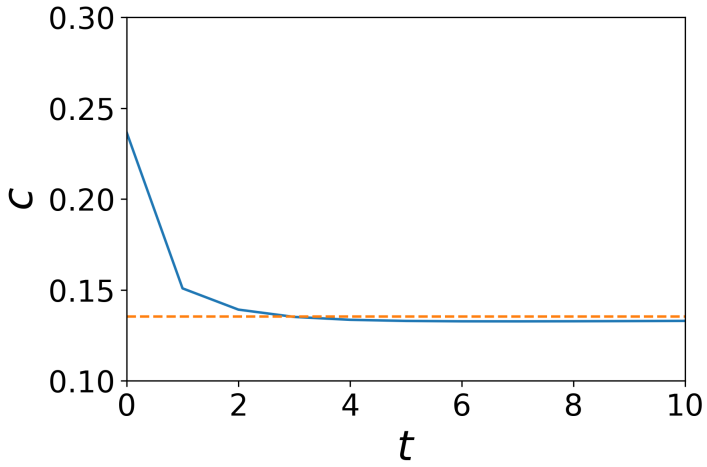

Figure 5.8: *Rate of Spread for the population density in front of the road: given by* (5.1.5)-(5.1.8) *(blue solid line) where* $R = A = 2.5$, $a = -5$, $b = 0$, $\delta = 0.2$, *and* $\tilde{N} = 0.01\phi$. *The asymptotic rate of spread Eq.* (5.1.9) *is indicated by the dashed orange line.*

Chapter 6

Conclusions

The aim of this work was to develop a new mathematical model of invasive plant species where a road is incorporated into the dispersal domain. The application of mathematics to ecological problems has long been studied with some seminal early results in [31, 26, 35]. However, the use of mathematics in ecological problems has significantly increased and continues to rise in popularity [40]. Results pertaining to how a population of invasive plants formed of a single continuous region grow and spread in the homogeneous landscape, an open field, for example, have long been known [43]. For example, travelling wave solutions with a continuous propagation speed. However, even in this seemingly well-studied integro-difference equation-based model with a single species, complex patterns of behaviour can emerge that warrant further investigation. In Chapter 2, an investigation of the transient propagation speed before the population transitions to its asymptotic behaviour with a constant asymptotic propagation speed was conducted. We found that the propagation speed and the time it takes to transition to the asymptotic solution behave non-monotonically with respect to the choice of the detection threshold. Furthermore, we have shown transition to the asymptotic regime when a travelling wave invades a spatial domain at a constant rate has been observed over a time span of several generations. Long transition times suggest that assumptions about immediate establishment of the asymptotic regime of invasion need further investigation and the transition regime cannot

be neglected. The non-linear spatio-temporal dynamics manifests itself in various ways before the initial population density evolves into a travelling wave propagating at a constant speed. The propagation speed at the transient scale is sensitive to the choice of the detection threshold density when the other parameters are fixed in the problem. The transition time to the asymptotic regime is also sensitive to the threshold density since the definition of the transition time is based on the propagation speed. One essential consequence of a non-linear behaviour of the propagation speed at the transient scale is that a small change in the detection threshold can lead to an abrupt change (a jump) in the transition time and therefore the question of how to choose the detection threshold density at early stages of invasion requires further careful investigation. The definition of the detection threshold density remains an open question in practical applications where very little information may be available about the initial density distribution. Here for the detection threshold if we observe an accelerating wave at the beginning of invasion this may indicate that the detection threshold density used is too high. Using an insufficiently small detection threshold density may result in a wrong conclusion about invasion, as the invasive species has already been spread in a larger spatial domain.

Recently, there has been an increased understanding that different landscape features can significantly alter invasive species' spatial distribution and propagation speed (see Chapter 3). One landscape feature that has been observed to alter the characteristics of plants with varying degrees of impact is forest roads. It has also been identified that the number of forest roads will significantly increase in the coming years. Although little was known about the mechanisms of how invasive plants interact with forest roads.

In Chapter 3, a new model incorporating a road into the dispersal domain was introduced in one-dimensional space. The road model is incorporated into the dispersal domain by splitting the time increment into two and implementing an additional dispersal step for any population density that lands on the road subdomain, finally applying a cleaning step on the road.

A number of previous studies have found that forest roads increase the rate of invasion.

However, our study shows that the behaviour is more complex, and a forest road does not always increase the rate of invasion. For the Ricker growth function, two regimes of behaviour were found. The first regime is the corridor regime; this is where the population density reaches the road, interacts with the road, and subsequently spreads to the domain in front of the road. The corridor regime, in most cases, temporarily impedes invasion rather than increasing the rate of invasion. The second regime observed is the barrier regime; this is where the species reaches the road and interacts with the road. Due to the width of the road, the strength of dispersal and the carrying capacity of the species, it is unable to become established in the domain in front of the road. Again, this regime does not lead to an increase in the invasiveness of the species. We also investigated the Allee growth function.

The Allee growth function displays more complex behaviour, where the growth is negative for small population densities. We found that due to this region of negative growth, three regimes of behaviour are observed. The first two cases of behaviour are the same as in the Ricker growth function, the barrier and corridor regime. However, the third is a new regime, which we call the beachhead regime. The beachhead regime is where the population density invades a region in front of the road; however, due to the relationship between the population density reaching the region in front from behind the road and the region of negative growth, it remains stable in front of the road. As is the case with the Ricker growth function, none of the regimes in the Allee growth function lead to an increase in the invasiveness of the species. The propagation speed for the Ricker growth function has also been investigated for the road case at the transient scale (see Chapter 3) in line with the no road case (see Chapter 2). Spatial heterogeneity makes a further impact on the propagation speed of the invasive species during the transition from the initial distribution to the constant asymptotic behaviour. It has been demonstrated here that the constant amount of the population density brought over the road contributes to the non-linear behaviour of the propagation speed and the transition time at the transient scale. This adds another layer of complexity to the problem, where, apart from

the changes in the detection threshold density, small changes in the population brought to the spatial domain in front of the road can also lead to different values of the transition time. Meanwhile, the amount of the population density brought over the road is defined by the road width, and that parameter alone can be used to control the propagation of the invasive species in the spatial domain. The distance the invasive species propagates over a given time from the location where it has been first detected in front of the road depends on the road width, and invasion slows down in the presence of a wide road. It is also worth noting here that formation of an accelerating wave at the beginning of invasion observed by practitioners may occasionally result in confusing short-distance dispersal with an accelerating wave appearing when long-distance dispersal kernels are considered. For instance, it has been mentioned in [9] that the spatial spread observed in their field studies had initial properties related to long-distance dispersal predominating and then properties related to short-distance dispersal predominating. Based on their observations, it has been concluded in [9] that the complex spatial spread can be attributed to a possible mix of long distance and short-distance dispersal events. Meanwhile, the results presented demonstrate that a complex behaviour of the spatial spread may occur in the short-distance dispersal mode alone and is not related to long-distance dispersal. Hence, the issue of identifying long-distance dispersal events at the early stage of biological invasion requires further careful attention.

All of the work conducted in Chapter 2 and Chapter 3 was conducted within a 1-D dispersal domain. In Chapter 4, the no road and road model is extended to a 2-D dispersal domain. Initially, in the 2-D model, the dispersal kernel is restricted to a 2-D Gaussian kernel. For the 2-D Gaussian dispersal kernel, the x-direction and y-direction components can be considered independently. Therefore, the knowledge and understanding gained in the 1-D problem can be transferred to the 2-D problem, where the dispersal is the same in the x and y directions on and off the road.

There are, however, mechanisms that can only be considered in the 2-D problem. The first additional trait that can be considered in the 2-D problem is that the dispersal can

differ in the x and y directions, anisotropic dispersal. This was considered in both the no road and the road cases. Due to the choice of the Gaussian kernel, the results from the 1-D case can again be applied here; however, instead of treating the dispersal in the x and y directions differently across the whole domain. In the road case, the dispersal can be the same across the whole of the no road region and in the x direction in the road region of the dispersal domain but different in the y direction along the road region of the dispersal domain. In this case, one observes if the dispersal is increased in the direction along the road compared to the rest of the domain, the rate of propagation, and, thus, the invasiveness of the population density increased in the domain along the direction of the road. This increase along the direction of the road is also dependent on the road width. We found that for a given fixed set of parameters in the problem where the dispersal parameter is increased along the direction of the road, there is a notion of an 'optimal' road width where the rate of invasion is at a maximum. If the road width is decreased or increased below this value, the propagation speed in the direction along the road is decreased.

In Chapter 5, an additional landscape heterogeneity was introduced in the problem in the form of edge effects in the vicinity around the road domain. The edge effects are implemented by either increasing or decreasing the carrying capacity of the growth function when approaching the edge of the road, representing either more or less favourable conditions of the plant species. For the Ricker growth function, the edge effects can either increase or decrease the set of parameters that lead to a barrier or corridor regime. The addition of the edge effects also slows down or increases the propagation speed when approaching and invading the domain in front of the road, depending on whether the edge effects are negative or positive. These edge effect results show that along with the road domain itself, the conditions surrounding the road can also have a significant impact on the propagation of plant species, requiring careful consideration.

Future Work

Possible directions of future work include extending the investigation of the propagation speed at the transient scale in the one-dimensional domain to the Allee growth function. However, analytical investigation of the Allee growth function would include additional complexities due to the negative growth for small population densities, and the method used for the Ricker growth function cannot easily be applied to the Allee case. Extension of the investigation of the propagation speed at the transient scale to the two-dimensional problem could also provide valuable insights into the problem. It remains unclear, however, whether the results obtained in the 1-D case can be immediately extended to the more realistic 2-D landscape as in the latter case possible directional dispersal has to be taken into account. Directional dispersal may change the propagation regime at the short-time scale, and this issue is left for future work. Furthermore, incorporation of the directional dispersal into the propagation speed problem may require employing long-distance dispersal in the direction along the road. The investigation of the propagation speed here was based on the existence of the constant asymptotic speed. Meanwhile, there is no constant asymptotic speed in problems with long-distance dispersal where the dispersal kernel is not exponentially bounded and therefore the definitions used in the present work would require revision for this problem. Another interesting topic of consideration could be to investigate if it is possible to choose an initial condition or set of initial conditions where the transient wave speed variation is not observed.

Further investigation of the effects of long-distance dispersal involving both the Ricker and Allee growth functions, as well as how time-varying conditions such as wind affect dispersal, would also be of interest to consider.

We have shown that edge effects can impact the spatio-temporal distribution of the population density. The completion of the investigation of the edge effect problem through a more sophisticated definition of the growth function and extension to the two-dimensional spatial domain, as well as combining an anisotropic dispersal kernel to the edge effect problem, would be a valuable area of future research.

Although informed by field work and real-world case studies, the work throughout this thesis is approached from a purely theoretical perspective. Another possible avenue of future work would be to validate the results and conclusions of this work with field data.

Bibliography

[1] W.C. Allee. Animal aggregations. *The Quarterly Review of Biology*, 2(3):367–398, 1927.

[2] L.J.S. Allen. *An Introduction to Mathematical Biology*. Pearson, 2007.

[3] L.J.S. Allen, J.F. Fagan, G. Högnäs, and H. Fagerholm. Population extinction in discrete-time stochastic population models with an allee effect. *Journal of Difference Equations and Applications*, 11(4-5):273–293, 2005.

[4] D.A. Andow, P.M. Kareiva, S.A. Levin, and Okubo. Spread of invading organisms. *Landscape Ecology*, 4:77 – 188, 1990.

[5] N. Bacaër. *A short history of mathematical population dynamics*, volume 618. Springer, 2011.

[6] P. Ball. In retrospect: On growth and form. *Nature*, 494(7435):32–33, Feb 2013.

[7] C. Bellard, P. Cassey, and T.M. Blackburn. Alien species as a driver of recent extinctions. *Biology letters*, 12(2):20150623, 2016.

[8] D.S. Boukal and L. Berec. Single-species models of the allee effect: Extinction boundaries, sex ratios and mate encounters. *Journal of Theoretical Biology*, 218(3):375 – 394, 2002.

[9] M.E. Braithwaite. How well has bsbi chronicled the spread of neophytes? *Watsonia*, 28:21–31, 2010.

[10] P.H.S. Brancalion *et al.* Global restoration opportunities in tropical rainforest landscapes. *Science advances*, 5(7), 2019.

[11] E.O. Brigham and R.E. Morrow. The fast fourier transform. *IEEE Spectrum*, 4(12):63–70, 1967.

[12] R.S. Cantrell and C. Cosner. *Spatial Ecology via Reaction-Diffusion Equations*. John Wiley & Sons, Ltd, 2003.

[13] N. Cappuccino. Allee effect in an invasive alien plant, pale swallow-wort vincetoxicum rossicum (asclepiadaceae). *Oikos*, 106(1):3–8, 2004.

[14] F.S. Chapin III *et al.* Consequences of changing biodiversity. *Nature*, 405(6783):234–242, 2000.

[15] J.S. Clark, M.A. Lewis, and L. Horvath. Invasion by extremes: population spread with variation in dispersal and reproduction. *The American Naturalist*, 157:537 – 554, 2001.

[16] Forestry Commission. Forestry commission open data. (accessed 9^{th} April 2021).

[17] Forestry Commission. Forestry statistics 2020. (accessed 9^{th} April 2021).

[18] C. DÁntonio and S.L. Flory. Long-term dynamics and impacts of plant invasions. *Journal of Ecology*, 105(6):1459–1461, 2017.

[19] C.M. DÁntonio, R.F. Hughes, and J.T. Tunison. Long-term impacts of invasive grasses and subsequent fire in seasonally dry hawaiian woodlands. *Ecological Applications*, 21(5):1617–1628, 2011.

[20] B.F. Deeley and N.B. Petrovskaya. Propagation of invasive plant species in the presence of a road. *Journal of Theoretical Biology*, 548:111196, 2022.

[21] B.F. Deeley and N.B. Petrovskaya. Propagation of the invasion front at the short-time scale in various landscapes. *Bulletin of Mathematical Biology*, 2023. (under review).

[22] Food Department for Environment and Rural Affairs. A green future: Our 25 year plan to improve the environment. (accessed 9^{th} April 2021).

[23] S. Elaydi. *An Introduction to Difference Equations*. Springer-Verlag New York, 2005.

[24] L. Euler. *An introduction to the analysis of the infinite (translated by John D. Blanton)*. Springer-Verlag, New York, 1988.

[25] F.H. Evans and A.J. Diggle. Fast dispersal simulation using bivariate quantiles. In *19th International Congress on Modelling and Simulation - Sustaining Our Future: Understanding and Living with Uncertainty, MODSIM2011*, 2011.

[26] R.A. Fisher. The wave of advance of advantageous genes. *Annals of eugenics*, 7:355 – 369, 1937.

[27] K.P. Hadeler and F. Rothe. Travelling fronts in nonlinear diffusion equations. *J. Math. Biol.*, 2:251 – 263, 1975.

[28] A. Hastings, K. Cuddington, K.F. Davies, C.J. Dugaw, S. Elmendorf, A. Freestone, S. Harrison, M. Holland, J. Lambrinos, U. Malvadkar, B.A. Melbourne, K. Moore, C. Taylor, and D. Thomson. The spatial spread of invasions: new developments in theory and evidence. *Ecology Letters*, 8:91 – 101, 2005.

[29] E. Heinsalu, E. Hernández-García, and C. López. Spatial clustering of interacting bugs: Lévy flights versus gaussian jumps. *Europhysics Letters*, 92(4):40011, nov 2010.

[30] L. Heneghan *et al.* The invasive shrub european buckthorn (rhamnus cathartica, l.) alters soil properties in midwestern u.s. woodlands. *Applied Soil Ecology*, 32(1):142–148, 2006.

[31] R. Hengeveld. *Dynamics of Biological Invasions*. Springer Netherlands, 1989.

[32] Y. Kang and A.-A. Yakubu. Weak allee effects and species coexistence. *Nonlinear Analysis: Real World Applications*, 12(6):3329 – 3345, 2011.

[33] H. Kierstead and L. Slobodkin. The size of water masses containing plankton blooms. *Journal of Marine Research*, 1953.

[34] M. Kot, M.A. Lewis, and P. van den Driessche. Dispersal data and the spread of invading organisms. *Ecology*, 77(7):2027 – 2042, 1996.

[35] M. Kot and W.M. Schaffer. Discrete-time growth-dispersal models. *Math. Biosci*, 80:109 – 136, 1986.

[36] I. Kowarik and L. Moritz Von der. Secondary wind dispersal enhances long-distance dispersal of an invasive species in urban road corridors. *NeoBiota*, 9, 2011.

[37] A.M. Kramer, B. Dennis, A.M. Liebhold, and J.M. Drake. The evidence for allee effects. *Population Ecology*, 51(3):341, 2009.

[38] K.-Y. Lam and Y. Lou. *Introduction to Reaction-Diffusion Equations*. Springer, 2022.

[39] J.M. Levine *et al.* Mechanisms underlying the impacts of exotic plant invasions. *Proceedings of the Royal Society of London. Series B: Biological Sciences*, 270(1517):775–781, 2003.

[40] M. Lewis, S.V. Petrovskii, and J. Potts. *The Mathematics Behind Biological Invasions*. Springer International Publishing, 2016.

[41] M.A. Lewis and S. Pacala. Modeling and analysis of stochastic invasion processes. *J. Math. Biol.*, 41:387 – 429, 2000.

[42] B. Li and G. Otto. Wave speed and critical patch size for integro-difference equations with a strong allee effect. *Journal of Mathematical Biology*, 85(5):1 – 23, 2022.

[43] F. Lutscher. *Integro-difference equations in spatial ecology*. Springer, 2019.

[44] M.C. Mack, C.M. DÁntonio, and R.E. Ley. Alteration of ecosystem nitrogen dynamics by exotic plants: A case study of c4 grasses in hawaii. *Ecological Applications*, 11(5):1323–1335, 2001.

[45] R.M. May. Limit cycles in predator-prey communities. *Science*, 177(4052):900–902, 1972.

[46] R.M. May. Biological populations obeying difference equations: stable points, stable cycles, and chaos. *Journal of Theoretical Biology*, 51(2):511–524, 1975.

[47] R.M. May and G.F. Oster. Bifurcations and dynamic complexity in simple ecological models. *The American Naturalist*, 110(974):573–599, 1976.

[48] C. Meunier, G. Lavoie. Roads as corridors for invasive plant species: New evidence from smooth bedstraw (galium mollugo). *Invasive Plant Science and Management*, 5, 2012.

[49] L.A. Meyerson and H.A. Mooney. Invasive alien species in an era of globalization. *Frontiers in Ecology and the Environment*, 5(4):199–208, 2007.

[50] J.D. Murray. *Mathematical biology: I. An introduction*, volume 17. Springer Science & Business Media, 2007.

[51] A.J. Nicholson and V.A. Bailey. The balance of animal populations.—part i. In *Proceedings of the zoological society of London*, volume 105, pages 551–598. Wiley Online Library, 1935.

[52] T. Onozaki. *Nonlinearity, Bounded Rationality, and Heterogeneity: Some Aspects of Market Economies as Complex Systems*. Springer Japan, 2018.

[53] N.B. Petrovskaya and N.L. Embleton. Evaluation of peak functions on ultra-coarse grids. *Proc. R. Soc. A*, 469:20120665, 2013.

[54] D. Pimentel, L. Lach, R. Zuniga, and D. Morrison. Environmental and economic costs of nonindigenous species in the united states. *BioScience*, 50(1):53–65, 2000.

[55] K.I. Powell, J.M. Chase, and T.M. Knight. A synthesis of plant invasion effects on biodiversity across spatial scales. *American journal of botany*, 98(3):539–548, 2011.

[56] B. Putten, M.D. Visser, H.C. Muller-Landau, and P.A. Jansen. Distorted-distance models for directional dispersal: a general framework with application to a wind-dispersed tree. *Methods in Ecology and Evolution*, 3(4):642–652, 2012.

[57] L.A.D. Rodrigues, D.C. Mistro, E.R. Cara, N.B. Petrovskaya, and S.V. Petrovskii. Patchy invasion of stage-structured alien species with short-distance and long-distance dispersal. *Bulletin of Mathematical Biology*, 77(8):1583 – 1619, 2015.

[58] O.E. Sala *et al.* Global biodiversity scenarios for the year 2100. *science*, 287(5459):1770–1774, 2000.

[59] S.K. Sasmal and J. Chattopadhyay. An eco-epidemiological system with infected prey and predator subject to the weak allee effect. *Mathematical Biosciences*, 246(2):260 – 271, 2013.

[60] D. Savage, M.J. Barbetti, W.J. MacLeod, M.U. Salam, and M. Renton. Can mechanistically parameterised, anisotropic dispersal kernels provide a reliable estimate of wind-assisted dispersal? *Ecological Modelling*, 222(10):1673–1682, 2011.

[61] J. Schank and C. Twardy. *Mathematical Models*, volume 6 of *The Cambridge History of Science*, page 416–431. Cambridge University Press, 2009.

[62] M.J. Schuster, P.D. Wragg, and P.B. Reich. Using revegetation to suppress invasive plants in grasslands and forests. *Journal of Applied Ecology*, 55(5):2362–2373, 2018.

[63] J.A. Sherratt and B.P. Marchant. Algebraic decay and variable speeds in wavefront solutions of a scalar reaction–diffusion equation. *IMA J. Appl. Math.*, pages 289 – 302, 1996.

[64] J.G. Skellam. Random dispersal in theoretical populations. *Biometrika*, 38(1/2):196–218, 1951.

[65] P.A. Stephens and W.J. Sutherland. Consequences of the allee effect for behaviour, ecology and conservation. *Trends in Ecology Evolution*, 14(10):401–405, 1999.

[66] J. Thomson. *On growth and form*. Nature Publishing Group UK London, 1917.

[67] W.J. Tsay, C.J. Huang, T.T. Fu, and I.L. Ho. A simple closed-form approximation for the cumulative distribution function of the composite error of stochastic frontier models. *Journal of Productivity Analysis*, 39:259 – 269, 2013.

[68] P.M. Vitousek, H.A. Mooney, J. Lubchenco, and J.M. Melillo. Human domination of earth's ecosystems. *Science*, 277(5325):494–499, 1997.

[69] M. Von der Lippe and K. Ingo. Long-distance dispersal of plants by vehicles as a driver of plant invasions. *Conservation Biology*, 21, 2007.

[70] J. Wang, J. Shi, and J. Wei. Predator–prey system with strong allee effect in prey. *Journal of Mathematical Biology*, 62:291–331, 2011.

[71] M.-H. Wang, M. Kot, and M. Neubert. Integrodifference equations, allee effects, and invasions. *J. Math. Biol.*, 44:150 – 168, 2002.

[72] H.F. Weinberger. Long-time behavior of a class of biological models. *SIAM journal on Mathematical Analysis*, 13(3):353 – 396, 1982.

[73] M. Williamson. *Biological invasions*. Clapham & Hall, UK, 1996.

Appendix A

Calculation of the amount of the population density brought over the road

Here we explain how to calculate the amount of the population density $\Psi = \Psi(\sigma, \delta)$ brought over from behind the road of width δ at each time increment. In [20], the population density was calculated in the heterogeneous landscape for the next time increment, given the initial condition,

$$N^*(x) = \begin{cases} \ln(A), & \text{for } x \in [a, b], \\ 0, & \text{otherwise,} \end{cases} \tag{A.0.1}$$

where b is the left edge of the road, and $a < b$. Here we want to calculate the amount of population density that spread from behind the road $x \in (-\infty, b]$ to in front of the road $x \in [b+\delta, \infty)$. Hence, in line with the initial condition behind the road (3.3.1), we choose $|b - a|$ to be sufficiently large to approximate the whole domain behind the road.

To calculate the total population density spread in front of the road from behind the road $\Psi(\delta, \sigma)$, with the condition (A.0.1), we need to solve

$$\Psi(\delta, \sigma) = \ln(A) \int_{b+\delta}^{\infty} \phi(x, \delta)\, dx,$$

where $\phi(x,\delta)$ is given by

$$\phi(x,\delta) = \Bigg[\frac{1}{4\sqrt{1-c_2}}\left(\exp\left(\frac{d_2^2}{4d_1}+d_3\right)\left(\operatorname{erf}\left(\frac{2d_1(b+\delta)-d_2}{2\sqrt{d_1}}\right)+\operatorname{erf}\left(\frac{d_2-2d_1b}{2\sqrt{d_1}}\right)\right)\right.$$
$$\left.-\exp\left(\frac{d_4^2}{4d_1}+d_5\right)\left(\operatorname{erf}\left(\frac{2d_1(b+\delta)-d_4}{2\sqrt{d_1}}\right)+\operatorname{erf}\left(\frac{d_4-2d_1b}{2\sqrt{d_1}}\right)\right)\right)$$
$$+\frac{1}{2}\left(\operatorname{erf}\left(\frac{b-x}{\sigma\sqrt{2}}\right)+\operatorname{erf}\left(\frac{x-a}{\sigma\sqrt{2}}\right)\right)\Bigg], \quad \text{(A.0.2)}$$

and,

$$d_1 = -\left(\frac{c_2-1}{2\sigma^2}\right), \quad d_2 = \left(\frac{2x+\sqrt{2}\sigma c_1-2c_2b}{2\sigma^2}\right), \quad d_3 = \left(\frac{-\sqrt{2}\sigma c_1 b+c_2b^2-x^2}{2\sigma^2}\right),$$
$$d_4 = \left(\frac{2x+\sqrt{2}\sigma c_1-2ac_2}{2\sigma^2}\right), \qquad d_5 = \left(\frac{-\sqrt{2}\sigma ac_1+a^2c_2-x^2}{2\sigma^2}\right).$$

One can write ϕ as follows,

$$\phi(x,\delta) = \lambda_1(\nu_1(\lambda_2,\lambda_3,\lambda_4,\lambda_5,\lambda_6)-\nu_1(\lambda_2,\lambda_3,\lambda_4,\lambda_7,\lambda_6)$$
$$-\nu_1(\lambda_8,\lambda_9,\lambda_4,\lambda_{10},\lambda_6)+\nu_1(\lambda_8,\lambda_9,\lambda_4,\lambda_{11},\lambda_6))+\frac{1}{2}(\nu_2),$$

where,

$$\lambda_1 = \frac{1}{4}\frac{1}{\sqrt{d_1}}\frac{1}{\sqrt{2\sigma^2}}, \quad \lambda_2 = \frac{c_1^2\sigma^2-2\sqrt{2}bc_1\sigma+2c_2b^2}{4(1-c_2)\sigma^2}, \qquad \lambda_3 = \frac{\sqrt{2}c_1\sigma-2bc_2}{2(1-c_2)\sigma^2},$$
$$\lambda_4 = \frac{c_2}{2(1-c_2)\sigma^2}, \quad \lambda_5 = \frac{2b+2\delta(1-c_2)-\sqrt{2}c_1\sigma}{4\sqrt{d_1}\sigma^2}, \qquad \lambda_6 = \frac{-1}{2\sigma^2\sqrt{d_1}},$$
$$\lambda_7 = \frac{2b-\sqrt{2}c_1\sigma}{4\sigma^2\sqrt{d_1}}, \qquad \lambda_8 = \frac{\sqrt{2}c_1\sigma-2ac_2}{2(1-c_2)\sigma^2}, \qquad \lambda_9 = \frac{c_1^2\sigma^2-2\sqrt{2}ac_1\sigma+2a^2c_2}{4\sigma^2(1-c_2)},$$
$$\lambda_{10} = \frac{2(1-c_2)(b+\delta)-\sqrt{2}\sigma c_1+2ac_2}{4\sigma^2\sqrt{d_1}} \quad \lambda_{11} = \frac{2b(1-c_2)-\sqrt{2}c_1\sigma+2ac_2}{4\sigma^2\sqrt{d_1}},$$

and

$$\nu_1(\alpha_1,\alpha_2,\alpha_3,\alpha_4,\alpha_5) = \exp\left(\alpha_1+\alpha_2x+\alpha_3x^2\right)\operatorname{erf}\left(\alpha_4+\alpha_5x\right)$$
$$\nu_2 = \operatorname{erf}(\frac{b-x}{\sigma\sqrt{2}})-\operatorname{erf}(\frac{a-x}{\sigma\sqrt{2}}).$$

In order to calculate Ψ one is required to integrate terms of the form,

$$\operatorname{erf}(\alpha_1 + \alpha_2 x)\exp(\alpha_3 + \alpha_4 x + \alpha_5 x^2). \tag{A.0.3}$$

The substitution used in [20], $\operatorname{erf}(x) \approx 1 - \exp(c_1 x + c_2 x^2)$, will be applied here again, where the coefficients c_1 and c_2 have been evaluated in [67] as $c_1 = -1.09599814703333$, and $c_2 = -0.75651138383854$. Using Eq. (A.0.3), one can now calculate the integral of ν_1 when $x \in [m, n]$. The two cases required to consider are as follows.

Case I: For $\alpha_1 + \alpha_2 x \geq 0$ we have

$$\int_m^n \nu_1(\mu_1, \mu_2, -\mu_3, \mu_4, \mu_5)\, dx \approx w_1(\mu_1, \mu_2, -\mu_3, \mu_4, \mu_5; m, n),$$

where w_1 is given by

$$\begin{aligned} w_1(\mu_1, \mu_2, -\mu_3, \mu_4, \mu_5; m, n) = {} & \frac{\sqrt{\pi}\exp(\frac{\mu_2^2}{4\mu_3} + \mu_1)}{2\sqrt{\mu_3}}(\operatorname{erf}(\frac{\mu_2 - 2\mu_3 m}{2\sqrt{\mu_3}}) - \operatorname{erf}(\frac{\mu_2 - 2\mu_3 n}{2\sqrt{\mu_3}})) \\ & - \frac{\sqrt{\pi}\exp(\frac{\beta_2^2}{4\beta_3} + \beta_1)}{2\sqrt{\beta_3}}(\operatorname{erf}(\frac{\beta_2 - 2\beta_3 m}{2\sqrt{\beta_3}}) - \operatorname{erf}(\frac{\beta_2 - 2\beta_3 n}{2\sqrt{\beta_3}})). \end{aligned}$$

Case II: For $\alpha_1 + \alpha_2 x < 0$ we have

$$\int_m^n \nu_1(\mu_1, \mu_2, -\mu_3, \mu_4, \mu_5)\, dx \approx w_2(\mu_1, \mu_2, -\mu_3, \mu_4, \mu_5; m, n),$$

where w_2 is given by

$$\begin{aligned} w_2(\mu_1, \mu_2, -\mu_3, \mu_4, \mu_5; m, n) = {} & \frac{\sqrt{\pi}\exp(\frac{\beta_5^2}{4\beta_3} + \beta_4)}{2\sqrt{\beta_3}}(\operatorname{erf}(\frac{\beta_5 - 2\beta_3 m}{2\sqrt{\beta_3}}) - \operatorname{erf}(\frac{\beta_5 - 2\beta_3 n}{2\sqrt{\beta_3}})) \\ & - \frac{\sqrt{\pi}\exp(\frac{\mu_2^2}{4\mu_3} + \mu_1)}{2\sqrt{\mu_3}}(\operatorname{erf}(\frac{\mu_2 - 2\mu_3 m}{2\sqrt{\mu_3}}) - \operatorname{erf}(\frac{\mu_2 - 2\mu_3 n}{2\sqrt{\mu_3}})). \end{aligned}$$

The coefficients β_i, $i \in \{1,2,3,4,5\}$, are

$$\beta_1 = \mu_4^2 c_2 + \mu_4 c_1 + \mu_1, \quad \beta_2 = 2\mu_4\mu_5 c_2 + \mu_5 c_1 + \mu_2, \quad \beta_3 = -\mu_5^2 c_2 + \mu_3,$$
$$\beta_4 = \mu_4^2 c_2 - \mu_4 c_1 + \mu_1, \quad \beta_5 = 2\mu_4\mu_5 c_2 - \mu_5 c_1 + \mu_2.$$

Calculation of the integral ν_2, when $x \in [b+\delta, \infty)$, proceeds as follows

$$\int_{b+\delta}^{\infty} \nu_2 \, dx = w_3 = b - a + \delta \operatorname{erf}\left(\frac{\delta}{\sqrt{2}\sigma}\right) - (a - b - \delta) \operatorname{erf}\left(\frac{a-b-\delta}{\sqrt{2}\sigma}\right) + \frac{\sqrt{2}\sigma}{\sqrt{\pi}}\left(\exp\left(\frac{-\delta^2}{2\sigma^2}\right) - \exp\left(\frac{-(a-b-\delta)^2}{2\sigma^2}\right)\right).$$

Finally, we define $M(\omega) = \max(\omega, b+\delta)$, and the integral becomes

$$\begin{aligned}\Psi(\delta,\sigma) = \ln(A) \int_{b+\delta}^{\infty} \phi(x,\delta)\, dx = \ln(A)[&\lambda_1(w_1(\lambda_2,\lambda_3,-\lambda_4,\lambda_5,\lambda_6; b+\delta, M(b+\delta-c_2\delta-\frac{1}{\sqrt{2}}c_1\sigma)) \\ &+ w_2(\lambda_2,\lambda_3,-\lambda_4,\lambda_5,\lambda_6; M(b+\delta-c_2\delta-\frac{1}{\sqrt{2}}c_1\sigma),\infty) \\ - w_1(\lambda_2,\lambda_3,-\lambda_4,\lambda_7,\lambda_6; b+\delta, M(b-\frac{1}{\sqrt{2}}c_1\sigma)) &- w_2(\lambda_2,\lambda_3,-\lambda_4,\lambda_7,\lambda_6; M(b-\frac{1}{\sqrt{2}}c_1\sigma),\infty) \\ &- w_1(\lambda_8,\lambda_9,-\lambda_4,\lambda_{10},\lambda_6; b+\delta, M((b+\delta)(1-c_2)+ac_2-\frac{1}{\sqrt{2}}c_1\sigma)) \\ &- w_2(\lambda_8,\lambda_9,-\lambda_4,\lambda_{10},\lambda_6; M((b+\delta)(1-c_2)+ac_2-\frac{1}{\sqrt{2}}c_1\sigma),\infty) \\ &+ w_1(\lambda_8,\lambda_9,-\lambda_4,\lambda_{11},\lambda_6; b+\delta, M(b(1-c_2)+ac_2-\frac{1}{\sqrt{2}}c_1\sigma)) \\ &+ w_2(\lambda_8,\lambda_9,-\lambda_4,\lambda_{11},\lambda_6; M(b(1-c_2)+ac_2-\frac{1}{\sqrt{2}}c_1\sigma),\infty)) + \frac{1}{2}w_3]. \quad \text{(A.0.4)}\end{aligned}$$

Below we calculate the amount of the population density Ψ in the extreme cases of an infinitely wide and infinitely narrow road.

A.1 Wide road

The first case we investigate is when the width of the road is $\delta \to \infty$. We note that the total amount of population density is

$$\int_{-\infty}^{\infty} \phi(x, \delta)\, dx = |b - a| \ln(A) := C,$$

where C is a constant for any given a. Thus the amount of the population density $\Psi(x, \delta)$ (A.0.4) in front of the road is

$$\Psi(x, \delta) = \int_{-\infty}^{\infty} \phi(x, \delta)\, dx - \int_{-\infty}^{X} \phi(x, \delta)\, dx = C - \int_{-\infty}^{X} \phi(x, \delta)\, dx,$$

where $X = b + \delta$. For an infinitely wide road $\delta \to \infty$, the spatial coordinate is $X \to \infty$, and we have

$$\begin{aligned} \Psi(x, \delta) &= C - \lim_{X \to \infty} \int_{-\infty}^{X} \phi(x, \delta)\, dx \\ &= C - C = 0. \end{aligned}$$

Hence, the road acts as a 'barrier' preventing the invasive spread in the domain $x > b$, cf. [20].

A.2 Narrow road

The second case we investigate is what happens when the width of the road is taken to be $\delta \to 0$. It has been shown in [20] that $\phi(\delta)$ is a decreasing function of the road width δ. Hence, the amount of the population density brought over the road $\Psi(\delta, \sigma)$ has a maximum value Ψ_{max} at $\delta = 0$,

$$\Psi_{max}(\delta, \sigma) = \Psi(0, \sigma) = \ln(A) \int_{b}^{\infty} \phi(x, 0)\, dx.$$

Substituting $\phi(x,0)$ and calculating the integral we arrive at

$$\Psi_{max}(\delta,\sigma) = \ln(A)\frac{1}{2}((b-a)(\text{erf}\,(\frac{a-b}{\sqrt{2}\sigma})+1) + \frac{\sqrt{2}\sigma}{\sqrt{\pi}}(1-\exp\,(\frac{-(a-b)^2}{2\sigma^2})).$$

We now take $a \to -\infty$ to obtain

$$\Psi_{max}(\delta,\sigma) = \ln(A)\frac{\sigma}{\sqrt{2\pi}}. \tag{A.2.1}$$

Appendix B

The Analytical Two-Dimensional Model

Here we explain how to calculate the amount of the population density $\Psi = \Psi(\sigma, \delta)$ brought over from behind the road of width δ at each time increment in the two-dimensional case. The problem is set up in the same way as in the one-dimensional case Appendix A for the two-dimensional analog. Here, the initial condition is given by

$$N^*(x,y) = \begin{cases} \ln(A), & \text{for } x \in [a,b], y \in (-\infty, \infty), \\ 0, & \text{otherwise.} \end{cases} \tag{B.0.1}$$

The analytical result can then be found to be

$$\tilde{N}_1^R(x,y) = F(h)\phi(x,\delta), \tag{B.0.2}$$

where the function $\phi(x,\delta)$ is given by

$$\phi(x,\delta) = \frac{1}{4}\left[\frac{1}{2}\frac{1}{\sqrt{2\sigma_x^2}}\frac{1}{\sqrt{f_1(x)}}\left(\exp\left(\frac{f_2^2(b,x)}{4f_1(x)}+f_3(b,x)\right)\left(\operatorname{erf}\left(\frac{2f_1(x)(b+\gamma)-f_2(b,x)}{2\sqrt{f_1(x)}}\right)\right.\right.\right.$$
$$\left.\left.\left.+\operatorname{erf}\left(\frac{f_2(b,x)-2f_1(x)b}{2\sqrt{f_1(x)}}\right)\right)-\exp\left(\frac{f_2^2(a,x)}{4f_1(x)}+f_3(a,x)\right)\left(\operatorname{erf}\left(\frac{2f_1(b+\gamma)-f_2(a,x)}{2\sqrt{f_1(x)}}\right)\right.\right.\right.$$
$$\left.\left.\left.+\operatorname{erf}\left(\frac{f_2(a,x)-2f_1(x)b}{2\sqrt{f_1(x)}}\right)\right)\right)\right]\left[\left(\operatorname{erf}\left(\frac{(n-y)}{\sigma_y\sqrt{2}}\right)+\operatorname{erf}\left(\frac{y-m}{\sigma_y\sqrt{2}}\right)\right)\right.$$
$$+\frac{1}{2}\frac{1}{\sqrt{2\sigma_y^2}}\frac{1}{\sqrt{f_1(y)}}\left[-\exp\left(\frac{f_4^2(n,y)}{4f_1(y)}+f_5(n,y)\right)\left(\operatorname{erf}\left(\frac{2f_1(y)n-f_4(n,y)}{2\sqrt{f_1(y)}}\right)+1\right)\right.$$
$$+\exp\left(\frac{f_2^2(n,y)}{4f_1(y)}+f_3(n,y)\right)\left(1+\operatorname{erf}\left(\frac{f_2(n,y)-2f_1(y)n}{2\sqrt{f_1(y)}}\right)\right)$$
$$+\exp\left(\frac{f_4^2(m,y)}{4f_1(y)}+f_5(m,y)\right)\left(\operatorname{erf}\left(\frac{2f_1(y)m-f_4(m,y)}{2\sqrt{f_1(y)}}\right)+1\right)$$
$$\left.\left.-\exp\left(\frac{f_2^2(m,y)}{4f_1(y)}+f_3(m,y)\right)\left(1+\operatorname{erf}\left(\frac{f_2(m,y)-2f_1(y)m}{2\sqrt{f_1(y)}}\right)\right)\right]\right], \quad \text{(B.0.3)}$$

where,

$$f_1(x) = -\left(\frac{c_2-1}{2\sigma_x^2}\right), \quad \text{(B.0.4)}$$

$$f_2(\alpha,x) = \left(\frac{2x+\sqrt{2}\sigma_x c_1 - 2c_2\alpha}{2\sigma_x^2}\right), \quad \text{(B.0.5)}$$

$$f_3(\alpha,x) = \left(\frac{-\sqrt{2}\sigma_x c_1\alpha + c_2\alpha^2 - x^2}{2\sigma_x^2}\right), \quad \text{(B.0.6)}$$

$$f_4(\alpha,x) = \left(\frac{2x-\sqrt{2}\sigma_x c_1 - 2c_2\alpha}{2\sigma_x^2}\right), \quad \text{(B.0.7)}$$

$$f_5(\alpha,x) = \left(\frac{\sqrt{2}\sigma_x c_1\alpha + c_2\alpha^2 - x^2}{2\sigma_x^2}\right). \quad \text{(B.0.8)}$$

Then,

$$\tilde{N}_{\frac{1}{2}}(x,y) = F(\alpha)\frac{1}{4}\left(\operatorname{erf}\left(\frac{(b-x)}{\sigma_x\sqrt{2}}\right)+\operatorname{erf}\left(\frac{x-a}{\sigma_x\sqrt{2}}\right)\right)\left(\operatorname{erf}\left(\frac{(n-y)}{\sigma_y\sqrt{2}}\right)+\operatorname{erf}\left(\frac{y-m}{\sigma_y\sqrt{2}}\right)\right), \quad \text{(B.0.9)}$$

where

$$\tilde{N}_1(x,y) = \tilde{N}_{\frac{1}{2}}(x,y) + \tilde{N}_1^R(x,y). \tag{B.0.10}$$

Appendix C

The Analytical Edge-Effect Model

As with the no edge effect case for the analytical solution a simplification of the population density behind the road was required, the same will be true for the edge effect case. We will first look at the case where the edge negatively impacts the species. The population density will be set to the carrying capacity for the growth function,

$$N_t(x) = \begin{cases} h, & \text{if } x \in [a, b-\delta), \\ h(\frac{b-x}{2\eta} + \frac{1}{2}), & \text{if } x \in [b-\eta, b], \\ 0, & \text{otherwise.} \end{cases}$$

We will assume that this population density will stay constant for any time t. One key detail that this neglects is what happens when the population density in front of the road is brought to the domain behind the road, increasing the population density at the edge of the road which we assume to be constant. However, with the analytical results we are solely interested in the cases of behaviour in front of the road. The aforementioned behaviour will only occur when the population density is of sufficient density in front of the road and thus in the corridor case. Therefore, for the purpose of this investigation, this behaviour can be ignored.

Because no growth occurs on the road we can consider the model for both components

separately. It is now possible to find the analytical result,

$$N_{t+\frac{1}{2}} = F(h)(\frac{1}{2}(\text{erf}\,(\frac{x-a}{\sqrt{2}\sigma}) - \text{erf}\,(\frac{x-(b-\eta)}{\sqrt{2}\sigma})) + (\frac{b+\eta}{4\eta})(\text{erf}\,(\frac{x-(b-\eta)}{\sqrt{2}\sigma}) - \text{erf}\,(\frac{x-b}{\sqrt{2}\sigma}))$$
$$-(\frac{x}{4\eta})(\text{erf}\,(\frac{x-(b-\eta)}{\sqrt{2}\sigma}) - \text{erf}\,(\frac{x-b}{\sqrt{2}\sigma})) - \frac{\sigma}{2\eta\sqrt{2\pi}}(\exp\,(\frac{-((b-\eta)-x)^2}{2\sigma^2}) - \exp\,(\frac{-(b-x)^2}{2\sigma^2}))).$$

Now we need to compute the additional dispersal step. In order to calculate this we first need to make the substitution

$$\text{erf}(x) \approx 1 - \exp(c_1 x + c_2 x^2),$$

where $c_1 = -1.09599814703333$, and $c_2 = -0.75651138383854$. Next we can make the following substitution and rearrange to obtain,

$$\begin{aligned} N^R_{t+1}(x) = \frac{1}{\sqrt{2\pi\sigma^2}} \int_b^{b+\delta} F(h)(\frac{1}{2}(-\exp(d_1 y^2 + d_2 y + d_3) + \exp(d_1 y^2 + d_4 y + d_5)) \\ +\frac{b+\eta}{4\eta}(-\exp(d_1 y^2 + d_4 y + d_5) + \exp(d_1 y^2 + d_6 + d_7)) \\ -(\frac{y}{4\eta})(-\exp(d_1 y^2 + d_4 y + d_5) + \exp(d_1 y^2 + d_6 + d_7)) \\ -\frac{\sigma}{2\eta\sqrt{2\pi}}(-\exp(d_8 y^2 + d_9 y + d_{10}) + \exp(d_8 y^2 + d_{11} + d_{12}))). \end{aligned}$$

Where,

$$d_1 = -\left(\frac{c_2 - 1}{2\sigma^2}\right), \qquad d_2 = \left(\frac{\sqrt{2}c_1\sigma - 2ac_2 + 2x}{2\sigma^2}\right),$$
$$d_3 = \left(\frac{-\sqrt{2}ac_1\sigma + a^2c_2 - x^2}{2\sigma^2}\right), \qquad d_4 = \left(\frac{\sqrt{2}c_1\sigma - 2(b-\eta)c_2 + 2x}{2\sigma^2}\right),$$
$$d_5 = \left(\frac{-\sqrt{2}nc_1\sigma + (b-\eta)^2c_2 - x^2}{2\sigma^2}\right), \qquad d_6 = \left(\frac{\sqrt{2}c_1\sigma - 2bc_2 + 2x}{2\sigma^2}\right),$$
$$d_7 = \left(\frac{-\sqrt{2}bc_1\sigma + b^2c_2 - x^2}{2\sigma^2}\right), \qquad d_8 = \left(\frac{2}{2\sigma^2}\right),$$
$$d_9 = \left(\frac{2(b-\eta) + 2x}{2\sigma^2}\right), \qquad d_{10} = \left(\frac{-(b-\eta)^2 - x^2}{2\sigma^2}\right),$$
$$d_{11} = \left(\frac{2b + 2x}{2\sigma^2}\right), \qquad d_{12} = \left(\frac{-b^2 - x^2}{2\sigma^2}\right)$$

For simplicity we have the solution to the following integrals

$$\begin{aligned}\psi(f_1, f_2, f_3) &= \int_b^{b+\delta} \exp(f_1y^2 + f_2y + f_3)\, dy \\ &= \frac{1}{2\sigma\sqrt{2}\sqrt{f_1}} \exp\left(\frac{f_2^2}{4f_1} + f_3\right)\left(\operatorname{erf}\left(\frac{2(b+\delta)f_1 - f_2}{2\sqrt{f_1}}\right) - \operatorname{erf}\left(\frac{2bf_1 - f_2}{2\sqrt{f_1}}\right)\right),\end{aligned} \tag{C.0.1}$$

$$\begin{aligned}\Psi(f_1, f_2, f_3) &= \int_b^{b+\delta} y\exp(f_1y^2 + f_2y + f_3)\, dy \\ &= \frac{1}{4\sigma\sqrt{2\pi}f_1^{3/2}} \exp(f_3)\Big(2\sqrt{f_1}(\exp\left(b(f_2 - bf_1)\right) - \exp\left((b+\delta)(f_2 - (b+\delta)f_1\right)) \\ &\quad -f_2\sqrt{\pi}\exp\left(\frac{f_2^2}{4f_1}\right)\left(\operatorname{erf}\left(\frac{2bf_1 - f_2}{2\sqrt{f_1}}\right) - \operatorname{erf}\left(\frac{2(b+\delta)f_1 - f_2}{2\sqrt{f_1}}\right)\right)\Big).\end{aligned} \tag{C.0.2}$$

Thus, the solution for the road dispersal step is as follows,

$$\begin{aligned}N_{t+1}^R(x) = F(h)(&\frac{1}{2}(-\psi(d_1, d_2, d_3) + \psi(d_1, d_4, d_5)) + (\frac{b+\eta}{4\eta})(-\psi(d_1, d_4, d_5) + \psi(d_1, d_6, d_7)) \\ &-(\frac{1}{4\eta})(-\Psi(d_1, d_4, d_5) + \Psi(d_1, d_6, d_7)) - (\frac{\sigma}{2\eta\sqrt{2\pi}})(-\psi(d_8, d_9, d_{10}) + \psi(d_8, d_{11}, d_{12}))).\end{aligned}$$

Therefore, the population density at $t+1$ is given by

$$N_{t+1}(x) = F(h)\phi_{edge}(x,\delta), \tag{C.0.3}$$

where,

$$\begin{aligned}\phi_{edge}(x,\delta) = (\frac{1}{2}(\text{erf}\,(\frac{x-a}{\sqrt{2}\sigma}) - \text{erf}\,(\frac{x-(b-\eta)}{\sqrt{2}\sigma})) + (\frac{b+\eta}{4\eta})(\text{erf}\,(\frac{x-(b-\eta)}{\sqrt{2}\sigma}) - \text{erf}\,(\frac{x-b}{\sqrt{2}\sigma}))\\ -(\frac{x}{4\eta})(\text{erf}\,(\frac{x-(b-\eta)}{\sqrt{2}\sigma}) - \text{erf}\,(\frac{x-b}{\sqrt{2}\sigma})) - \frac{\sigma}{2\eta\sqrt{2\pi}}(\exp\,(\frac{-((b-\eta)-x)^2}{2\sigma^2}) - \exp\,(\frac{-(b-x)^2}{2\sigma^2})))\\ +(\frac{1}{2}(-\psi(d_1,d_2,d_3) + \psi(d_1,d_4,d_5)) + (\frac{b+\eta}{4\eta})(-\psi(d_1,d_4,d_5) + \psi(d_1,d_6,d_7))\\ -(\frac{1}{4\eta})(-\Psi(d_1,d_4,d_5) + \Psi(d_1,d_6,d_7)) - (\frac{\sigma}{2\eta\sqrt{2\pi}})(-\psi(d_8,d_9,d_{10}) + \psi(d_8,d_{11},d_{12}))).\end{aligned} \tag{C.0.4}$$